uOttawa

L'Université canadienne
Canada's university

FACULTÉ DES ÉTUDES SUPÉRIEURES ET POSTOCTORALES

u Ottawa

L'Université canadienne
Canada's university

FACULTY OF GRADUATE AND POSDOCTORAL STUDIES

Duvinh Tran

AUTEUR DE LA THÈSE / AUTHOR OF THESIS

M.Sc. (Neuroscience)

GRADE / DEGREE

Department of Cellular and Molecular Medicine

FACULTÉ, ÉCOLE, DÉPARTEMENT / FACULTY, SCHOOL, DEPARTMENT

The ALS8-Associated P56S Mutation of VAPB Alters ER Morphology and ER Function

TITRE DE LA THÈSE / TITLE OF THESIS

Johny Ngsee

DIRECTEUR (DIRECTRICE) DE LA THÈSE / THESIS SUPERVISOR

CO-DIRECTEUR (CO-DIRECTRICE) DE LA THÈSE / THESIS CO-SUPERVISOR

William Staines

Mario Tiveri

Gary W. Slater

Le Doyen de la Faculté des études supérieures et postdoctorales / Dean of the Faculty of Graduate and Postdoctoral Studies

THE ALS8-ASSOCIATED P56S MUTATION OF VAPB ALTERS ER MORPHOLOGY AND ER FUNCTION

Duvinh Tran

This thesis is submitted as a partial fulfilment of the M.Sc. program in Neuroscience

November 3rd, 2010

Faculty of Medicine
Department of Cellular & Molecular Medicine
Neuroscience Program
University of Ottawa

Your file Votre référence
ISBN: 978-0-494-74208-2
Our file Notre référence
ISBN: 978-0-494-74208-2

ABSTRACT

Amyotrophic lateral sclerosis is a neurodegenerative disease that affects motor neurones of the central nervous system leading to the loss of voluntary muscle control. The objective of this study is to characterize the cellular effects of the P56S mutation in the VAPB gene identified in ALS8, and how these might lead to neurodegeneration.

Over-expression of VAPB-P56S induced formation of expanded endoplasmic reticulum tubules and caused nuclear envelope defects resulting in functional deficits. The mutation inhibited transport of correctly folded membrane proteins from the ER to the Golgi complex and dampened activation of the IRE1 and ATF6 signaling pathways of the unfolded protein response. VAPs interact with lipid binding proteins containing a FFAT motif and co-expression of a FFAT motif resolved the morphological and functional deficits, suggesting that VAPB-P56S might be a gain of toxic function and that the FFAT motif acts as a competitive agonist in counteracting this toxic effect.

TABLE OF CONTENTS

LIST OF FIGURES

LIST OF ABBREVIATIONS

(ATF6) activating transcription factor 6
(ALS) amyotrophic lateral sclerosis
(ARE) anti-oxidant response element
(bZIP) basic leucine zipper
(BSA) bovine serum albumin
(FFAT) two phenylalanines in an acidic tract
(CHOP) CAAT/enhancer binding protein homologous protein
(CNS) central nervous system
(CHO) Chinese hamster ovary
(CgB) ChromograninB
(cDNA) complimentary DNA
(CCD) coiled-coil domain
(CMV) cytomegalovirus
(DIM) dimerization
(DTT) dithiothreitol
(EM) electron microscopy
(EF1α) elongation factor 1α
(ER) endoplasmic reticulum
(ERG30) endoplasmic reticulum and Golgi 30-kDa protein
(ERAD) ER-associated degradation
(EDEM1) ER degradation enhancer, mannosidase alpha-like 1
(ERGIC) ER-Golgi Intermediate Compartment
(ERSE) ER stress response element
(eIF2α) eukaryotic translation initiation factor 2α
(EPSPs) excitatory postsynaptic potentials
(FRAP) fluorescence recovery after photobleaching
(FALS) familial ALS
(GFP) green fluorescent protein
(GRP78) glucose-regulated protein 78
(GLUT4) glucose transporter 4
(GLS) Golgi complex localization sequence
(HERP) homocysteine-induced ER protein
(IRE1) inositol requiring enzyme 1
(LINC) linker of the nucleocytoskeleton to the cytoskeleton
(MSP) major sperm protein
(mRNA) messenger RNA
(MEM) minimum essential medium
(MND) motor neurone disease
(NSC34) Neuroblastoma-spinal cord 34
(NE) nuclear envelope
(NLS) nuclear localization signal
(NPCs) nuclear pore complexes
(Nups) nucleoporins

(NRF2) nuclear respiratory factor 2
(OSER) organized smooth ER
(OHD) OSBP homology domain
(ORD) OSBP-related ligand-binding domain
(ORPs) OSBP-related proteins
(OSBP) oxysterol-binding protein
(PNS) perinuclear space
(PM) plasma membrane
(PH) pleckstrin homology
(PCR) polymerase chain reaction
(PERK) pancreatic ER kinase-like endoplasmic reticulum kinase
(RT-PCR) real-time PCR
(rdgB) retinal degeneration type B protein
(SMA) spinal muscular atrophy
(SALS) sporadic ALS
(SNARE) soluble *N*-ethylmaleimide-sensitive factor attachment protein receptor
(SCS2) suppressor of choline sensitivity 2
(TDP-43) TAR-DNA-binding protein-43
(TAD) transcriptional activation domain
(TMD) transmembrane domain
(TRAF2) tumor necrosis factor receptor-associated factor 2
(UPR) unfolded protein response
(UPRE) unfolded protein response element
(VAMP) vesicle-associated-membrane protein
(VAP33) VAP of 33kDA
(VAPB) vesicle-associated-membrane protein-associated protein B
(VSVG) vesicular stomatitis viral glycoprotein
(XBP1) X-box-binding protein-1

ACKNOWLEDGEMENTS

I would like to thank Peter Rippstein, manager of the Stewart Whitman Core Histopathology Laboratory and Electron Microscopy Laboratory at the University of Ottawa Heart Institute for his contribution to the electron microscopy images in this study. I would like to acknowledge Derek Prosser for his contribution to the ChromograninB (CgB) transport experiment.

I would also like to thank my thesis supervisor, John Ngsee for allowing me the opportunity to study and work in his laboratory. His knowledge and guidance have provided others and myself with a great learning environment. I would also like to acknowledge the members of my thesis advisory committee, Drs. Marie-Andrée Akimenko and Xiaohui Zha for their time and guidance.

I cannot forget the group of people that I have been privileged to work with over these years. The term lab mate and friend have become interchangeable thanks to these people. I would like to thank them for making my time here extremely enjoyable. Thanks Allana, Stephanie, Julie, Derek, Carine, Wendy, Jess, Tony, Kalina, Yves, Darren, Beata and Kristen. I hope I didn't forget anyone.

To all my friends that I've known all these years that have been there but have not been in the lab. Thanks to all you guys. You know who you are.

Finally, thank you to mom and dad. Thanks for giving Duvien and myself the opportunities to do the some of the things that you were not able to do. I will never be able to thank you enough. This thesis is for the both of you as much as it is for me.

INTRODUCTION

The ALS8-linked VAPB-P56S mutation affects motor neurones

The premature death of neurones is a common characteristic of several neurodegenerative diseases such as Alzheimer's, Parkinson's, Huntington's, and amyotrophic lateral sclerosis (ALS) (Xiong and McNamara, 2002). VAPB is an integral membrane protein expressed in all tissues, however the ALS8 causing P56S mutation specifically results in the loss of motor neurones (Teuling et al., 2007). The reason behind the preferential vulnerability of motor neurones to VAPB-P56S is not known. Previous studies have documented that expression of VAPB-P56S caused aggregates (Hetz et al., 2009) that are resistant to degradation (Forman et al., 2003), a hallmark of many neurodegenerative diseases. In spite of this, the origin and effect on cellular processes of these aggregates is not well understood and the cellular mechanism underlying the pathogenesis of ALS8 is incomplete. The potential functional deficits caused by these aggregates may explain the susceptibility of motor neurones to death compared non-motor neurone cells.

The motor neurone

Motor neurones are localized to the motor cortex, a region of the cerebral cortex in the brain that function in voluntary muscle movement (Shaw, 2005). They are classified as efferent neurones because they carry information from the CNS to the muscles as opposed to afferent or sensory neurones that carry information from sensory organs and tissues back to the CNS. A motor neurone is composed of the cell body or

soma, dendrites and axons (James and Talbot, 2006). The dendrites branch out from the cell body and receive electrochemical signals from other areas of the nervous system and the soma is the area of the cell that contains all the cellular components and genetic information needed to keep the motor neurone functional (Kabashi et al., 2010). The axon, composed of a long and thin fiber, conducts electrical impulses and sends signal from the soma. Upper motor neurones in the motor cortex project their axon to the brainstem and spinal cord where they release glutamate onto post-synaptic receptors of lower motor neurones (Bruijn et al., 2004). Lower motor neurones then continue this excitatory transmission by releasing acetylcholine at the neuromuscular junction to trigger a contractile response of the muscle fiber (Jiang et al., 2003). ALS is referred to as motor neurone disease (MND) or Lou Gehrig's disease in the United States (James and Talbot, 2006) and is characterized by death the upper motor neurones and lower motor neurones resulting in the loss of voluntary muscle movement (Boillee et al., 2006).

VAPB is ubiquitously expressed in most tissues. In mice, VAPA and VAPB are expressed in the kidney, heart, skeletal muscle, liver, spleen, lung and various areas of the central nervous system (Teuling et al., 2007). Results obtained from human sections displayed VAPB labeling in the hippocampus and cerebellum as well as in the motor neurones of the spinal cord and caudal brainstem (Teuling et al., 2007). Furthermore, localization of VAPB in neurones was concentrated to the cell bodies and their proximal dendrites (Teuling et al., 2007). Motor neurones are large in size and have a complex morphology requiring tightly regulated cellular processes (Boillee et al., 2006). In addition, these cells have extensive ER as indicated by Nissl staining of rough ER and VAPB is localized to the ER. Interestingly, the P56S mutation of VAPB affects only

motor neurones and this may be due to alteration of ER morphology and ER function, which may explain the selective damage. Moreover, these motor neurones are post-mitotic and do not regenerate implying that selective damage to motor neurones by expression of the P56S mutant may be additive with aging and potentially explain the late-onset nature of ALS8 (D'Angelo et al., 2009).

Genetic studies link the P56S mutation of VAPB to ALS8

A study in 2004 identified a large Brazilian family of Portuguese ancestry that carried one of the eleven loci linked to a form of Familial ALS (FALS) (Mitne-Neto et al., 2007). This study revealed that approximately 200 individuals from nine related families numbering about 1500 people suffered from ALS symptoms (Nishimura et al., 2005). Haplotype analysis revealed that these individuals shared a common single point mutation ($C_{166}T$) in exon 2 that resulted in a substitution of a proline to serine at residue 56 (P56S) (Landers et al., 2008). The mutation was mapped to chromosome 20q13.3, the site for a six exon gene spanning approximately 58Kb for vesicle-associated-membrane protein-associated protein B (VAPB) (Nishimura et al., 2005). The locus was designated as ALS8 (Nishimura et al., 2005), a dominant adult-onset form of ALS (Chai et al., 2008) where both sexes are affected equally and the patients range between the ages of 25 to 52 years with a speed of disease progression between 2 and 30 years (Nishimura et al., 2004). The symptoms were categorized into three distinct conditions ranging from late-onset, slowly progressing form of spinal muscular atrophy (SMA), to a slowly progressing form of ALS (ALS8), and finally to a severe and rapidly progressing ALS (Ackerman and Cox, 2008).

The symptoms of ALS

The death of motor neurones causes involuntary muscle movement manifested by muscle twitches, cramps and postural tremors (Ratnaparkhi et al., 2008). Patients also displayed muscle weakness and atrophy (Hetz et al., 2009), and had difficulties in speech and swallowing that progressed to paralysis leading to respiratory failure and death approximately five years after onset (Cozzolino et al., 2008). The disease is made even more difficult because individuals with ALS maintain their cognitive abilities and are aware of the progression and loss of their motor functions (Xiong and McNamara, 2002).

The majority of ALS cases occur at about 50 years of age (Cozzolino et al., 2008) and affects 4-6 persons out of 100,000 and the risk of development is 1-2 persons out of 100,000 (Kanekura et al., 2009). Sporadic ALS (SALS) makes up 90-95% of the cases while the remaining 5-10% have a genetic link and are classified as FALS (Conforti et al., 2006). Despite the differences in frequency between SALS and FALS, disease manifestation between the two is not distinguishable (Hirano, 2008). For that reason, the understanding of ALS8 disease progression and possible therapeutic strategies can potentially be applied to other ALS cases.

VAP family of proteins

In humans, there are three members in the VAP family of proteins, including VAPA, VAPB and VAPC (Nishimura et al., 1999). The first VAP was identified in *Aplysia californica* as VAP of 33kDA (VAP33) (Nishimura et al., 1999) and later studies revealed that VAPs were expressed in all eukaryotic organisms (Lev et al., 2008). The acronym VAP was coined from its association with vesicle-associated-membrane protein

(VAMP)-2, a protein that is part of the soluble *N*-ethylmaleimide-sensitive factor attachment protein receptor (SNARE) complex (Foster et al., 2000) responsible for mediating membrane fusion and vesicle docking to specific target membranes in the secretory and endocytic pathway of eukaryotic cells (Weir et al., 2001).

Despite being grouped in the same protein family, differences exist between the three VAPs. VAPA is encoded from gene found on chromosome 18 whereas VAPB and VAPC are encoded from a gene on chromosome 20 (Nishimura et al., 1999). In addition, there are small variations in protein size where VAPA is 249 amino acids long with a molecular mass of 27.3kDa compared to VAPB that is 243 amino acids long and has a molecular mass of 27 kDa (Nishimura et al., 1999). VAPC is an alternatively spliced version of VAPB and contains only the first 70 amino acids of VAPB followed by 29 unrelated amino acids (Kukihara et al., 2009).

VAP major domains and subcellular localization

VAPA and VAPB have three major domains that are essential for their function and localization. The A and B isoforms are 63% identical at the amino acid level (Nishimura et al., 2004) and contain an amino-terminal major sperm protein (MSP) domain, a middle coiled-coil domain (CCD), and a carboxyl-terminal transmembrane domain (TMD) (Fig. 1A) (Prosser et al., 2008). VAPA and VAPB are integral membrane proteins in which there are 4 types for single-spanning membrane proteins. Type I and type IV integral membrane proteins have cleavable signal sequences and have their amino-terminal oriented towards the ER lumen and the cytoplasm, respectively. Type II and type III integral membranes have non-cleavable signal anchors and have their amino-terminal oriented towards the cytoplasm and ER lumen, respectively. The amino-

terminal of VAP is oriented towards the cytoplasm and its carboxyl-terminal is embedded into the lipid bilayer of the endoplasmic reticulum (ER) membrane thus classifiying VAPA and VAPB as single-pass type II integral membrane proteins (Fig. 1C) (Teuling et al., 2007). The P56S mutation of VAPB is located within the MSP domain (Teuling et al., 2007), a 150 amino acid domain organized into a seven-stranded immunoglobin-like β sandwich with S-type topology (Baker et al., 2002) that interacts directly with the FFAT motif of lipid binding or transfer proteins and also interacts indirectly with microtubules (Prosser et al., 2008). The CCD is approximately 40 amino acids in size and is also predicted to function in protein-protein interaction (Hamamoto et al., 2005). The TMD anchors VAP to the ER membrane, and contains a dimerization motif (GxxxG) for homo- and heterodimerization (Fasana et al., 2009).

Subcellular localization studies of VAPA and VAPB showed that the proteins are localized to the ER (Skehel et al., 2000) and the Golgi apparatus (Soussan et al., 1999). The ER is a large, continuous network of membrane-enclosed structures or cisternae held together by the cytoskeleton (Gorelick and Shugrue, 2001). The ER tubules are formed by action of reticulon and reticulon-like proteins. The perinuclear ER constitutes the outer nuclear membrane whereas the peripheral ER is the remaining part of the ER that extends throughout the cytoplasm and can be decorated with ribosomes (rough ER) or free of ribosomes (smooth ER) (Schroder and Kaufman, 2005). The Golgi apparatus is an organelle composed of stacks of cisternae and functions in packaging and processing proteins and lipids on their way through the secretory pathway to their final destination (Lee et al., 2004).

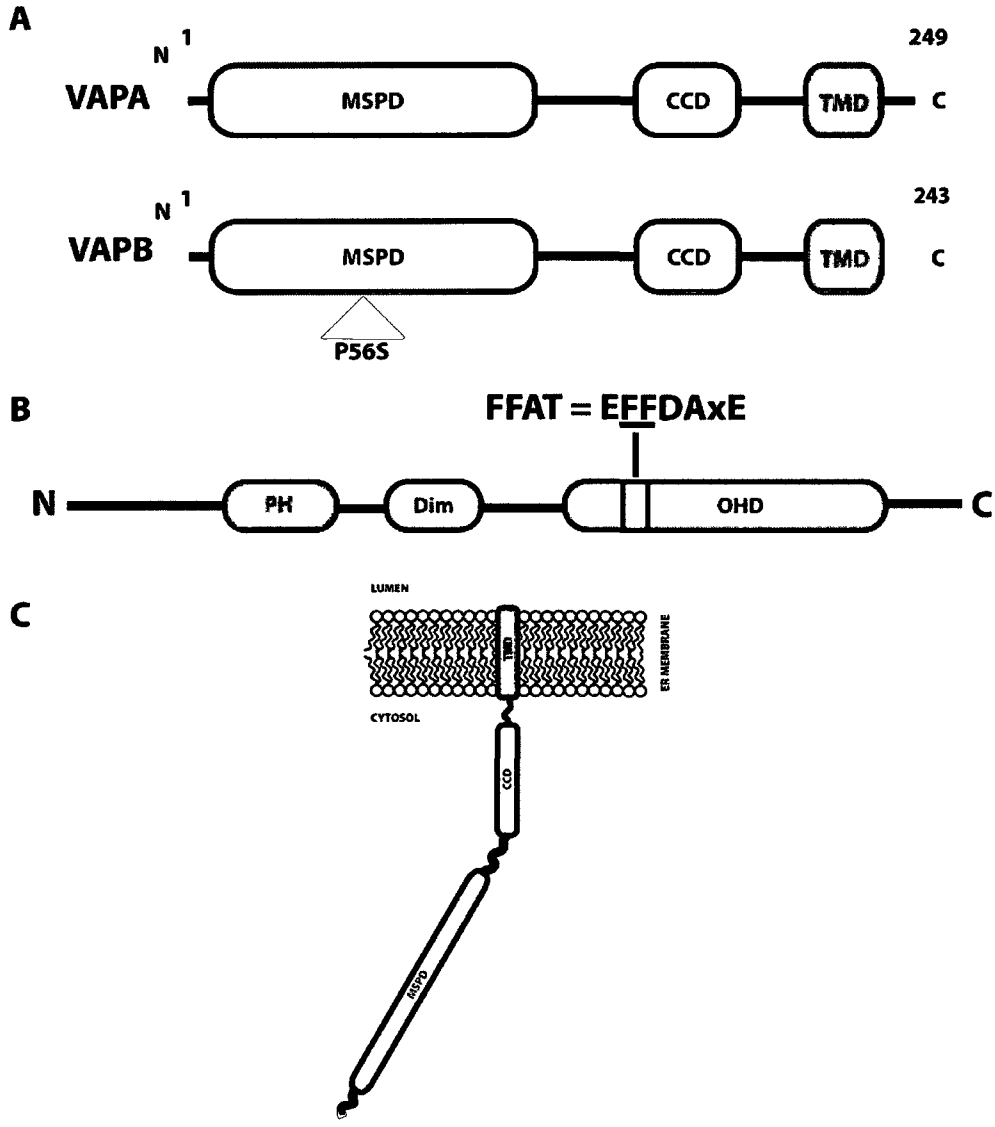

Figure 1. Diagram of VAP and OSBP protein structures.
(*A*) Schematic of VAP A and B isoforms illustrating major domains. VAPA and VAPB contain an N-terminal major sperm (MSP) domain, a middle coiled-coil domain (CCD), and the C-terminal transmembrane domain (TMD). P56S indicates the site of the missense mutation associated with ALS8 in VAPB. (*B*) Schematic of OSBP protein structure illustrating major domains. OSBP contains a pleckstrin homology (PH) domain, a dimerization (DIM) domain, and an OSBP homology domain (OHD) spanning 417-772. The FFAT containing fragment of OSBP that was cloned for this study spanned residues 347-468. (*C*) Cartoon of VAP protein structure orientation. VAPA and VAPB are a type II integral membrane protein with its TMD anchored to the ER membrane and the MSP domain oriented towards the cytosol.

VAPB-P56S mutation induces a change in protein conformation

The effect of the P56S mutation of VAPB at the level of the protein structure is predicted to cause a change in protein conformation (Nishimura et al., 2004). The proline at codon 56 is located within an S-shape loop connecting the d1- and d2-strands within the MSP domain (Nishimura et al., 2004) and stabilizes the S-shape loop by maintaining it in a less energetically favourable *cis*-peptide bond conformation (Teuling et al., 2007). This conformation is vital to for proper positioning of the d1-strand so that it can shield the hydrophobic core residues of the MSP domain (Teuling et al., 2007). The proline to serine substitution is predicted to destabilize the S-shape loop and cause a shift to a more energetically favourable *trans*-peptide bond conformation resulting in exposure of the hydrophobic residues to the solvent (Teuling et al., 2007). Consequently, exposure of the hydrophobic residues of VAPB-P56S promotes clustering of neighbouring P56S mutant VAPB proteins as a means of shielding the hydrophobic core residues (Teuling et al., 2007). Due to its cyclic structure, proline provides a much greater confirmational rigidity compared to other amino acids. Also, it appears that that it is the loss of the proline residue rather than the introduction of the serine residue that is important. Matsuoka's group demonstrated that substitution of the 56th residue with other amino acids such as alanine, lysine or aspartic acid resulted in insolubility of VAPB similar to the P56S mutation (Kanekura et al., 2006). Nothing is known about the phopshorylation of VAPB and it is unclear if the serine residue at position 56 is phophorylated. However, based on the study by Matsuoka's group, it does not appear as though phosphorylation of serine and changes in post-translational modification of VAPB can account for the gain in toxic function because mutating the 56th residue to other non-phosphorylatable amino acids

yield the same effect as the serine substitution (Kanekura et al., 2006). Unfortunately, no autopsy material has been available for familial cases of VAPB-P56S to confirm that these aggregates are replicated in humans (Chai et al., 2008). However, these aggregates have been reproduced in animal models, such as *Drosophila melanogaster* where transgenic expression of mutant dVAPP58S corresponding to human VAPB-P56S, reproduced these structures (Chai et al., 2008). Also, transgenic mice expressing the human P56S mutation of VAPB have displayed aggregates described as cytoplasmic ubiquitin accumulations which is a neuropathological marker (Tudor et al., 2010). Ubiquitination is associated with misfolded proteins supporting the model that the P56S prevents proper folding of VAPB amd the loss of the correct protein conformation (Kanekura et al., 2006). *In vitro* studies have consistently shown that over-expression of VAPB-P56S results in the formation of highly polyubiquitinated, detergent-insoluble, membrane-aggregates (Kanekura et al., 2006). Despite these findings, the origin of these structures and their effect on cellular functions remains unclear.

Possible VAP functions

Previous VAPB studies revealed a protein with different possible functions. Some of the earlier literature focused on VAP33/VAPA and the knowledge gained from those studies might be applicable to VAPB because the two isoforms share similar protein structure (Nishimura et al., 2004). Altogether, the VAPB-P56S mutation is predicted to have an effect on candidate functions including intracellular trafficking, the unfolded protein response (UPR), and phospholipid metabolism (Tudor et al., 2010). A defect of one of these functions may be responsible for pre-mature cell death and explain the pathogenesis of ALS8 and the susceptibility of motor neurones.

Intracellular trafficking

In eukaryotes, the protein secretory pathway is a dynamic system involving a series of vesicle budding and fusion events to allow cargo to be transported between specific organelle compartments (Weir et al., 2001). The fidelity of this pathway is essential to maintain the integrity of membrane-bound organelles and various cellular functions (Skehel et al., 2000). The involvement of VAP in intracellular trafficking is well studied but their specific function is controversial and the effect of the P56S mutation of VAPB is unknown.

VAP is implicated in protein trafficking between the ER and the Golgi complex

In *Aplysia californica*, ApVAP33 is associated with VAMP/synaptobrevin, a protein that functions in neurotransmitter release (Skehel et al., 2000). This group observed that intracellular injection of antibody against ApVAP33 inhibited excitatory postsynaptic potentials (EPSPs) in cultured cells suggesting that ApVAP33 regulated neurotransmission (Skehel et al., 2000). This role was clarified in mice where mVAP33 was shown to be involved in microtubule-dependent delivery of vesicle-associated proteins to synaptic terminals rather than directly participating in synaptic vesicle exocytosis (Nishimura et al., 2004). The study showed that mVAP33 localization in primary neuronal cultures was limited to the ER and intracellular vesicles but was excluded from the PM or synaptic vesicles and that the protein associated with microtubules (Skehel et al., 2000). In support of this premise, human VAP33/VAPA was demonstrated to function in regulating the availability of the SNARE protein, VAMP-2 for glucose transporter 4 (GLUT4) and that sequestering of VAMP-2 prevented fusion of GLUT4-containing vesicles with the plasma membrane (Foster et al., 2000). In another

study, *in vitro* binding assays showed that VAPA interacted with SNARE proteins Rbet1 and Rsec22, two proteins implicated in ER to Golgi complex trafficking (Lev et al., 2008). Furthermore, Elazar's group identified that ER and Golgi 30-kDa protein (ERG30), which would later be named VAPB, functioned in the transport pathway between the ER and the Golgi complex (Soussan et al., 1999). Their study revealed that the addition of ERG30 antibodies *in vitro* resulted in the accumulation of COPI-coated vesicles at the Golgi complex (Soussan et al., 1999). COPI coatomers are involved in retrograde traffic within the Golgi and from the *cis*-Golgi region to the ER (Gorelick and Shugrue, 2001). Together, these findings implicate VAPA and VAPB in intracellular trafficking between the ER and the Golgi complex. One of the objectives of the current study is to determine how disruption of the movement of proteins between these two compartments by mutant VAPB-P56S might contribute to motor neurone degeneration in ALS8.

Unfolded protein response

In higher eukaryotic cells, the UPR is an adaptive mechanism that addresses ER stress brought on by the accumulation of misfolded proteins (Schroder and Kaufman, 2005). The UPR is an intracellular signalling pathway that initiates adaptive responses via activation of three proximal sensors including inositol requiring kinase 1 (IRE1), activating transcription factor 6 (ATF6) and pancreatic ER kinase-like endoplasmic reticulum kinase (PERK) (Fig. 2) (Liu and Kaufman, 2003). The overarching goal of the UPR is to adapt to ER stress and mitigate the stress condition (Rutkowski and Kaufman, 2004). The understanding of the involvement of VAPB in the UPR is still novel and the effect of VAPB-P56S on this adaptive mechanism is still unclear.

The ER acts as a quality control compartment and activates the UPR

The UPR is tightly linked to the ER, a membrane enclosed network that is continuous with the nuclear envelope and extends into the cytoplasm (Zhang and Kaufman, 2004). It is the site of secretory and membrane protein biosynthesis, translocation, glycosylation, folding, assembly, and the site of lipid biosynthesis (Amarilio et al., 2005). Furthermore, the organelle functions as a quality control compartment to ensure that only properly modified and folded proteins are able to proceed through the secretory pathway to other intracellular organelles and the cell surface (Ellgaard and Helenius, 2001). The biosynthetic function of the ER puts it at risk for ER stress that occurs when the normal physiological state of the ER is disturbed and this can occur when the influx of nascent, unfolded proteins exceeds the folding and processing capacity of the ER (Schroder and Kaufman, 2005).

The adaptive response

The adaptive UPR branch is controlled by a master regulator, BiP/glucose-regulated protein 78 (GRP78) that functions as a molecular chaperone (Forman et al., 2003). BiP plays a pivotal role in activation of the UPR by acting as a negative master regulator for the three UPR proximal sensors (Sommer and Jarosch, 2002). It does this by binding to the ER luminal domain of the three UPR sensors thereby preventing their mobility and activation (Fig. 2A) (Schroder and Kaufman, 2005). However, under conditions of ER stress, BiP will preferentially bind to exposed hydrophobic regions (Fig. 2B) (Kaufman, 2002), a characteristic of underglycosylated, misfolded, or unassembled proteins, resulting in its dissociation from the UPR proximal sensors and their activation (Shang, 2005).

The most conserved sensor in higher eukaryotic cells is IRE1, a type I integral membrane protein (Urano et al., 2000). BiP dissociation allows IRE1 to oligomerize, triggering autophosphorylation and activation of endoribonuclease activity at the carboxyl-terminal that extends in the cytosol (Zhang and Kaufman, 2004). The substrate for IRE1 endoribonuclease is XBP1 mRNA (Schroder and Kaufman, 2005) which undergoes a cytoplasmic splicing event by IRE1 (Yoshida, 2007) where a 26 nucleotide intron of XBP1 mRNA is removed followed by a re-ligation event that results in the generation of a translational frameshift (Forman et al., 2003). The newly spliced XBP1 codes for a potent basic leucine zipper (bZIP) transcription activator that containing a transcriptional activation domain (TAD) that will translocate to the nucleus where it will activate gene transcription of chaperones and genes for protein degradation via ER-associated degradation (ERAD) (Szegezdi et al., 2006) by binding to the unfolded protein response element (UPRE) and the ER stress response element (ERSE) (Schroder and Kaufman, 2005).

A second proximal sensor is ATF6, a type II integral membrane protein (Zhang and Kaufman, 2004). Upon disassociation of BiP, a Golgi complex localization sequence (GLS) is unmasked (Schroder and Kaufman, 2005), initiating translocation of an ATF6 precursor to the Golgi complex where it undergoes two cleavages to free a cytosolic bZIP domain of ATF6 (Shen and Prywes, 2005). Once freed, the transcription factor translocates to the nucleus and binds to ERSE to activate gene transcription of chaperones and XBP1 (Wang et al., 2000).

The third proximal sensor is a type I integral membrane protein called PERK (Schroder and Kaufman, 2005). When BiP is titrated away from PERK, the protein

oligomerizes and phosphorylates eukaryotic translation initiation factor 2α (eIF2α) at the α subunit, and nuclear respiratory factor 2 (NRF2) (Malhotra and Kaufman, 2007b), a bZIP transcriptional factor (Forman et al., 2003). Phosphorylation of eIF2α results in the reduction in concentration of the protein translation 43S pre-initiation complexes and the increase translation of short upstream open reading frames (uORFs) that repress downstream ORF (Schroder and Kaufman, 2005). The overall effect is attenuation of general protein translation (Schroder and Kaufman, 2005). Phosphorylation of Nrf2 causes the protein to localize to the nucleus where it binds to anti-oxidant response element (ARE) and regulates transcription of genes that have a potential to cause oxidative stress (Zhao and Ackerman, 2006).

In combination, the three UPR transducers are responsible for transcription of UPR genes to increase the folding capacity in the ER by upregulating chaperones and foldases and increasing the ER in size to dilute the protein load (Szegezdi et al., 2006). Moreover, the UPR addresses the protein folding demand by attenuating global protein synthesis and activating the ERAD for degradation by the proteasome machinery (Chang et al., 2004). The caveat to this system is that prolonged UPR activation due to unresolvable stress can trigger a switch from the adaptive response to an apoptotic response (Szegezdi et al., 2006).

The apoptotic response

There are two pathways by which the UPR can initiate programmed cell death by apoptosis. Activation of the receptor-independent pathway occurs when ATF6 and PERK via ATF4, induce expression of CAAT/enhancer binding protein homologous protein (CHOP) (Fig. 2B), a proapoptotic bZIP transcription factor (Schroder and

Kaufman, 2005). CHOP functions by repressing transcription of antiapoptotic Bcl-2 and promoting apoptosis (Schroder and Kaufman, 2005). The PERK signaling pathway also attenuates cyclin D1 translation and arrests the cell cycle during G1 phase (Liu and Kaufman, 2003). The receptor-dependent pathway occurs when IRE1 recruits tumor necrosis factor receptor-associated factor 2 (TRAF2) to the ER membrane (Fig. 2B) (Schroder and Kaufman, 2005). The recruitment of TRAF2 eventually causes its release from procaspase-12 resulting in clustering and activation of caspase-12 which initiates the caspase activation cascade (Forman et al., 2003).

VAPB is associated with IRE1 and ATF6 activation

The involvement of VAPB with the UPR was deduced from early studies in yeast. The yeast orthologue of VAP is known as suppressor of choline sensitivity 2 (SCS2) (Suzuki et al., 2009) and was isolated as a suppressor of defective IRE1 and HAC, which are orthologues of mammalian IRE1 and X-box-binding protein-1 (XBP1), respectively (Kanekura et al., 2006). Functional studies revealed that over-expression of wild-type VAPB induced IRE1 activation whereas VAPB-P56S dampened activation in NSC-34 motor neurones (Kanekura et al., 2006) treated for a brief period with thapsigargin, an ER Ca^{2+} Atlases inhibitor and inducer of ER stress (DuRose et al., 2006). In addition, knockdown of VAPB by siRNA attenuated IRE1 activation to chemically induced ER stressors thapsigargin or dithiothreitol (DTT), which reduces disulfide bonds (Back et al., 2005) suggesting that VAPB is a mediator of IRE1 activation (Kanekura et al., 2006). The link between VAPs and ATF6 was discovered by a yeast two-hybrid screen that identified an interaction between a partial clone of ATF6 with the MSP domain of VAPA (Gkogkas et al., 2008). More recently, findings have shown that over-expression of

VAPB-P56S and to lesser extent, VAPB-WT, attenuated the activity of ATF6-regulated transcription (Gkogkas et al., 2008).

Collectively, these studies reveal that the UPR can be adaptive or apoptotic and they implicate VAPB in the IRE1 and ATF6 signaling. The effects of VAPB on the UPR subjected to short periods of ER stress are documented, however, the effects of chronic ER stress, which is more relevant to the late-onset nature of ALS8, has not been studied. The effect of chronic ER stress in combination with the expression of VAPB-P56S might cause prolonged IRE1 and ATF6 activation, and contribute to initiation of the apoptosis. This prediction could explain the loss of motor neurones in ALS8 and forms another one of the objectives of the current study.

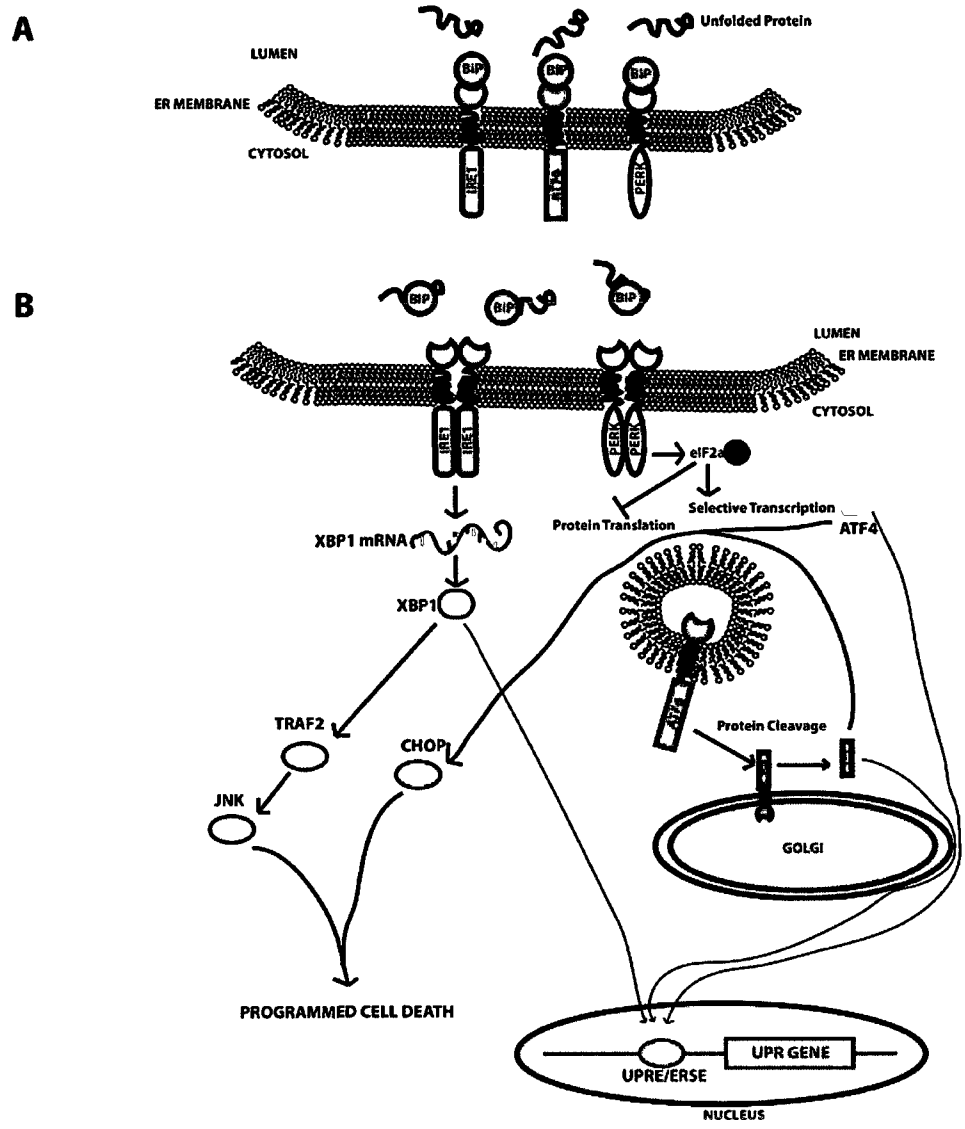

Figure 2. Diagram of UPR signaling pathways.
(*A*) BiP maintains the three proximal sensors of the UPR in their inactive form. However, ER stress brought on by accumulation of unfolded protein in the ER lumen results in BiP dissociation from IRE1, ATF6 or PERK. (*B*) Upon BiP dissociation, IRE1 dimerizes and undergoes autophosphorylation to activate its RNAse activity resulting in splicing of XBP1 mRNA. Spliced XBP1 mRNA yields an XBP1 transcription factor that upregulates UPR target genes in the nucleus. The ATF6 precursor is transported to the Golgi complex where it is cleaved by proteases and gives rise to the active ATF6 fragment that goes to the nucleus and activates UPR genes. PERK dimerizes and phosphorylates eIF2α causing reduction of general mRNA translation and an upregulation of selective transcription. Unresolvable stress activates programmed cell death via TRAF2 or CHOP.

Phospholipid metabolism

Membrane-bound VAPs directly bind to proteins containing two phenylalanines in an acidic tract (FFAT) motif that have the consensus sequence EFFDAxE (Fig. 1B) and this interaction is linked to VAP function (Lev et al., 2008). This interaction promotes recruitment of FFAT motif-containing lipid binding or transfer proteins to the membrane as a mechanism to adjust the local lipid composition and influence membrane dynamics (Beh and Rine, 2004). The VAP-FFAT interaction at the level of the protein structure is well characterized but the effect of VAPB-P56S on lipid sensing at the ER is not well understood.

Lipid binding or transfer protein function

The FFAT motif is found in lipid binding or transfer proteins that are localized to the cytosol or the membrane of compartments upon recruitment (Perry and Ridgway, 2006). Their function is to stabilize hydrophobic lipids in the aqueous environment by solubilizing them during transport across the cytoplasm that occurs in the absence of vesicular membranes (Loewen et al., 2003). Once these FFAT motif-containing lipid binding or transfer proteins reach their target membrane, the lipids are then re-inserted into the membrane (Olkkonen and Levine, 2004).

In humans, proteins from three different families of lipid binding or lipid transfer proteins contain the FFAT motif (Loewen and Levine, 2005). These proteins include oxysterol-binding protein (OSBP), several OSBP-related proteins (ORPs) (ORP1L, ORP2, ORP3, ORP4L, ORP6, ORP7, and ORP9) and retinal degeneration type B protein (rdgB) including Nir1, Nir2, and Nir3 (Olkkonen and Levine, 2004). OSBP is a high-

affinity cytosolic receptor that binds to different oxysterols such as 25-hydroxycholesterol and its distribution is regulated by the cellular cholesterol status (Wyles et al., 2002). ORPs differ from OSBP with respect to protein sequence but all contain an OSBP-related ligand-binding domain (ORD) and act as sterol sensors for various cellular processes (Olkkonen et al., 2006). Nir/rdgB are a group of proteins that regulate membrane trafficking, phospholipid metabolism and signaling (Amarilio et al., 2005).

VAP is implicated in regulating lipid synthesis at the ER

The initial characterization of the VAP-FFAT interaction was carried out in *Saccharomyces cerevisiae* (Loewen et al., 2003). This study showed that Opi1, a transcriptional regulator of phospholipid synthesis directly interacted via its FFAT motif with the MSP domain of yeast homologue of VAP, SCS2 (Loewen et al., 2003). This interaction was clarified in a later study by crystallography using recombinant rat ORP1 FFAT motif (residues 454-546) with rat VAPA amino-terminal (residues 1-125) (Kaiser et al., 2005). The crystal structure revealed a 2:2 complex composed of two VAP MSP domains and two FFAT motifs (Kaiser et al., 2005). More importantly, the structure revealed the key protein regions required for binding. The phenylalanine at residue 476 of the FFAT motif contacted VAPA residue Met89 in a hydrophobic pocket created by aliphatic side chains of Lys45, Thr47, Ly87, and Lys118 (Kaiser et al., 2005).

Defective binding between VAP and FFAT motif-containing proteins have severe consequences in regards to cellular processes and ER morphology. Brunger's group showed that a FFAT binding-defective mutant blocked the growth function of SCS2 in yeast (Kaiser et al., 2005). The study involved the mutation of key residues in the

hydrophobic pocket and aliphatic side chains of SCS2 equivalent to K87D/M89D in rat (Kaiser et al., 2005). The outcome showed a failure for SCS2 to interact with the FFAT motif of Opi1 and this resulted in a loss of growth and survival function because yeasts expressing this mutation were unable to initiate translation of INO1 that would allow growth in the absence of inositol (Kaiser et al., 2005). Expression of the same mutant in COS7 cells altered ER morphology where over-expression of VAPA K87D/M89D resulted in a pattern of regularly spaced patches that co-localized with ER markers in place of the normal reticular ER pattern (Kaiser et al., 2005). Recent evidence revealed that defective binding of VAP with FFAT motif-containing proteins has consequences to the UPR where expression of VAPB K87D/M89D failed to trigger a stress response via the IRE1 pathway (Kanekura et al., 2006). Altogether, the P56S mutation of VAPB may affect its interaction with lipid binding or transfer proteins resulting in changes in VAPB function and lipid composition at the ER. One of the objectives of this current study is to determine if these changes affect vesicle trafficking or the UPR and therefore are contributing factors to motor neurone degeneration of ALS8.

Hypotheses and objectives

I hypothesize that VAPA and VAPB regulate the transport of proteins between the ER and Golgi complex. The expression of the P56S mutation of VAPB causes morphological changes at the ER that will interfere with protein movement between these two compartments. The three proximal sensors of the UPR are localized to the ER membrane. Consequently, morphological changes at the ER will be manifested by changes in UPR activation. Since binding to the FFAT motif of lipid binding or transfer proteins is essential for maintaining the lipid profile at the ER membrane and VAP

function, its co-expression is predicted to affect the morphological changes at the ER and induce changes in protein trafficking and activation of the UPR.

To test these hypotheses, *in vitro* experiments were performed to study the effects of VAPB-P56S on cell morphology, protein transport and UPR activation. The approach taken to determine the morphological effect of the VAPB-P56S mutation involved transfecting VAPB-P56S DNA and subsequent analysis of cell morphology by confocal and electron microscopy. The effect of the P56S mutation on protein transport was assessed using the well-characterized vesicular stomatitis viral glycoprotein (VSVG), a protein that mediates virus attachment to the host cell and the fusion of the viral envelope with the endosomes, as a marker to track movement between the ER and Golgi complex (Lefrancois and Lyles, 1983). The effect of VAPB-P56S on the UPR subjected to chronic ER stress was established by monitoring IRE1 and ATF6, two of the three UPR sensors that previous studies have demonstrated to be associated with VAPB (Gkogkas et al., 2008; Kanekura et al., 2006). PERK was excluded from this thesis because current knowledge does not link VAPB to this pathway of the UPR. However, to obtain a more complete story of the effect of VAPB on the UPR, future studies should include the PERK pathway. Chinese hamster ovary (CHO) fibroblasts were used throughout this study because the interest of this thesis focused on ER morphology and ER function and CHO fibroblasts are ideal for these experiments because of their flat cell morphology. Neuroblastoma-spinal cord (NSC-34) motor neurones were chosen as a cell culture model to assess the two UPR pathways because they have morphological and functional properties of motor neurones making them applicable to the study of chronic ER stress associated that may be a contributing factor to late-onset ALS8. Morphological

properties include the expression of neurofilament proteins, extension of neuritic processes. Functional properties are the generation of action potentials and acetylcholine synthesis, storage, and release (Cashman et al., 1992). This thesis represents the results obtained from these studies.

MATERIALS AND METHODS

DNA plasmid constructs

Human VAPA and VAPB complimentary DNA (cDNA) were amplified by polymerase chain reaction (PCR) with a sense primer (5'-ATCAGTATGCGGCCGCTAT GGCGAAGCACGAGCAG-3') and an antisense primer (5'-ACGGATCCCTACAAGAT GAATTTCCCTAGA-3') for VAPA, and with a sense primer (5'-CTGCGGCCGCTATG GCGAAGGTGGAGCAGGTCC-3') and an antisense primer (5'-GCGGATCCTACAAG GCAATCTTCCCAAT-3') for VAPB, and subcloned at the carboxyl-terminal of the Flag epitope of pFlag-CMV2 at *NotI* and *BamHI* sites to construct the wild-type variants. The P56S mutation was made by site-directed mutagenesis from either wild-type VAPA or VAPB with a sense primer (5'-TACTGTGTGAGGTCCAACAGTGGAATT-3') and an antisense primer (5'-AATTCCACTGTTGGACCTCACACAGTA-3') for VAPA, and with a sense primer (5'-TACTGTGTGAGGTCCAACAGCGGAATC-3') and an antisense primer (5'-GATTCCGCTGTTGGACCTCACACAGTA-3') for VAPB and subcloned into pFlag-CMV2 at *NotI* and *EcoRI* sites. The FFAT motif of rabbit OSBP (residues 347-468) (Fig. 1B) was amplified by PCR from rabbit OSBP with a sense primer (5'-CCGGATCCTCTGGCAAAGGGGACATGAGT-3') and an antisense primer (5'-GAGAATTCTAACATTTTGCAGCTCGGTCTAA-3') subcloned into pcDNA3.1 (+)-Myc with the Myc epitope at the amino-terminal of the FFAT motif using *BamHI* and *EcoRI* sites. For the AAAT motif of rabbit OSBP, the sense primer (5'-CCGGGATCCG ATGATGAAAATGAAGCTGCTGATGCCCCTGAGATCATCACC-3') was used with the antisense primer to clone the FFAT motif into pcDNA3.1 (+)-Myc at the *BamHI* and

EcoRI sites.

Cell culture

CHO fibroblasts were maintained in minimum essential medium (MEM) α (Invitrogen) supplemented with 5 % fetal bovine serum (FBS) (Invitrogen), 100 U/ml penicillin and 100 μg/ml streptomycin (Invitrogen). NSC-34 motor neurones (CELLutions) were maintained in MEM/high glucose (Invitrogen) supplemented with 10 % FBS, 100 U/ml penicillin and 100 μg/ml streptomycin (Invitrogen). Experiments involving NSC-34 cells required coating of the adhering surface with 100 μg/ml poly-L-lysine (Roche). Both cell lines were maintained at 37°C with 5% CO_2.

Transient DNA transfection

CHO fibroblasts were transfected with 400 ng of DNA plasmid and 1 μl LipofectAMINE reagent (Invitrogen) in 200 μl Opti-MEM (Invitrogen) for a 24-well plate (VWR) format for 4 hours. After 4 hours, the transfection mix was removed and replaced with complete MEM α described earlier. Similarly, NSC-34 motor neurones were transfected with 200 ng of DNA plasmid, 2 μl LipofectAMINE reagent and 2 μl of Plus reagent (Invitrogen) in 200 μl Opti-MEM for a 24-well plate format for 4 hours. After 4 hours, the transfection mix was removed and replaced with complete MEM/high glucose described earlier. DNA plasmid LipofectAMINE, Plus reagent and Opti-MEM volumes were scaled according to plate surface area for other experiments.

Subcellular localization of VAP and ER morphology

DNA transfection

To determine the subcellular localization of VAPA or VAPB and their effect on ER morphology, CHO fibroblasts were seeded at $0.8x10^5$ cells on 12 mm glass coverslips (Fisher) 16 hours prior to transfection. Flag-epitope tagged wild-type or P56S mutant VAPA or VAPB were co-transfected with either pcDNA3.1 (+)-Myc empty vector or pcDNA3.1 (+)-Myc/OSBP-FFAT for conditions that were in the absence or presence of FFAT, respectively.

Immunocytochemistry

Sixteen hours after the end of transfection, the cells were washed with (1X) 0.0067 M phosphate-buffered saline (PBS) (Fisher) and fixed with 4 % paraformaldehyde (Cedarlane) in PBS for 30 minutes followed by 3 X 3 minute washes with PBS wash solution (PBS containing 0.1M glycine (Roche) and 0.01 % sodium azide/NaN_3 (JT Baker)). The cells were then permeabilized in blocking solution (PBS containing 0.4 % saponin (Sigma), 1 % bovine serum albumin (Sigma), 2 % normal goat serum (Invitrogen) and 0.01 % sodium azide/NaN_3 (JT Baker)) for 30 minutes followed by 3 X 3 minute washes with PBS wash solution. The cells were then incubated with mouse anti-Flag (1:1000) (Applied Biological Materials) for VAP and rabbit anti-Calreticulin (1:200) (Stressgen) primary antibodies for 1 hour at room temperature or overnight at 4°C followed by 3 X 3 minute washes with PBS wash solution. The proteins were visualized with Alexa Fluor 488- (1:500) or Texas-Red (1:300) -conjugated secondary antibodies (Invitrogen and Jackson Laboratories, respectively). Prior to mounting, the

cells were equilibrated to the SlowFade Gold reagent (Invitrogen) mounting solution by employing equilibration buffer (1X PBS, 30% glycerol and 0.01 % NaN_3) and then the coverslips were mounted in SlowFade Gold reagent (Invitrogen) on 3x1x1 mm frosted glass microscope slides (Fisher) and sealed with commercial nail polish.

Image collection

Images were captured on an Olympus IX70 microscope equipped with a Bio-Rad MRC1024 laser-scanning confocal unit using a 60x, 1.4 NA oil-immersion objective and LaserSharp image acquisition software.

Cell phenotype quantification and statistical analysis

A CHO fibroblast with expanded ER-localized structures was defined as such by having at least one of these structures with a diameter of at least 200 nm in addition to having the loss of the reticular ER pattern. An average of 200 VAP expressing cells were counted for each condition and the values were expressed as the percentage of VAP expressing cells with expanded ER-localized structures relative to the total population of cells with VAP expression. A student unpaired t-Test, with two-tailed distribution was used to compare the mean percentage ± S.E.M., n=3, of VAP expressing cells with expanded ER-localized structures of VAPB-P56S without FFAT to VAPB-P56S with FFAT.

Electron microscopy of VAPB-P56S

DNA transfection

To determine the effect of the VAPB-P56S mutation on the ER morphology at the

level of the ultrastructure, CHO fibroblasts were seeded at $2.4x10^5$ cells on 24mm square glass coverslips (VWR) 16 hours prior to transfection. Flag-epitope tagged P56S mutant VAPB was co-transfected with either pcDNA3.1 (+)-Myc /OSBP-FFAT or pcDNA3.1 (+)-Myc/OSBP-AAAT.

Cell preparation

Sixteen hours after the end of transfection, the cells were washed with PBS and fixed with 1.6 % glutaraldehyde (Polysciences) in PBS. The cells were prepared for electron microscopy by Peter Rippstein of the Stewart Whitman Core Histopathology Laboratory and Electron Microscopy Laboratory at the University of Ottawa Heart Institute. The cells were resuspended in 15 % bovine serum albumin (BSA) infiltrated for 30 minutes and pelleted by centrifugation. The supernatant was removed and the cell pellets were coagulated with 1.6 % glutaraldehyde in 0.1 M sodium cacodylate buffer pH 7.2. The resulting firm pellets were cut into 1 mm pieces post-fixed in 1 % osmium tetroxide dehydrated in ascending alcohols and embedded in Spurr epoxy resin. Thin sections were stained with uranyl acetate and lead citrate.

Image collection

Digital images were taken with a JEOL 1230 TEM at 60kV adapted with a 2000 x 2000 pixel bottom mount CCD digital camera (Hamamatsu, Japan) and AMT software.

Perinuclear space quantification and statistical analysis

Analysis of the perinuclear space (PNS) was performed using ImageJ software. The distance between the outer and inner membrane was measured by taking three different sections of the NE at the widest distance for each cell. An average of 36 cells

were measured for each condition and values were expressed as the distance in nm. A student unpaired t-Test, with two-tailed distribution was used to compare the mean distance in nm ± S.E.M. of the PNS between cells co-expressing VAPB-P56S in the presence of AAAT or FFAT.

Time course of VSVG^{ts045} transport

DNA transfection

To monitor the effect of VAPA and VAPB on anterograde protein transport, CHO fibroblasts were seeded at $0.8x10^5$ cells on 12 mm glass coverslips 16 hours prior to transfection. The cells were co-transfected with pCDM8.1/VSVG^{ts045}-green fluorescent protein (GFP) (Presley et al., 1997) and with either pFlag-CMV2 vector for the control or Flag-epitope tagged wild-type or P56S mutant VAPA or VAPB. In addition, the cells were co-transfected with either pcDNA3.1 (+)-Myc empty vector or pcDNA3.1 (+)-Myc/OSBP-FFAT for conditions that were in the absence or presence of FFAT, respectively.

Temperature trapping conditions and immunocytochemistry

Sixteen hours after transfection, the cells were shifted to 42°C for 6 hours to accumulate VSVG^{ts045}-GFP in the ER and allow VSVG^{ts045}-GFP that had already exited the ER to traffic to the plasma membrane (PM) and clear the cell. After 6 hours, cycloheximide (20 μg/ml) (Sigma) was added 10 minutes prior to shifting to 32°C, after which the cells were chased at 32°C for 30, 60 and 90 minutes. Immediately before the shift to 32°C and at each time interval, the cells were prepared using the immunocytochemistry protocol outlined in the Subcellular localization of VAP and ER

morphology experiment. VAP expressing cells were stained for mouse anti-Flag primary antibody and visualized with Texas-Red-conjugated secondary antibody using dilutions described earlier.

Image collection

Images were captured using the same protocol outlined in the Subcellular localization of VAP and ER morphology experiment.

Quantification of VSVG localization

VSVG phenotype was quantified for VSVG localization at three distinct compartments, the ER, the Golgi complex and the PM. The labeling patterns for the ER was defined as GFP staining that appeared as reticular ER. The Golgi complex and the PM were defined as perinuclear Golgi complex and surface PM, respectively. An average of 100 cells were measured for each condition and time point and the values were expressed as the mean percentage ± S.E.M., n=3, with localization to one of the compartments.

VSVG folding

DNA transfection

To validate the effect of over-expression of VAPA and VAPB on VSVG^{ts045}-GFP folding, CHO fibroblasts were seeded and transfected according to the conditions outlined in Time course of VSVG^{ts045}-GFP transport, however, pcDNA3.1 (+)-Myc/OSBP-FFAT was not used.

Temperature trapping conditions and immunocytochemistry

The temperature conditions for trapping VSVG^{ts045}-GFP and release from the ER as well as the use of cycloheximide were the same as those described in Time course of VSVG^{ts045}-GFP transport. VSVG^{ts045}-GFP was chased for 30 minutes after which the cells were prepared using the immunocytochemistry protocol outlined in the Subcellular localization of VAP and ER morphology experiment. VAP expressing cells were stained for mouse anti-Flag primary antibody and visualized with Texas-Red-conjugated secondary antibody using dilutions described earlier. Correctly folded VSVG was stained with conformation specific monoclonal I14 antibody (1:50) (kindly provided by Dr. Xiaohui Zha, University of Ottawa, Ottawa, ON) and visualized using Texas Red goat anti-mouse secondary antibody.

Image collection

Images were captured using the same protocol outlined in the Subcellular localization and ER morphology experiment.

CgB and VSVG transport with 15°C block

DNA transfection

To compare the effect of VAPA and VAPB over-expression on anterograde protein transport between the ER and the Golgi complex of soluble cargo protein Chromogranin B (CgB) and membrane-associated cargo protein VSVG, CHO fibroblasts were seeded and transfected according to the conditions outlined in Time course of VSVG^{ts045}-GFP transport, however, pcDNA3.1 (+)-Myc/OSBP-FFAT was not used. In

addition pCDM8/CgB-GFP (S65T) (Wacker et al., 1997) was used in for conditions where CgB transport was being monitored.

Temperature trapping conditions and immunocytochemistry

Sixteen hours after transfection, the cells were shifted to 15°C for 2 hours to enhance the fluorescent signal and to prevent transport to the Golgi complex by trapping the cargo in the ERGIC. After 2 hours, cycloheximide (20 μg/ml) was added 10 minutes prior to shifting to 37°C, after which the cells were chased at 37°C for 30 minutes. The cells were prepared using the immunocytochemistry protocol outlined in the Subcellular localization of VAP and ER morphology experiment immediately before the shift to 37°C and 30 minutes afterwards. VAP expressing cells were stained for mouse anti-Flag primary antibody and visualized with Texas-Red-conjugated secondary antibody using dilutions described earlier.

Image collection

Images were captured using the same protocol outlined in the Subcellular localization and ER morphology experiment.

XBP1 splicing as a read-out of IRE1 activation

DNA transfection

An XBP1-GFP reporter was used to determine the effect of chronic ER stress in cells over-expressing VAPB-P56S on the IRE1 activation by fluorescent microscopy. CHO fibroblasts and NSC-34 motor neurones were seeded at $0.8x10^5$ cells directly into 24-well plates (VWR) 16 hours prior to transfection. The cells were co-transfected with

pXBP1u-GFP (Yu et al., 2006), pmRFP-N1 and with either pFlag-CMV2 vector for the control or Flag-epitope tagged wild-type or P56S mutant VAPB. In addition, the cells were co-transfected with either pcDNA3.1 (+)-Myc empty vector or pcDNA3.1 (+)-Myc/OSBP-FFAT for conditions that were in the absence or presence of FFAT, respectively.

Inducing ER stress

The cells were allowed to recover for 36 hours after transfection to decrease the amount of GFP expressing cells that may have resulted from non tunicamycin-induced ER stress. After 36 hours, tunicamycin (10 μg/ml) (Cedarlane) was added to the cells to induce ER stress.

Image collection

Live cells were imaged before the introduction of tunicamycin and at 4, 8, 16 hours afterwards using an Olympus IX70 microscope equipped with a Bio-Rad MRC1024 laser-scanning confocal unit using a 20x, 1.4 NA water-immersion objective and LaserSharp image acquisition software.

XBP1s-GFP expression and statistical analysis

Endogenous IRE1 activation was indicated by expression of GFP fluorescence signifying that XBP1u-GFP mRNA had been spliced by endogenous IRE1 to allow translation of XBP1s-GFP protein. An average of 100 cells were counted for each condition and time point and expressed as the percentage of GFP fluorescent cells relative to the RFP fluorescent cells. A student unpaired t-Test, with two-tailed distribution was used to compare the mean percentage ± S.E.M., n=5, between the control

and VAPB-WT or VAPB-P56S in the absence or presence of FFAT at the 8 hour time point.

XBP1s localization to the nucleus

DNA transfection

To test if over-expression of VAPB-P56S interfered with XBP1s-GFP localization to the nucleus, CHO fibroblasts were seeded at $0.8x10^5$ cells on 12 mm glass coverslips 16 hours prior to transfection. The cells were co-transfected with pXBP1u-GFP and with either pFlag-CMV2 vector for the control or Flag-epitope tagged wild-type or P56S mutant VAPB. In addition, the cell were co-transfected with either pcDNA3.1 (+)-Myc empty vector or pcDNA3.1 (+)-Myc/OSBP-FFAT for conditions that were in the absence or presence of FFAT, respectively.

Inducing ER stress

The cells were permitted to recover for 36 hours after transfection to decrease the amount of GFP expressing cells that may have resulted from non tunicamycin-induced ER stress. After 36 hours, β-Mercaptoethanol (10 mM) (Sigma) was added to the cells to induce ER stress.

Immunocytochemistry

The cells were collected immediately after introduction of tunicamycin and 30 minutes afterwards. At each time point, the cells were prepared using the immunocytochemistry protocol outlined in the Subcellular localization and ER morphology experiment and mounted using SlowFade Gold reagent with DAPI

(Invitrogen). VAP expressing cells were stained for mouse anti-Flag primary antibody and visualized with Texas-Red-conjugated secondary antibody using dilutions described earlier.

Image collection

Images were captured using a Zeiss LSM510 confocal microscope equipped with a 20x, 1.4 objective and LSM510 image acquisition software.

Quantification of XBP1s-GFP to the nucleus and statistical analysis

Using ImageJ software, the percentage of GFP fluorescence in the nucleus was taken as the integrated density of the GFP signal localized to the nucleus outlined by DAPI staining relative to the total integrated density of the GFP signal of the whole cell. The cells were categorized as having less than 60%, 61-80% or 81-100% relative to GFP fluorescence in the nucleus. A cell with 81-100% of its relative GFP fluorescence in the nucleus was defined as cell having XBP1s-GFP localized to the nucleus. An average of 50 cells were counted for each condition and time point and expressed as the mean percentage ± S.E.M., n=3. A student unpaired t-Test, with two-tailed distribution was used to compare the frequency of cells with 81-100% of its relative GFP fluorescence in the nucleus between the VAPB-P56S and the control or VAPB-WT in the absence of FFAT.

XBP1s protein turnover

DNA transfection

To establish the effect of over-expression of VAPB-P56S on the rate of XBP1s-GFP degradation, CHO fibroblasts were seeded at $1.3x10^6$ cells in 10 cm tissue culture dishes (Sarstedt) 16 hours prior to transfection. The cells were co-transfected with pXBP1u-GFP, pcDNA3.1 (+)-Myc empty vector and with either pFlag-CMV2 vector for the control or Flag-epitope tagged wild-type or P56S mutant VAPB.

Inducing ER stress

The cells were allowed to recover for 36 hours after transfection to decrease the amount of GFP expressing cells that may have resulted from non tunicamycin-induced ER stress. The cells were transferred from the 10 cm tissue culture dishes to 15 ml snap-cap polypropylene tubes (VWR) and tunicamycin (10 μg/ml) was added to induce ER stress for 8 hours at 37°C in a dry incubator with gentle shaking at ~150 rpm to maximize XBP1s-GFP expression. Moreover, 10mM Hepes (Gibco) was added to maintain the pH because the incubator was not equipped with a CO_2 injection system.

Collection of cell lysate

After 8 hours, the cells were harvested immediately before cycloheximide (20 μg/ml) was added and at 2, 4, 6 and 8 hours after protein synthesis was stopped. The cells were lysed in RIPA buffer (25 mM Tris-HCl, pH 7.6, 150 mM NaCl, 1 % NP-40, 1 % Na-Deoxycholate, 0.1 % SDS, 1mM PMSF) on ice for 20 minutes. The lysates were

sonicated at 30 % power for 1 X 10 seconds and the insoluble debris was spun out at 15,000 g for 10 minutes at 4°C.

Immunoblotting using a slot blot apparatus

Protein concentration was determined using a Bio-Rad DC protein assay kit (Bio-Rad). Thirty μg of total protein for each condition was loaded onto a Bio-Rad slot blot apparatus (Bio-Rad) and the proteins were collected under suction on a 0.45 um Protran® nitrocellulose membrane (Perkin Elmer). The membrane was blocked in 5 % skim milk made with 1X Western wash (150mM NaCl and 10mM Tris-HCl pH 7.5). Rabbit anti-GFP (1:2000) (Invitrogen) primary and Alexa Fluor 488-conjugated (1:2000) secondary were used to detect XBP1s-GFP. The protein was visualized using a GE Storm 820 Phosphor Imager and densitometry analysis was performed using GE ImageQuant TL software.

Quantification of relative XBP1s-GFP and half-life

The amount of XBP1s-GFP remaining was calculated relative to the protein density at the initial time point, N_0. The values were recorded as the mean relative XBP1s-GFP ± S.E.M., n=3. The half-life of each condition was calculated based on the amount of XBP1s-GFP remaining after 8 hours using the equation $t_{1/2} = t\ln(2)/\ln(N_0/N_8)$, where $t_{1/2}$ is the half-life, t is the time, N_0 is the initial quantity of XBP1s-GFP and N_8 is the quantity of XBP1s-GFP at time t.

ATF6-dependent luciferase reporter as a read-out of ATF6 activity

DNA transfection

A luciferase reporter assay was used to determine the effect of chronic ER stress on ATF6 activation in cells over-expressing VAPB-P56S. CHO fibroblasts and NSC-34 motor neurones were seeded at $0.8x10^5$ cells directly into 24-well plates 16 hours prior to transfection. The cells were co-transfected with p5xATF6-GL3 (Addgene), *Renilla* luciferase and with either pFlag-CMV2 vector for the control or Flag-epitope tagged wild-type or P56S mutant VAPB. In addition, the cell were co-transfected with either pcDNA3.1(+)-Myc empty vector or pcDNA3.1(+)-Myc/OSBP-FFAT for conditions that were in the absence or presence of FFAT, respectively.

Inducing ER stress

The cells were allowed to recover for 36 hours after transfection to decrease the amount of ATF6-dependent luciferase activity resulted from non tunicamycin-induced ER stress. After 36 hours, tunicamycin (10 μg/ml) (Cedarlane) was added to the cells to induce ER stress.

Cell preparation and luciferase measurements

The cells were washed with PBS and lysed using the reagents and protocol described for the Dual Glo™ Luciferase Assay System (Promega) immediately after tunicamycin treatment and at 8, 24, 36 and 48 hours after induction of ER stress. Firefly luciferase and *Renilla* luciferase luminescence were read at wavelengths of 560 nm and

480 nm, respectively, in a 96-well black micro-plate (Fisher) using a SpectroMax L micro-plate reader (Molecular Devices).

Quantification of ATF6 luciferase activity and statistical analysis

Endogenous ATF6 activity was given as a measure of ATF6 luciferase activity that was determined by normalizing ATF6-dependent firefly luciferase luminescence values to *Renilla* luciferase luminescence values. The values for the ATF6 luciferase activity ± S.E.M., n=8 or n=6 for CHO or NSC-34, respectively, were subjected to a student unpaired t-Test, with two-tailed distribution to compare the ATF6 luciferase activity between the VAPB-P56S and the control or VAPB-WT at the 24 hour time point in the absence or presence of FFAT for both cell lines.

RESULTS

VAPB-P56S induces formation of expanded ER-localized structures

Previous studies have documented VAPA and VAPB localization to the ER (Nishimura et al., 1999), and expression of VAPB-P56S results in membrane-aggregate structures (Hirano, 2008). This opens the possibility that aggregate structures originate from the ER and that expression of VAPB-P56S affects ER morphology. To determine the effect of VAPB-P56S on ER morphology, wild-type or P56S VAPA or VAPB were transfected into CHO fibroblasts. VAPA-WT and VAPB-WT displayed characteristic reticular ER pattern that partially co-localized with endogenous calreticulin (Fig. 3), a protein chaperone that resides in storage compartments associated to the ER (Ellgaard and Helenius, 2001). Over-expression of VAPA-P56S was performed to examine if this mutation mimicked the effects of VAPB-P56S. Similar to wild-type VAPA and VAPB, over-expression of VAPA-P56S had similar reticular ER pattern and partial co-localization with endogenous ER luminal chaperone, calreticulin (Fig. 3). In contrast, cells transfected with VAPB-P56S did not have the characteristic reticular ER pattern (Fig. 3) and instead, showed expanded structures that co-localized with calreticulin. The four different VAP conditions were quantified for the presence of these expanded ER-localized structures (Fig. 5). A cell with an expanded ER-localized structure was defined as having at least one of these structures with a diameter of at least 200 nm in addition to having the loss of the reticular ER pattern. CHO over-expressing VAPB-P56S had a greater frequency of cells (70.2 ± 1.2%) with these expanded ER-localized structures compared to VAPA-WT (0.7 ± 0.4%, p=0.000001; Fig. 5), VAPA-P56S (0.4 ± 0.4%,

p=0.000001; Fig. 5), and VAPB-WT (4.3 ± 2.8%, p=0.000002; Fig. 5). Despite VAPA and VAPB sharing structural similarities, the P56S mutation in VAPA did not cause the collapse of the reticular ER pattern that gave rise to expanded ER-localized structures. This suggests that VAPA and VAPB function in different subsets of the ER (Gkogkas et al., 2008) or are functionally distinct.

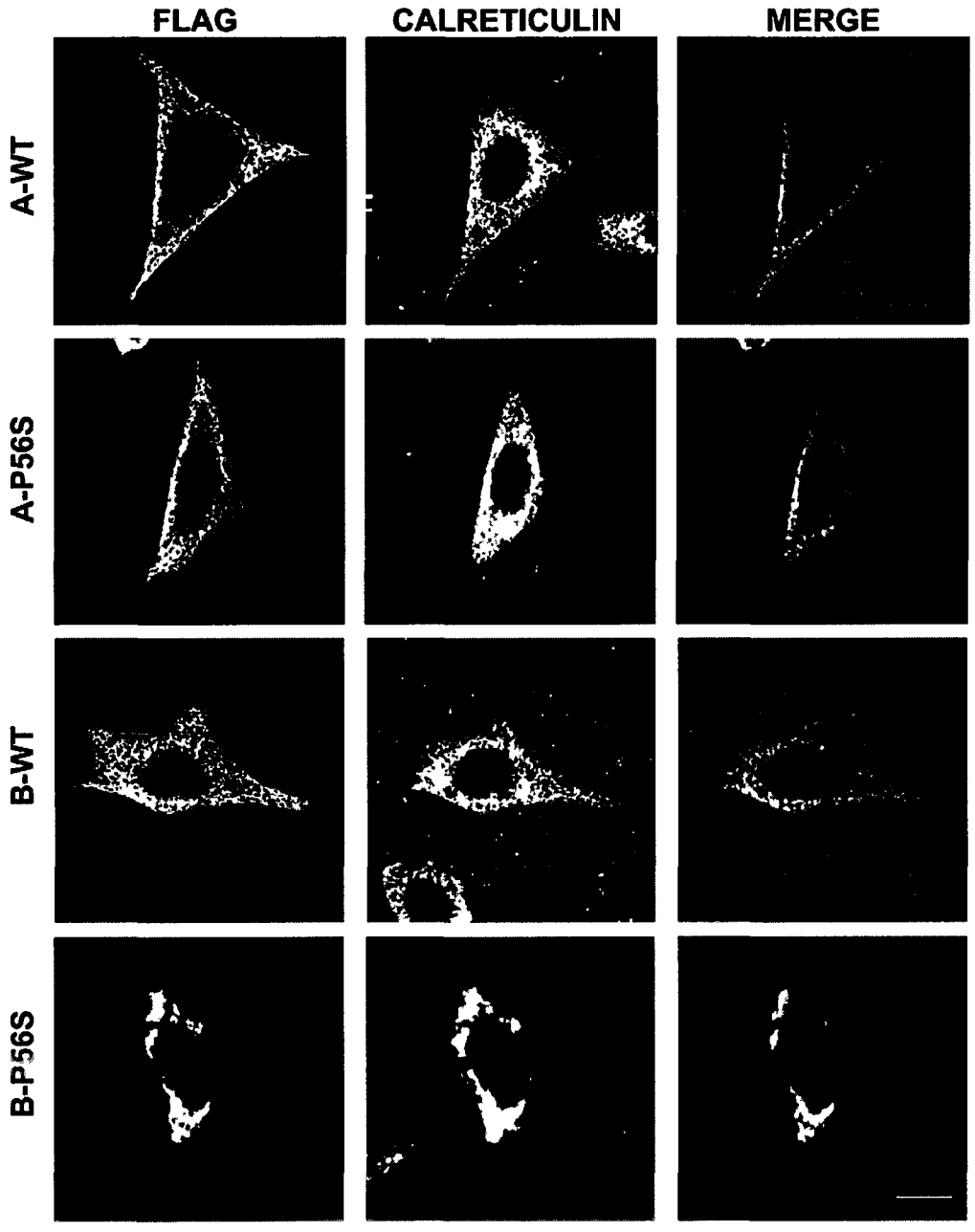

Figure 3. Subcellular localization of WT or P56S VAPA or VAPB in the absence of FFAT.

CHO fibroblasts were co-transfected with Flag-epitope tagged wild-type or P56S mutant VAPA or VAPB and pcDNA3.1 (+)-Myc empty vector. Representative images were captured by confocal microscopy and the proteins were visualized with anti-Flag for VAP (left column) and anti-calreticulin (middle column). Flag (red) and calreticulin (green) images were merged (right column) to illustrate co-localization. Scale bar: 10 μm.

Simultaneous over-expression of the FFAT motif decreases the frequency of VAPB-P56S cells with expanded ER-localized structures

VAPA interacts directly through its MSP domain with the FFAT motif of OSBP (Kaiser et al., 2005), one member of a class of lipid binding proteins tasked with preserving the lipid content and profile of intracellular organelles (Peretti et al., 2008). Studies have shown that the interaction between VAP and FFAT-motif-containing lipid proteins induced reorganization of the ER (Amarilio et al., 2005). To test if this interaction affects ER morphology, wild-type or P56S variant of VAPA or VAPB were co-transfected in CHO fibroblasts with the FFAT motif from rabbit OSBP. The FFAT construct used in this study contained only the FFAT domain of rabbit OSBP (Fig. 1B) but excluded the other functional domains such as the pleckstrin homology (PH) domain and the dimerization (DIM) domain; therefore any effect of FFAT expression should be attributed to the FFAT motif only. In a complete OSBP protein, the PH domain is tasked with recognizing phosphorylated phosphoinositol 4-phosphates found on the membranes of the Golgi complex and the DIM domain is important for homodimerization (Wyles et al., 2002). These two excluded OSBP domains are not determinants implicated in VAP-OSBP interaction. Interaction studies have shown that VAP directly binds with OSBP from amino acids 351-442 and the FFAT motif construct in this thesis spans amino acids 347-468 of rabbit OSBP, therefore the interaction is predicted to be preserved (Wyles et al., 2002). There was no change in subcellular localization or co-localization with calreticulin in VAPA-WT, VAPA-P56S or VAPB-WT co-expressing the FFAT motif (Fig. 4). However, the frequency of VAPB-P56S transfected cells exhibiting the expanded ER-localized structures was reduced from 70.2 ± 1.2% to 37.7 ± 6.0%; p=0.006

(Fig. 5). In addition, the return of the characteristic reticular ER pattern was observed in VAPB-P56S cells co-expressed with FFAT (Fig. 4). The frequency of cells containing these expanded ER-localized structures was still greater in VAPB-P56S (37.7 ± 6.0%) over-expressing cells compared to VAPA-WT (1.1 ± 0.6%, p=0.004; Fig. 5), VAPA-P56S (1.9 ± 1.2%, p=0.004; Fig. 5) and VAPB-WT (4.5 ± 0.3%, p=0.004; Fig. 5). Co-expression of the FFAT motif resolved the ER morphological effect of VAPB-P56S suggesting that the motif might counter any functional defects associated with the mutation.

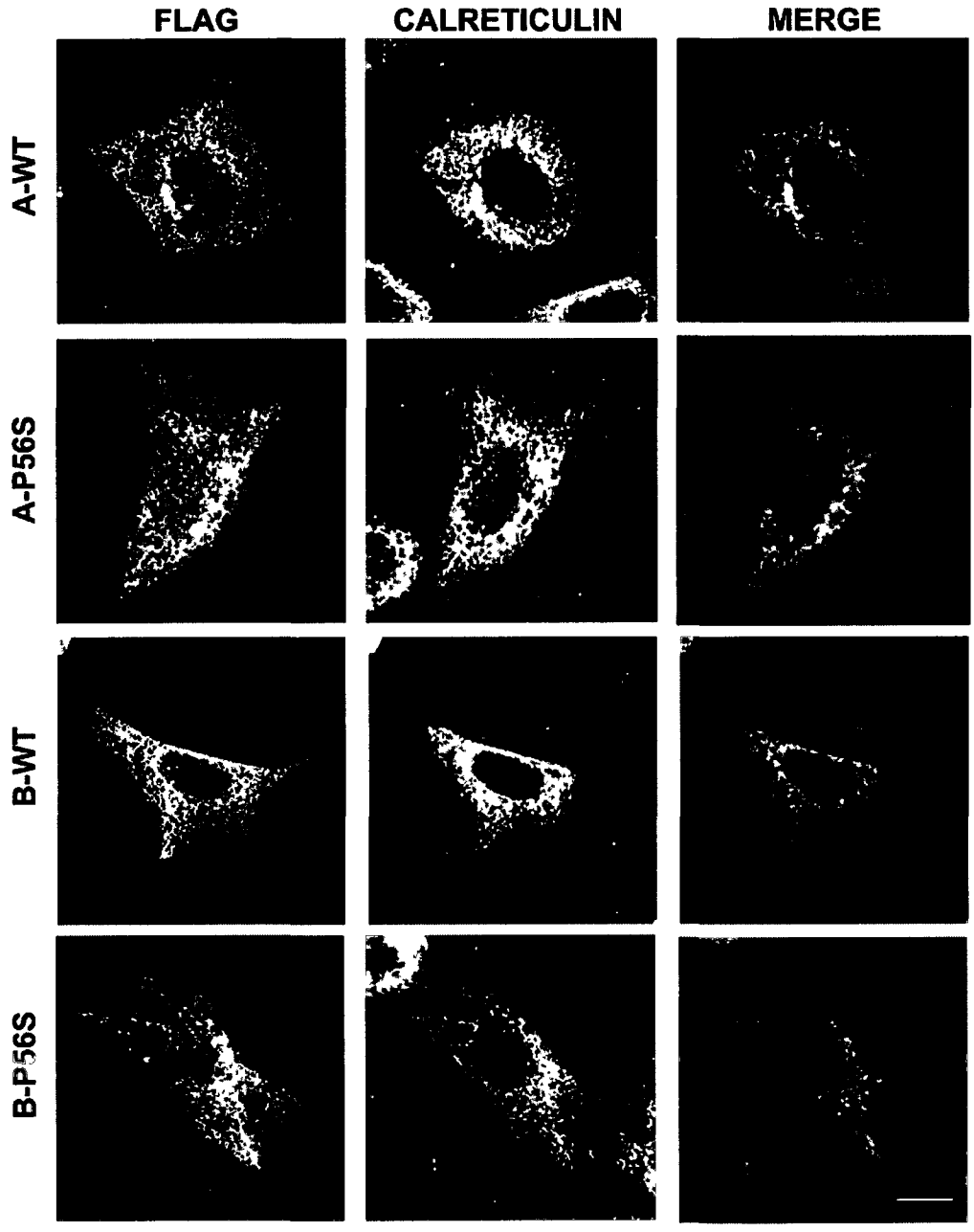

Figure 4. Subcellular localization of WT or P56S VAPA or VAPB in the presence of FFAT.

CHO fibroblasts were co-transfected with Flag-epitope tagged wild-type or P56S mutant VAPA or VAPB and pcDNA3.1 (+)-Myc/OSBP-FFAT. Representative images were captured by confocal microscopy and the proteins were visualized with anti-Flag for VAP (left column) and anti-calreticulin (middle column). Flag (red) and calreticulin (green) images were merged (right column) to illustrate co-localization. Scale bar: 10 μm.

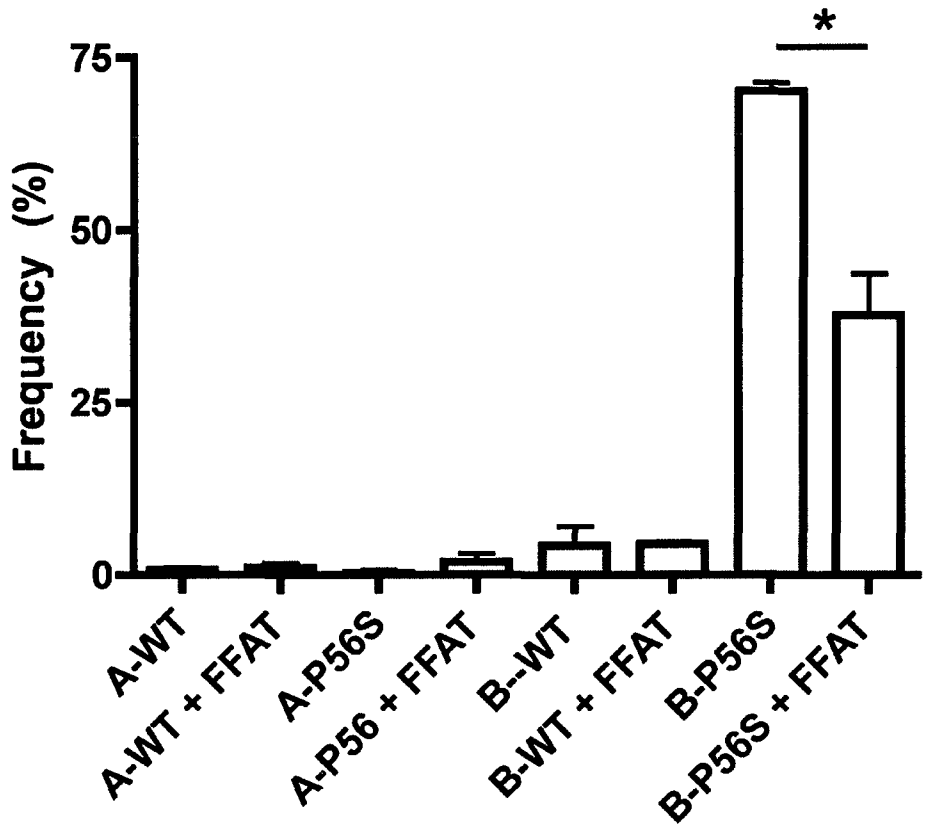

Figure 5. Distribution of WT or P56S VAPA or VAPB cells with expanded ER-localized structures in the absence or presence of FFAT.

CHO fibroblasts were co-transfected with Flag-epitope tagged wild-type or P56S mutant VAPA or VAPB and either pcDNA3.1 (+)-Myc empty vector or pcDNA3.1 (+)-Myc/OSBP-FFAT. A cell with expanded ER-localized structures was defined as having at least one of these structures with a diameter of at least 200 nm in addition to having the loss of the reticular ER pattern. An average of 200 Flag-tagged cells were counted for each condition and the values represent the mean percentage ± S.E.M., n=3, of cells containing expanded ER-localized structures relative to Flag-tagged cells. Statistical analysis comparing VAPB-P56S to VAPB-P56S + FFAT expressing cells was performed using a Student unpaired t-Test, with two-tailed distribution, *p=0.006.

VAPB-P56S causes expansion of ER tubules and the perinuclear space

Fluorescent microscopy of over-expressed VAPB-P56S in the absence of the FFAT motif showed the loss of the characteristic reticular ER pattern and the presence of expanded structures that appeared to originate from the ER. Previous studies have employed electron microscopy (EM) in combination with fluorescent microscopy (Fasana et al., 2009; Teuling et al., 2007) to uncover the origins of these structures. In this context, high-resolution EM was used to characterize the effect of VAPB-P56S at the level of the ultrastructure and to clarify the origins of these expanded structures. CHO fibroblasts were co-transfected with VAPB-P56S and either the FFAT motif or the AAAT motif of rabbit OSBP. The AAAT motif was employed as a negative control for the FFAT motif and had two alanines substituted in place of the two phenylalanines of the FFAT motif. High-resolution EM images of CHO co-expressed with VAPB-P56S and the AAAT motif exhibited large vacuoles that resembled expanded ER tubules (Fig. 6C) but were absent in FFAT co-transfected cells (Fig. 6A). The typical separation of inner and outer nuclear membranes is 30-50 nm (Zwerger et al., 2010), however, in the AAAT condition, the nuclear envelope (NE) appeared distorted and there was expansion of the perinuclear space (PNS) between the outer and inner membrane of the NE in AAAT co-transfected cells (160.7 ± 32.1nm) (Fig. 6D and 7) compared to FFAT co-transfected cells (70.0 ± 5.3nm; p=0.008; Fig. 6B and 7). These findings indicate that these expanded structures originate from ER tubules. Consequently, over-expression of VAPB-P56S may interfere with cellular processes that are associated with the ER. Moreover, the mutation caused expansion of the PNS suggesting that changes of the ER morphology are also associated with defects of the NE.

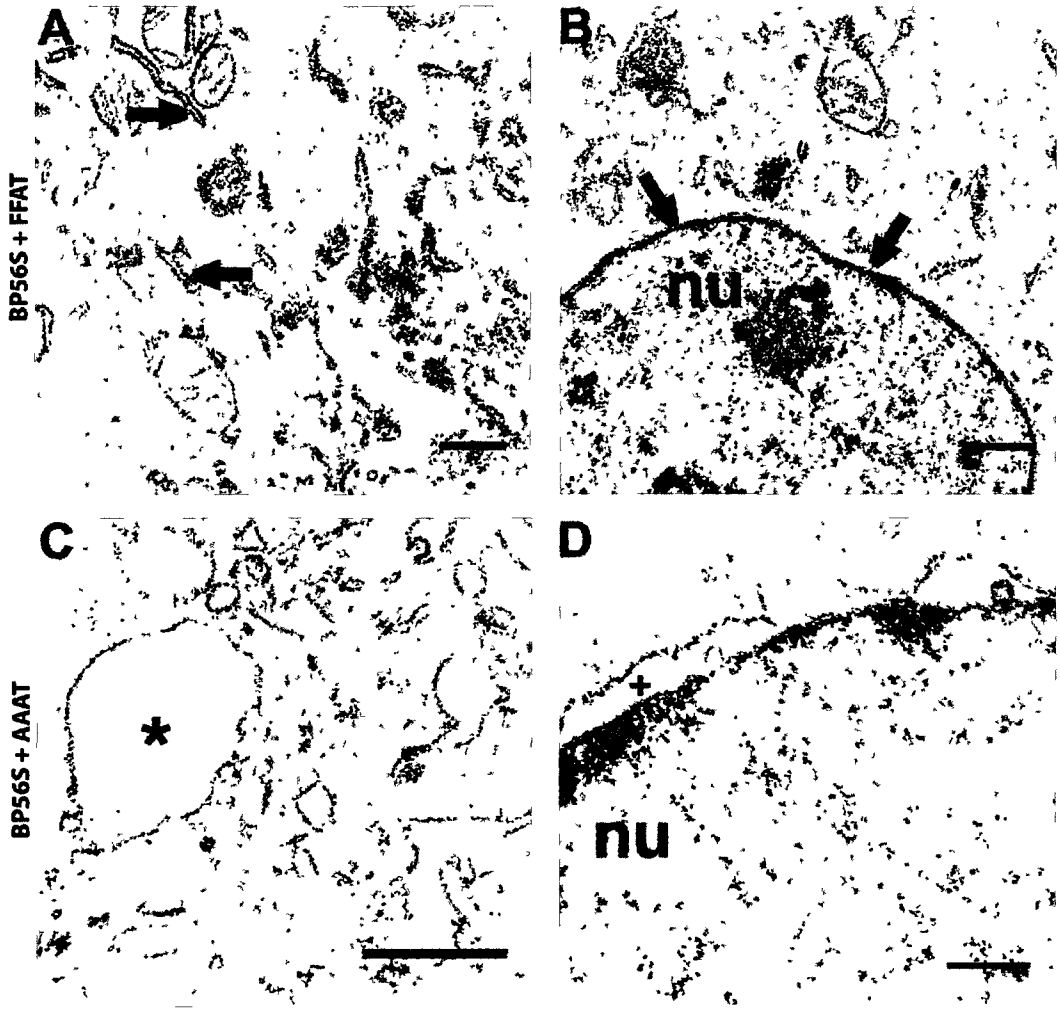

Figure 6. Electron microscopy analysis of CHO fibroblasts co-expressing VAPB-P56S with FFAT or AAAT.

CHO fibroblasts were co-transfected with Flag-epitope tagged P56S VAPB and either pcDNA3.1 (+)-Myc/OSBP-FFAT or pcDNA3.1 (+)-Myc/OSBP-AAAT. Transmission electron microscopy was used to capture high-resolution images of intracellular structures. (***A***) VapB-P56S co-transfected with FFAT displayed normal ER tubules (arrows) and (***B***) tight perinuclear spacing (PNS) of the nuclear envelope (NE). (***C***) VapB-P56S co-transfected with AAAT displayed expanded ER tubules (*) and (***D***) expansion of the PNS due to separation of the outer and inner membrane of the NE (+). nu, nucleus. Scale bars: ***A***, ***B***, ***C***, 1000 nm; ***D***, 200 nm.

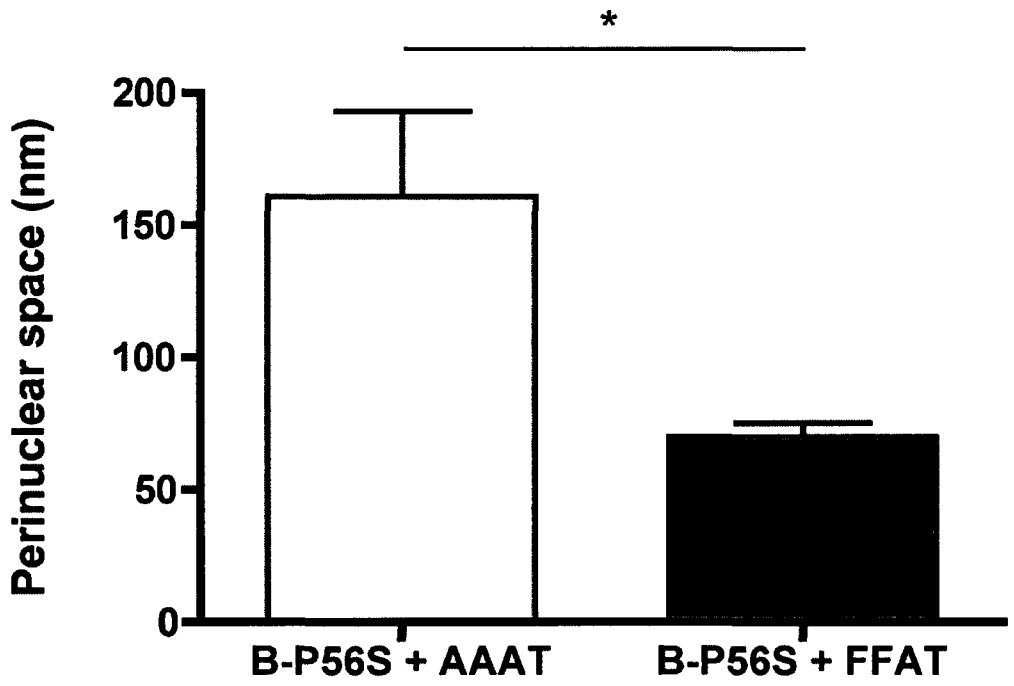

Figure 7. Distance of the perinuclear space of the nuclear envelope in CHO fibroblasts over-expressing the VAPB-P56S mutation in the absence or presence of FFAT.

CHO fibroblasts were co-transfected with Flag-epitope tagged P56S VAPB and either pcDNA3.1 (+)-Myc/OSBP-FFAT or pcDNA3.1 (+)-Myc/OSBP-AAAT. The perinuclear space was taken as the distance between the outer and inner membrane at three different sections of the nuclear envelope at the widest distances for each cell. The values are presented as the mean distance in nm ± S.E.M., AAAT n=38 and FFAT n=36. Statistical analysis comparing VAPB-P56S + AAAT to VAPB-P56S + FFAT expressing cells was performed using Student unpaired t-Test, with two-tailed distribution, *p=0.008.

VAPA and VAPB-P56S inhibit ER exit of correctly folded VSVG

The ER is the site of protein synthesis and the starting point of the secretory pathway. VAPA and VAPB are localized to the ER and are documented to function in intracellular trafficking (Shi et al., 2010) but their exact function is not known. Also, over-expression of VAPB-P56S generated expanded ER tubules; therefore morphological changes of the ER might have an effect on protein trafficking. In this context, the temperature sensitive $VSVG^{ts045}$-GFP was used as a membrane-associated vesicle cargo marker (Nehls et al., 2000) to track the anterograde flow of secretory proteins from the ER to Golgi complex. VSVG is an integral membrane protein that must assemble into non-covalently associated trimers (Lefrancois and Lyles, 1983) before exiting from the ER (Fig. 8). $VSVG^{ts045}$ has a mutation at the amino-terminal ectodomain that project into the ER lumen (Lefrancois and Lyles, 1983) and this mutation blocks initial folding of VSVG and prevents trimerization and ER exit at a non-permissive temperature of 42°C (Doms et al., 1988). The assay involved co-expressing $VSVG^{ts045}$-GFP in CHO fibroblasts with either pFlag-CMV2 control vector or the wild-type or P56S variants of VAPA or VAPB followed by incubation for 6 hours at a non-permissive temperature of 42°C. Trapping at 42°C for 6 hours promoted accumulation of VSVG in the ER and the removal of any VSVG that had already exited the ER by way of the PM. The cells were treated with cycloheximide ten minutes prior to the beginning of the chase period, which interferes with the translocation step and blocks protein translation elongation (Szegezdi et al., 2006). The addition of cycloheximide ensured that the VSVG being tracked during the chase period were not newly synthesized proteins that would interfere with quantification. The cells were then shifted to a permissive temperature of 32°C to allow

synchronized release of VSVG from the ER and fixed immediately after the shift to 32°C and at 30, 60, 90 minute time points (Fig. 8). The effect on protein trafficking was quantified based on the VSVG localization at three distinct compartments, the ER, the Golgi complex and the PM. The labeling patterns for the ER was defined as GFP staining that appeared as reticular ER. The Golgi complex and the PM were defined as perinuclear Golgi complex and surface PM, respectively.

In the control, VSVG was present in the ER immediately after the 42°C incubation (Fig. 9 and 10), and by 30 minutes had reached the Golgi complex. At 60 and 90 minutes, VSVG had reached the PM. Transfection of VAPA wild-type and P56S inhibited VSVG exit from the ER (Fig. 9 and 10) for the duration of the chase period. In contrast, the effect of over-expression of wild-type VAPB was similar to the control since VSVG was able to exit the ER (Fig. 9 and 10). Over-expression of VAPB-P56S displayed large structures that were GFP-labeled (Fig. 9) and resembled expanded ER tubules. These structures were quantified as ER and were present for the duration of the chase period (Fig. 10) suggesting that VSVG did not exit the ER and was unable to transport to the Golgi complex. VAPA-WT and VAPA-P56S blocked VSVG exit from the ER suggesting that they regulate anterograde transport of secretory proteins from the ER to the Golgi complex. In contrast, VAPB-WT did not inhibit VSVG exit from the ER opening the possibility that it is involved in retrograde flow of secretory proteins (Soussan et al., 1999).

The ER retains misfolded proteins as a quality control mechanism to ensure proper folding and assembly of proteins before exit from the ER (Szegezdi et al., 2006). It is possible that VSVG remained in an unfolded or misfolded state when shifted to 32°C

causing it to be retained in the ER. To elucidate the conformation of VSVG, a monoclonal I14 antibody that recognizes correctly folded trimeric VSVG was used (Lefrancois and Lyles, 1983). At the beginning of the chase period, all conditions showed VSVG localization to the ER (Fig. 11 and 12) but no I14 immunoreactivity was present and this is consistent with misfolded VSVG retention in the ER. Thirty minutes after the beginning of the chase period, I14 immunoreactivity was present for all conditions (Fig. 11 and 12) implying that VSVG was folded properly. Therefore, properly folded trimeric VSVG remained localized to the ER in over-expressed VAPA-WT, VAPA-P56S or VAPB-P56S confirming that the failure of VSVG to traffic to the Golgi complex is due to inhibition of ER exit. Therefore, over-expression of VAPB-P56S induced changes in ER morphology resulting in a block of the anterograde transport of properly folded VSVG.

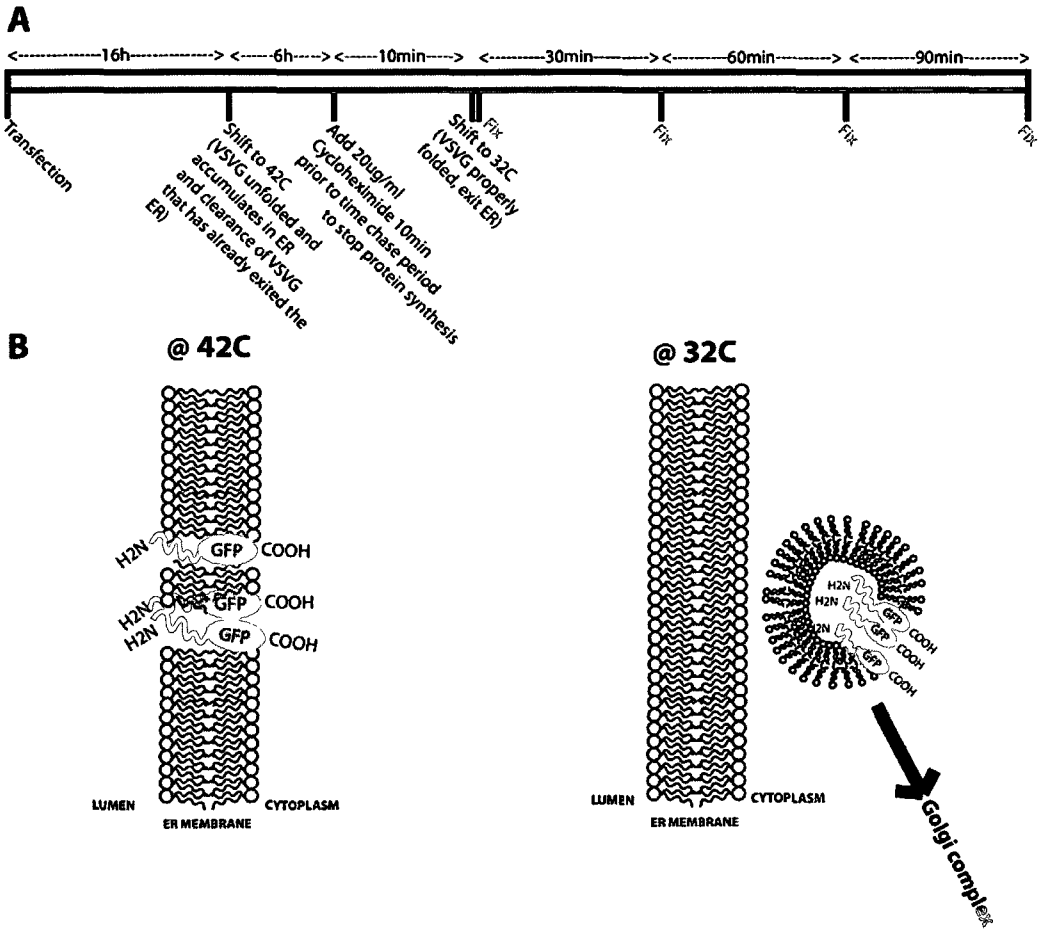

Figure 8. Schematic of VSVG^{ts045}-GFP transport experiment.
(*A*) Timeline indicating important time points of the VSVG^{ts045}-GFP transport experiment. (*B*) Cartoon of temperature-sensitive folding defect of VSVG^{ts045}-GFP indicating that at 42°C, VSVG is unable to fold properly into a trimer and is unable to exit the ER, thereby accumulating in the ER. At a permissive temperature of 32°C, VSVG^{ts045}-GFP is able to fold properly and form a trimer and can now exit the ER.

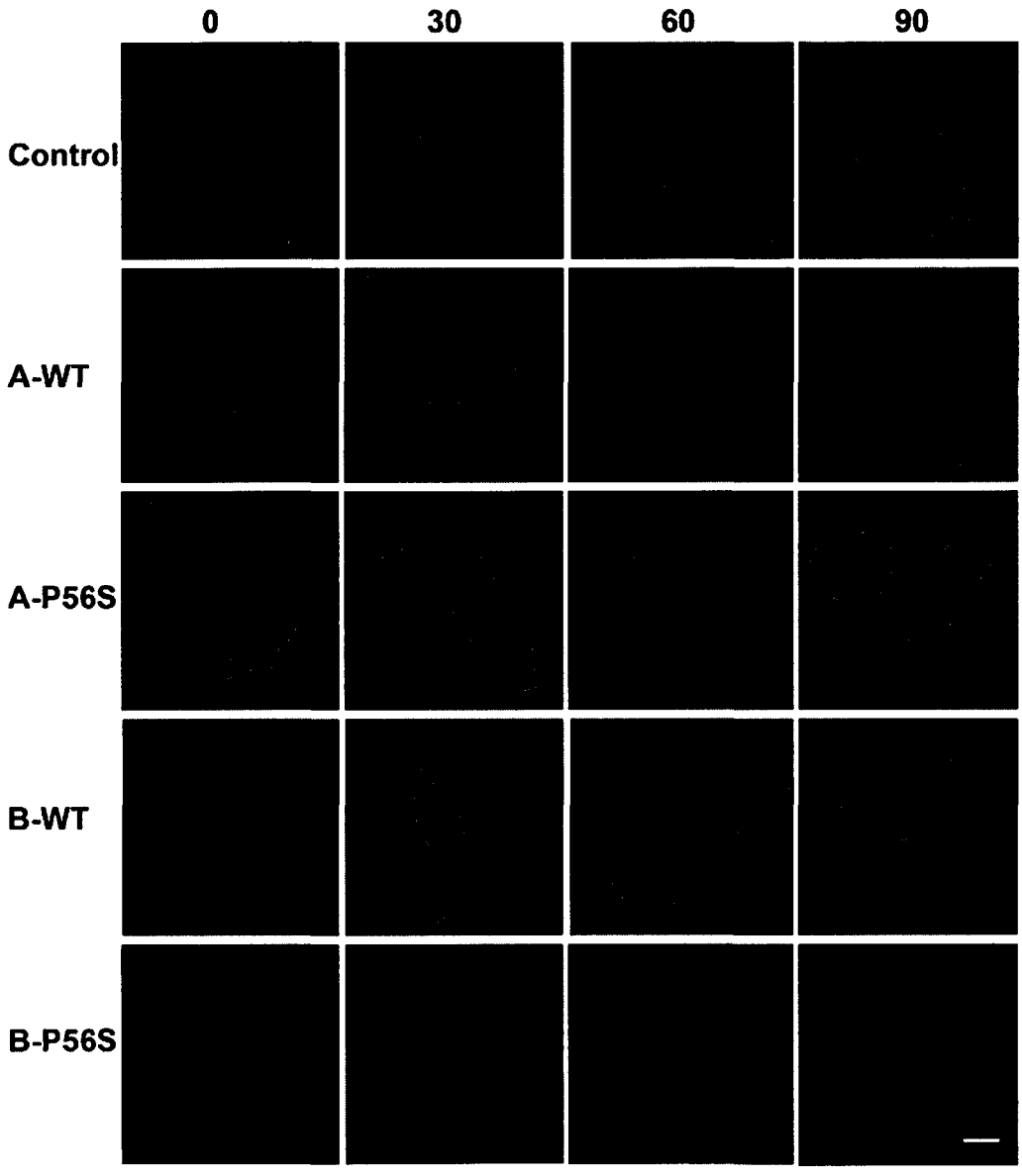

Figure 9. Time course of VSVG^{ts045}-GFP trafficking in CHO fibroblasts over-expressing WT or P56S VAPA or VAPB in the absence of FFAT.
CHO fibroblasts were co-transfected with pCDM8.1/VSVG^{ts045}-GFP, pcDNA3.1 (+)-Myc empty vector and either Flag-epitope tagged empty vector or wild-type or P56S mutant VAPA or VAPB. VSVG was trapped in the ER at 42°C for 6 hours and shifted to 32°C to synchronize ER exit. The cells were fixed with 4% paraformaldehyde at the indicated time (minutes) and representative images were captured by confocal microscopy and VSVG was visualized by its GFP signal (green). Scale bar: 10 μm.

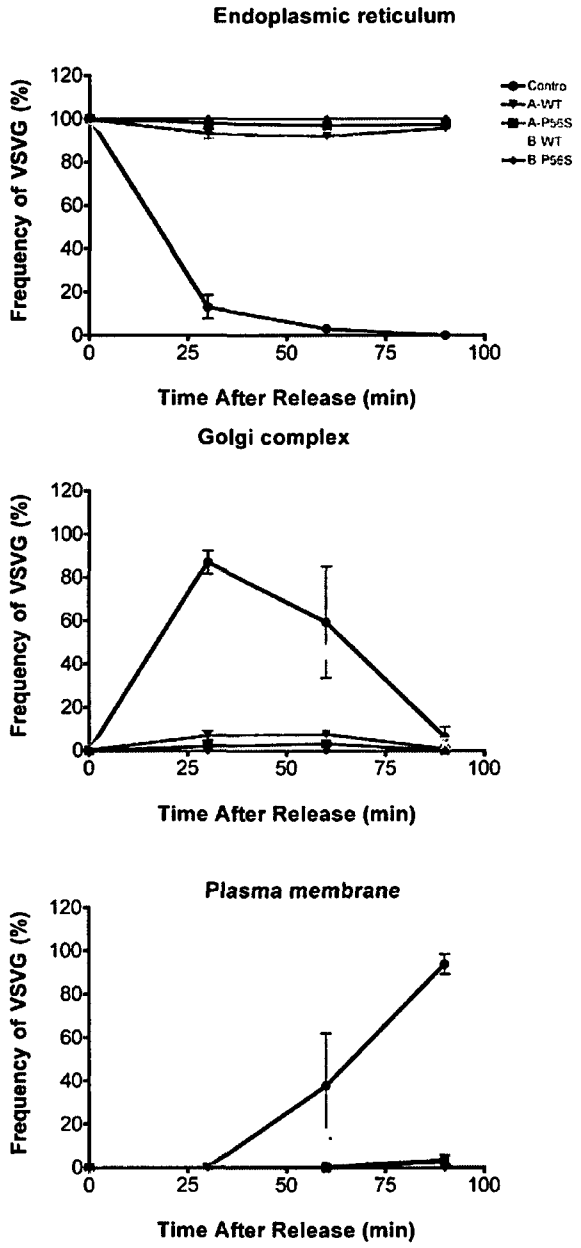

Figure 10. Distribution of VSVG^{ts045}-GFP localization in CHO fibroblasts over-expressing WT or P56S VAPA or VAPB in the absence of FFAT.

CHO fibroblasts were co-transfected with pCDM8.1/VSVG^{ts045}-GFP, pcDNA3.1 (+)-Myc empty vector and either Flag-epitope tagged empty vector or wild-type or P56S mutant VAPA or VAPB. VSVG localization was quantified for each condition and at each time point for either ER (top), Golgi complex (middle) or plasma membrane (bottom) with a minimum of 50 cells counted for each time point per condition. The frequencies are expressed as a mean percentage ± S.E.M., n=3, of CHO fibroblasts with given VSVG localization. Control (●), VAPA-WT (▼), VAPA-P56S (■),VAPB-WT ( ), and VAPB-P56S (◆).

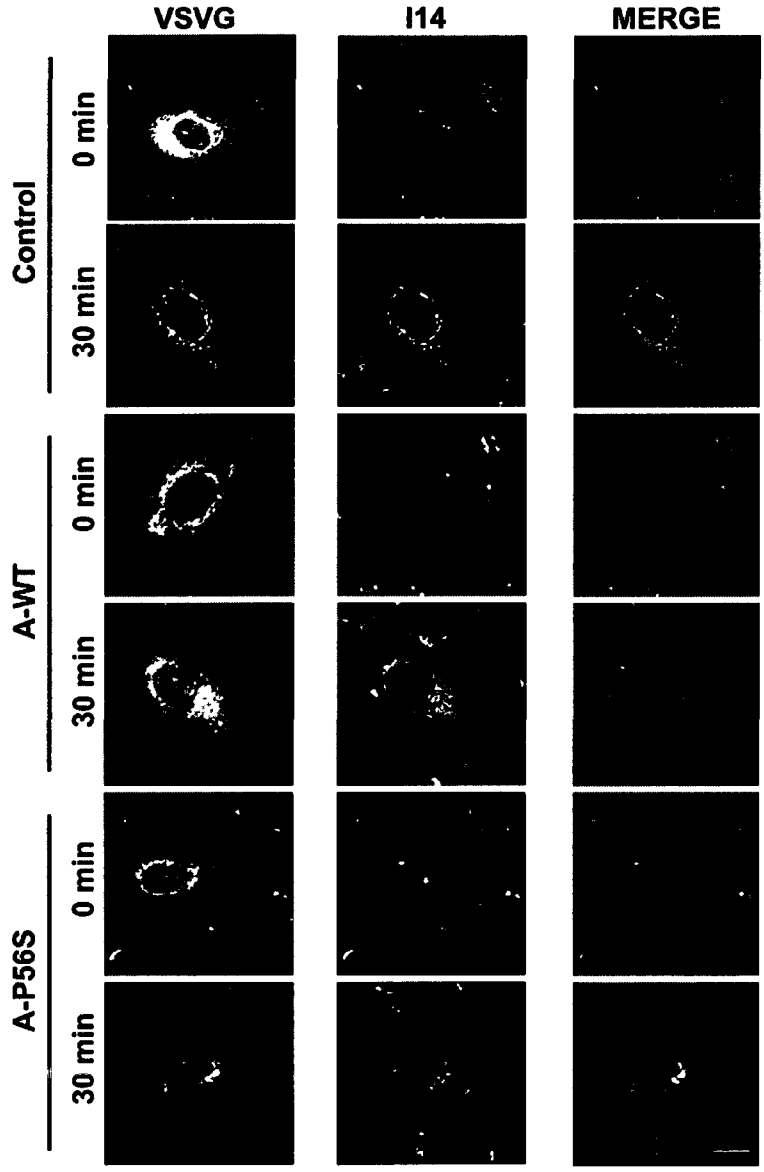

Figure 11. The effect of over-expression of WT or P56S VAPA on VSVG^{ts045}-GFP folding in CHO fibroblasts.

The images shown in Fig. 11 and 12 were obtained from the same experiment, therefore the same images for the control are displayed. CHO were co-transfected with pCDM8.1/VSVG^{ts045}-GFP, pcDNA3.1 (+)-Myc empty vector and either Flag-epitope tagged empty vector or wild-type or P56S mutant VAPA. VSVG was trapped in the ER at 42°C for 6 hours and shifted to 32°C to synchronize ER exit. The cells were fixed with 4% paraformaldehyde at the indicated time points and representative images were taken by confocal microscopy. VSVG was visualized by its GFP signal (left column) and properly folded VSVG was detected by confirmation-specific I14 (middle column). VSVG (green) and I14 (red) images were merged (right column) to show co localization. Scale bar: 10 μm.

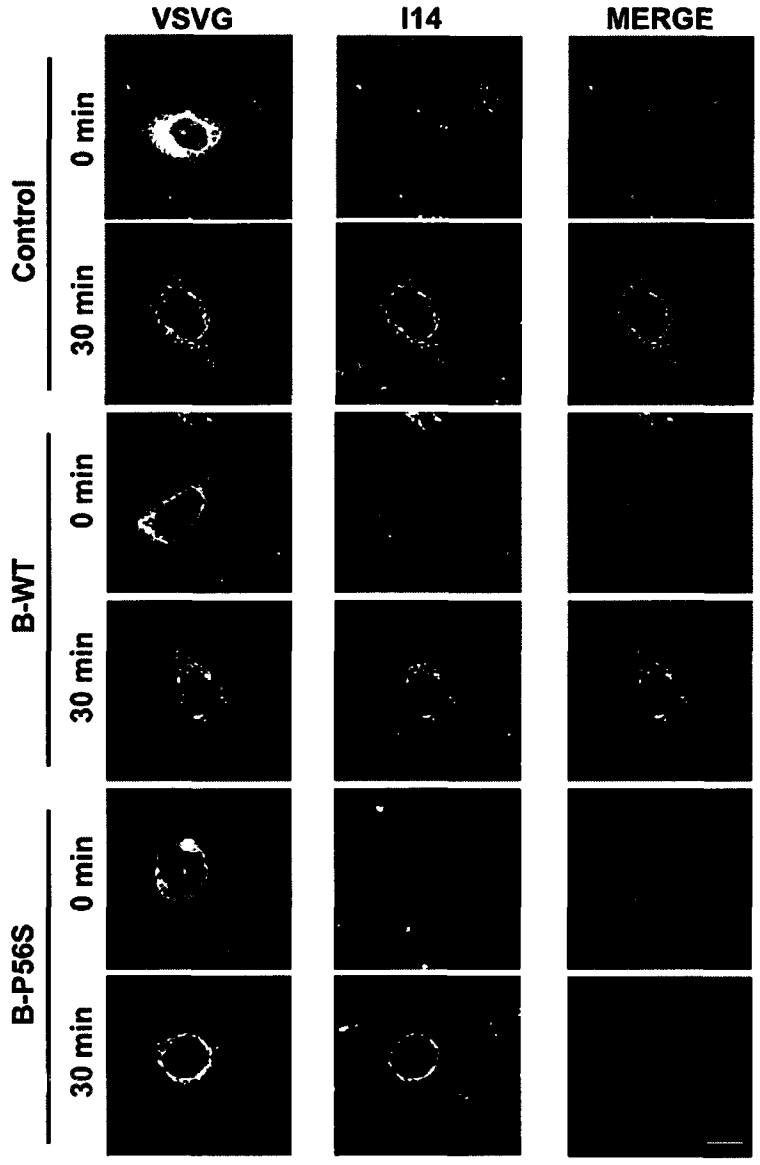

Figure 12. The effect of over-expression of WT or P56S VAPB on VSVG^{ts045}-GFP folding in CHO fibroblasts.

The images shown in Fig. 11 and 12 were obtained from the same experiment, therefore the same images for the control are displayed. CHO were co-transfected with pCDM8.1/VSVG^{ts045}-GFP, pcDNA3.1 (+)-Myc empty vector and either Flag-epitope tagged empty vector or wild-type or P56S mutant VAPB. VSVG was trapped in the ER at 42°C for 6 hours and shifted to 32°C to synchronize ER exit. The cells were fixed with 4% paraformaldehyde at the indicated time points and representative images were taken by confocal microscopy. VSVG was visualized by its GFP signal (left column) and properly folded VSVG was detected by confirmation-specific I14 (middle column). VSVG (green) and I14 (red) images were merged (right column) to illustrate co-localization. Scale bar: 10 μm.

Simultaneous over-expression of the FFAT motif restores ER exit of VSVG caused by VAPA and VAPB-P56S

Studies have shown that the direct interaction between VAP and FFAT-motif-containing proteins resulted in the reorganization of the ER (Amarilio et al., 2005) and affects VAP function (Loewen et al., 2003). Co-expression of the FFAT motif resolved the ER morphological effect of VAPB-P56S suggesting that it may counteract functional defects associated with the mutation. To examine if co-expression of FFAT had an effect on protein transport, $VSVG^{ts045}$-GFP was co-transfected into CHO fibroblasts with either pFlag-CMV2 control vector or wild-type or P56S variants of VAPA or VAPB in the presence of the FFAT motif of rabbit OSBP. Co-expression of FFAT did not change the transport dynamics of the control (Fig. 13 and 14) compared to transfection without the FFAT motif (Fig. 9 and 10). However, the inhibition of VSVG exit from the ER was reversed in VAPA-WT and VAPA-P56S (Fig. 13 and 14). VABP-WT co-expressed with the FFAT motif also behaved similarly to conditions where no FFAT motif was transfected (Fig. 13 and 14). In VAPB-P56S expressing cells, co-transfection with the FFAT motif restored the characteristic reticular ER pattern and protein trafficking (Fig. 13 and 14). These results demonstrate that expression of FFAT is able to restore protein transport in VAPA and VAPB-P56S expressing cells. In the case of VAPB-P56S, expression of FFAT appears to rescue the functional deficit that is associated with the change in ER morphology.

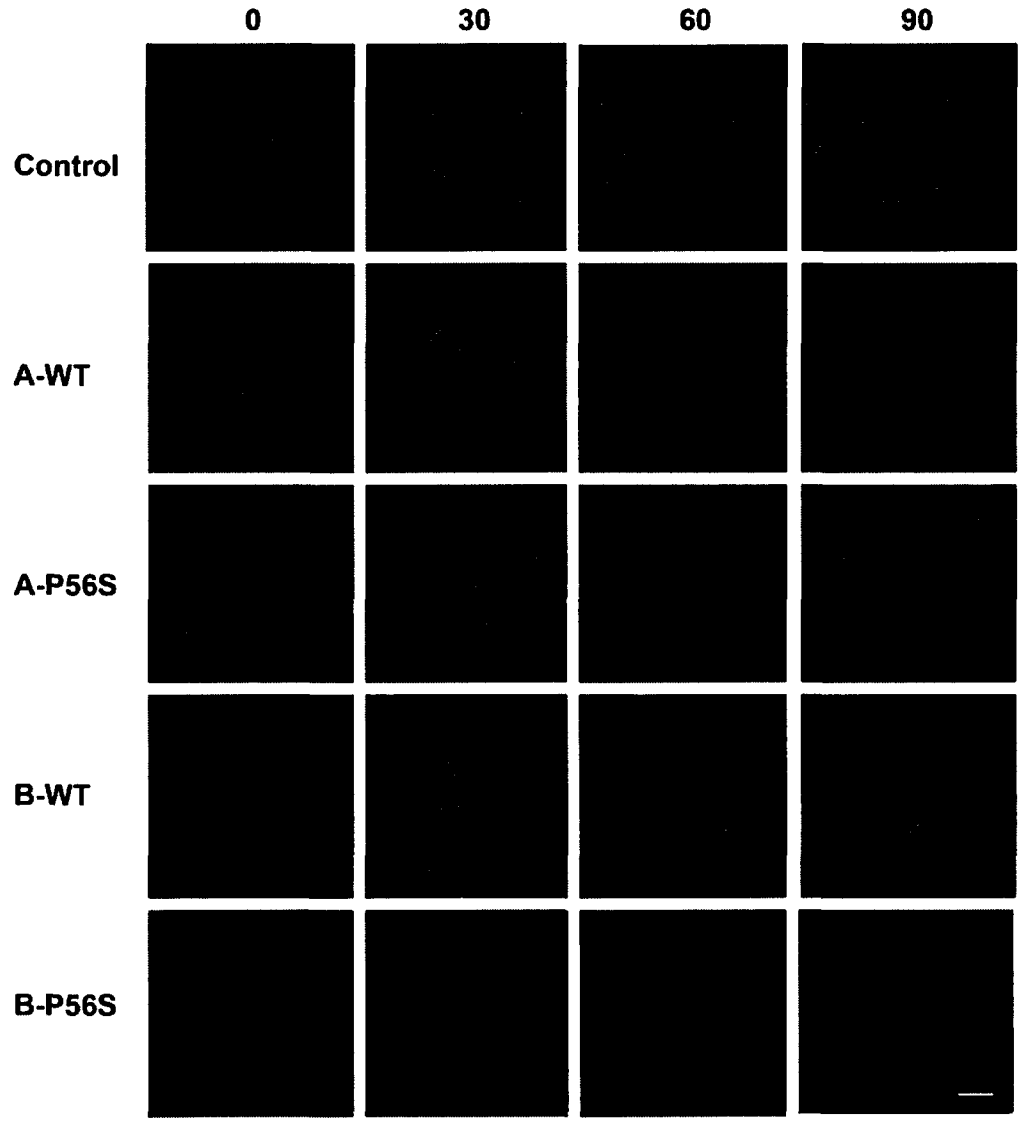

Figure 13. Time course of VSVG^{ts045}-GFP trafficking in CHO fibroblasts over-expressing WT or P56S VAPA or VAPB in the presence of FFAT.
CHO fibroblasts were co-transfected with pCDM8.1/VSVG^{ts045}-GFP, pcDNA3.1 (+)-Myc/OSBP-FFAT and either Flag-epitope tagged empty vector or wild-type or P56S mutant VAPA or VAPB. VSVG was trapped in the ER at 42°C for 6 hours and shifted to 32°C to synchronize ER exit. The cells were fixed with 4% paraformaldehyde at the indicated time (minutes) and representative images were captured by confocal microscopy and VSVG was visualized by its GFP signal (green). Scale bar: 10 μm.

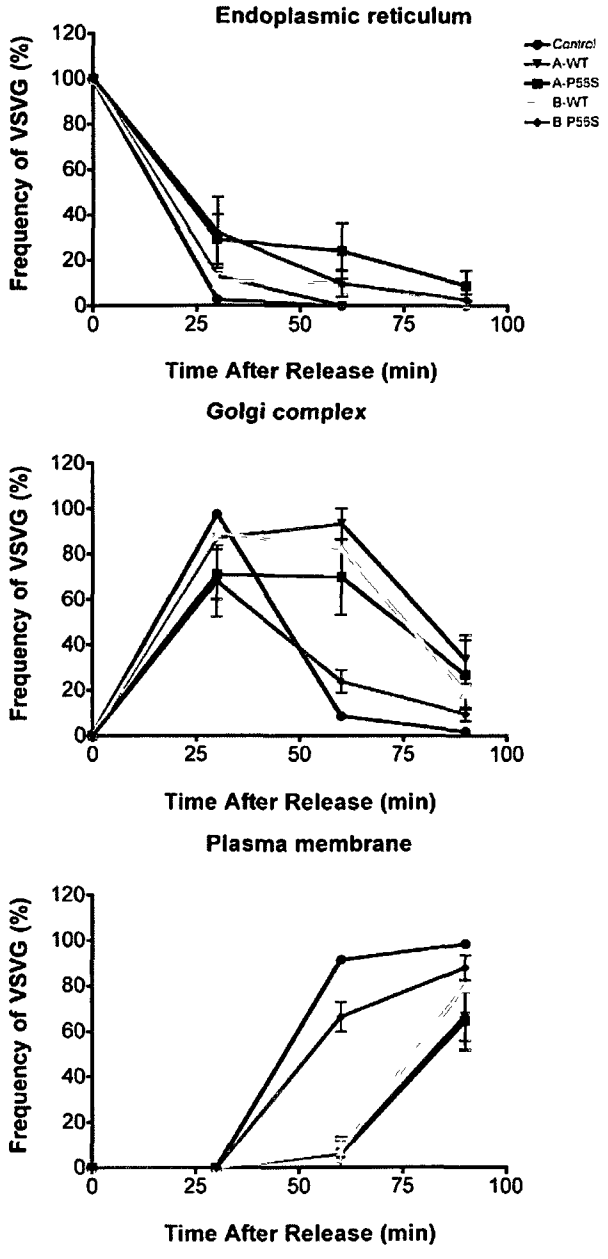

Figure 14. Distribution of VSVG^{ts045}-GFP localization in CHO fibroblasts over-expressing WT or P56S VAPA or VAPB in the presence of FFAT.
CHO fibroblasts were co-transfected with pCDM8.1/VSVG^{ts045}-GFP, pcDNA3.1 (+)-Myc/OSB-FFAT and either Flag-epitope tagged empty vector or wild-type or P56S mutant VAPA or VAPB. VSVG localization was quantified for each condition and at each time point for either ER (top), Golgi complex (middle) or plasma membrane (bottom) with a minimum of 50 cells counted for each time point per condition. The frequencies are expressed as the mean percentage ± S.E.M., n=3, of CHO cells with given VSVG localization. Control (●), VAPA-WT (▽), VAPA-P56S (■),VAPB-WT ( ), and VAPB-P56S (◆).

VAP inhibition of ER exit is specific to membrane-bound proteins

VAPA-WT, VAPA-P56S and VAPB-P56S inhibited ER exit of membrane-associated vesicle cargo protein, VSVG. However, vesicle cargo is not limited to membrane-bound proteins and can include soluble cargo proteins as well. The pathway of membrane-bound proteins to the ER exit site occurs by lateral movement in a two-dimensional plane whereas soluble proteins are not constrained by the same conditions (Jacobson et al., 1987). To determine if the inhibition of protein exit from the ER affects all cargo proteins or if it is specific to membrane-associated proteins, trafficking of soluble Chromogranin B (CgB) was compared to membrane-associated VSVG in CHO fibroblasts transfected with either pFlag-CMV2 control vector or wild-type or P56S VAPA or VAPB. The CgB plasmid used was fused to a temperature-sensitive GFP(S65T) (Wacker et al., 1997) that is a folding defective mutation at 37°C that results in low fluorescence. However, at 15°C, the GFP is able to fold correctly and this results in greater fluorescence intensity. The cells were incubated at 15°C for 2 hours to allow enhanced fluorescence of CgB-GFP(S65T) and inhibit biogenesis of vesicles at the ER-Golgi Intermediate Compartment (ERGIC). The cessation of vesicle biogenesis would trap all proteins that have already exited the ER in the ERGIC (Ben-Tekaya et al., 2005). If ER exit of soluble proteins were not affected, then CgB would be trapped in the ERGIC at 15°C but would be able to progress to the Golgi complex after the shift to 37°C because biogenesis of vesicles at the ERGIC is restored. However, if it is a general block of ER exit, then CgB would remain in the ER at 15°C and after the shift to 37°C because only cargo trapped at the ERGIC can be transported to the Golgi complex. Similar temperature conditions were used for cells co-transfected with $VSVG^{ts045}$-GFP.

Before the shift to 37°C, control cells exhibited CgB staining that resembled reticular ER and perinuclear punctate staining that is characteristic of the ERGIC (Fig. 15). After 30 minutes at 37°C, CgB was localized to the Golgi apparatus (Fig. 15) defined by its characteristic perinuclear staining and this effect was observed in all VAP conditions. Under similar temperature conditions, control cells showed $VSVG^{ts045}$-GFP staining resembling the ERGIC (Fig. 15) before the shift to 37°C and subsequently localization at the Golgi apparatus 30 minutes after the temperature change. VAPA-WT and VAPA-P56S had staining patterns that were reminiscent of reticular ER before the shift to 37°C and this localization was maintained 30 minutes after the chase period. The effect of VAPB-WT was similar to control cells and expression of VAPB-P56S resulted in VSVG-labeled structures that resembled the expanded ER tubules. These results demonstrate the inhibition of cargo protein exit out of the ER by VAPA-WT, VAPA-P56S and VAPB-P56S does not include soluble cargo proteins and is specific to membrane-associated cargo proteins.

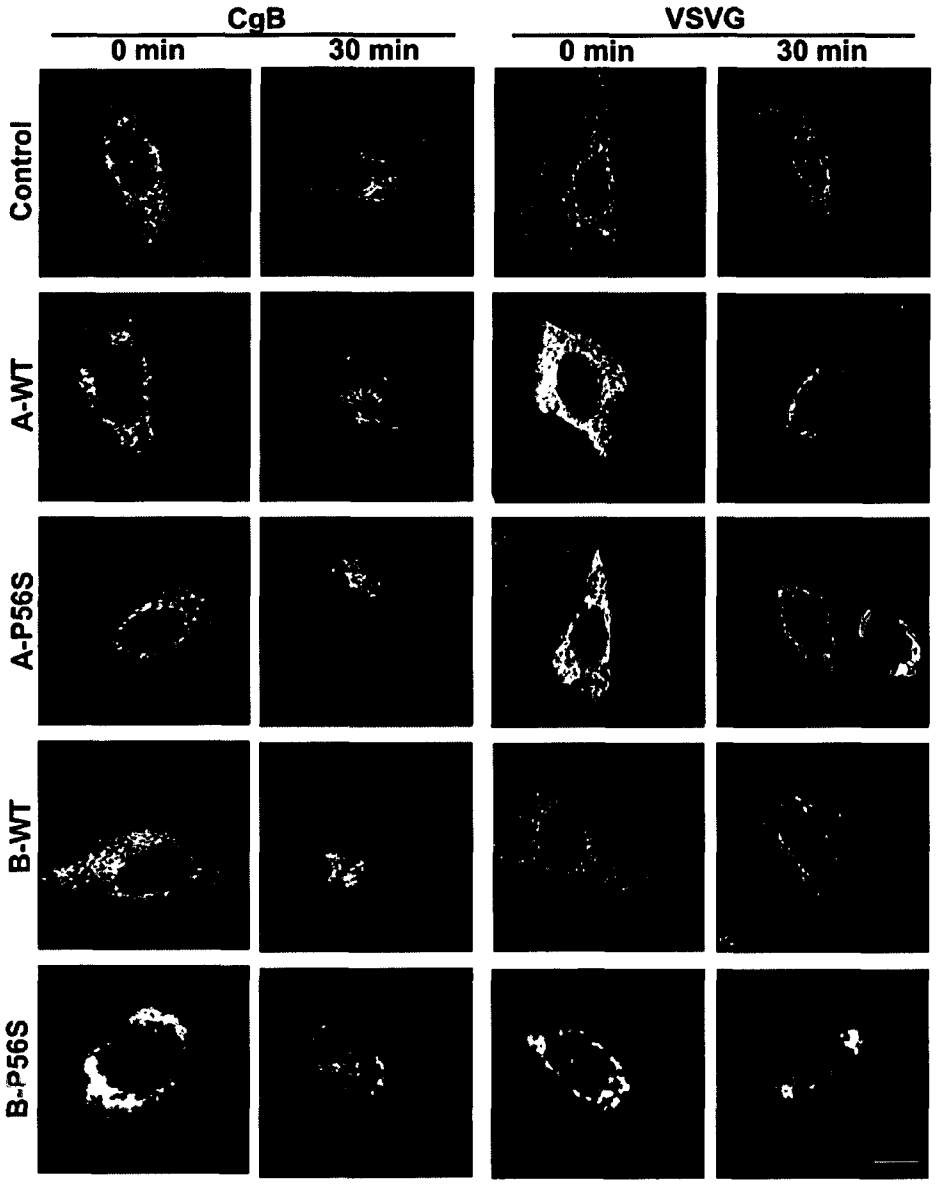

Figure 15. Comparison of the effect of WT or P56S VAPA or VAPB on the transport of soluble CgB-GFP(S65T) and membrane-bound VSVG^{ts045}-GFP. CHO fibroblasts were co-transfected with pCDM8/CgB-GFP (S65T) or pCDM8.1/VSVG^{ts045}-GFP, pcDNA3.1 (+)-Myc empty vector and either Flag-epitope tagged empty vector or wild-type or P56S mutant VAPA or VAPB. The cells were incubated at 15°C for 2 hours to enhance the fluorescent signal of CgB-GFP(S65T) and to trap all proteins in the ERGIC before being shifted to 37°C to restore vesicle biogenesis. Similar temperature conditions were applied to cells transfected with VSVG^{ts045}-GFP. The cells were fixed with 4 % paraformaldehyde at the indicated time points and representative images were captured by confocal microscopy and CgB or VSVG was visualized by their GFP signal. Scale bar: 10 μm.

Over-expression of VAPB dampens IRE1 activity

Over-expression of VAPB-P56S traps properly folded membrane-associated cargo proteins in expanded ER tubules which has the potential of increasing the protein load, triggering ER stress and activating the UPR (Schroder and Kaufman, 2005). These expanded ER structures were documented to be very stable and resistant to degradation (Kanekura et al., 2006) suggesting that prolonged UPR activation does not resolve the stress thereby triggering the apoptotic response. VAPB has been implicated in mediating the IRE1 signaling pathway of the UPR, however, previous studies have focused on the effect of VAPB-P56S over a short-time periods (Suzuki et al., 2009). It is more relevant to study the effect of chronic ER stress in VAPB-P56S expressing cells because ALS8 is a late-onset disease (Boillee et al., 2006). Therefore, the remainder of this study focused on the effects of VAPB on the UPR. Firstly, to assess the effects of VAPB-P56S on the IRE1 activation under conditions of chronic ER stress, CHO fibroblasts and NSC-34 motor neurones were co-transfected with pmRFP-N1, pXBP1u$_{(unspliced)}$-GFP and either pFlag-CMV2 control vector or wild-type or P56S VAPB in the absence or presence of the FFAT motif of rabbit OSBP. NSC-34 is a fusion of the murine aminopterin-sensitive neuroblastoma N18TG2 line with mouse motor neurone-enriched embryonic spinal cord that has the properties of motor neurones (Cashman et al., 1992) making it a cell culture model that is more relevant to the study of ALS.

pXBP1u-GFP plasmid was used as a GFP-based reporter and under conditions of ER stress will cause endogenous IRE1 to splice out a 26-nucleotide sequence from XBP1u$_{(unspliced)}$ mRNA to yield an XBP1s$_{(spliced)}$ sequence with a frameshift (Fig. 16A) (Yu et al., 2006). The splicing removes a stop codon and results in a frameshift that

places the GFP sequence in frame and gives rise to an XBP1s protein fused to GFP (Fig. 16B). Thus, the expression of XBP1s-GFP can be used to measure endogenous IRE1 activity. The cells were treated with N-glycosylation inhibitor, tunicamycin (Yoshida et al., 2006), to induce ER stress and inhibit protein exit from the ER resulting in an increased protein load in the ER. Also chronic treatment of tunicamycin is documented to cause irreversible toxicity of to neurones (Lin et al., 1999). Live cells were imaged immediately after treatment of tunicamycin and at 4, 8, and 16 hours after treatment and the values were given as a percentage of the population with GFP expression relative to RFP expression which served as a transfection control.

In CHO fibroblasts, the frequency of XBP1s-GFP cells over-expressed with either control plasmid, VAPB-WT or VAPB-P56S was not different from one another (Fig. 17) before tunicamycin treatment in the absence of FFAT. This indicates that in the absence of ER stress, VAPB-WT or VAPB-P56S do no stimulate endogenous IRE1 activity. In all three conditions, peak IRE1 activity occurred at 8 hours (Fig. 17A). However, the frequency of GFP cells was less for VAPB-WT (16.7 ± 0.9%, p=0.0001; Fig. 17A) and VAPB-P56S (18.5 ± 1.5%, p=0.001; Fig. 17A) over-expressed CHO compared to the control (30.0 ± 1.0%; Fig. 17A). Co-transfection of the FFAT motif did not have an effect on XBP1s-GFP expression in control, VAPB-WT or VAPB-P56S before tunicamycin treatment and at 4, 8 and 16 hours after treatment compared to their respective conditions in the absence of FFAT. However, the non-significant decrease of XBP1s-GFP expression in the control co-transfected with the FFAT motif was enough to result in the three conditions being not significantly different at the 8-hour peak time (Fig. 17B).

In NSC-34 motor neurones, the frequency of XBP1s-GFP cells over-expressed with either control plasmid, VAPB-WT or VAPB-P56S was not different from one another (Fig. 17C) before tunicamycin treatment in the absence of FFAT. Again, this suggests that in the absence of ER stress, VAPB-WT or VAPB-P56S do no stimulate endogenous IRE1 activity. In control cells, peak IRE1 activity occurred after 8 hours of treatment with tunicamycin (Fig. 17C). Over-expression of VAPB-WT and VAPB-P56S also had peak endogenous IRE1 activity at 8 hours but the frequency of XBP1s-GFP cells was significantly less in VAPB-WT (21.0 ± 2.0%, p=0.003; Fig. 17C) and VAPB-P56S (24.8 ± 3.6%, p=0.046; Fig. 17C) expressed cells compared to the control (35.1 ± 2.5%; Fig. 17C). Co-expression of the FFAT motif decreased the frequency of GFP expressing cells in the control at 8 hours from 35.1 ± 2.5% to 24.5 ± 2.2%, p=0.0131 (Fig. 17D) but did not have an effect in VAPB-WT or VAPB-P56S over-expressing NSC-34 compared their untransfected FFAT conditions. The expression of XPB1s-GFP was not different at 8 hours between control, VAPB-WT and VAPB-P56S in the presence of the FFAT motif of rabbit OSBP.

Dampening of IRE1 activity by VAPB-P56S suggest that apoptosis by way of prolonged IRE1 activation may not be a contributing factor to motor neurone degeneration in ALS8. Moreover, the lower frequency of XBP1s-GFP expressing cells in over-expressed VAPB-P56S may be due to inhibition of IRE1 splicing of XBP1u mRNA or rapid turnover of XBP1s protein.

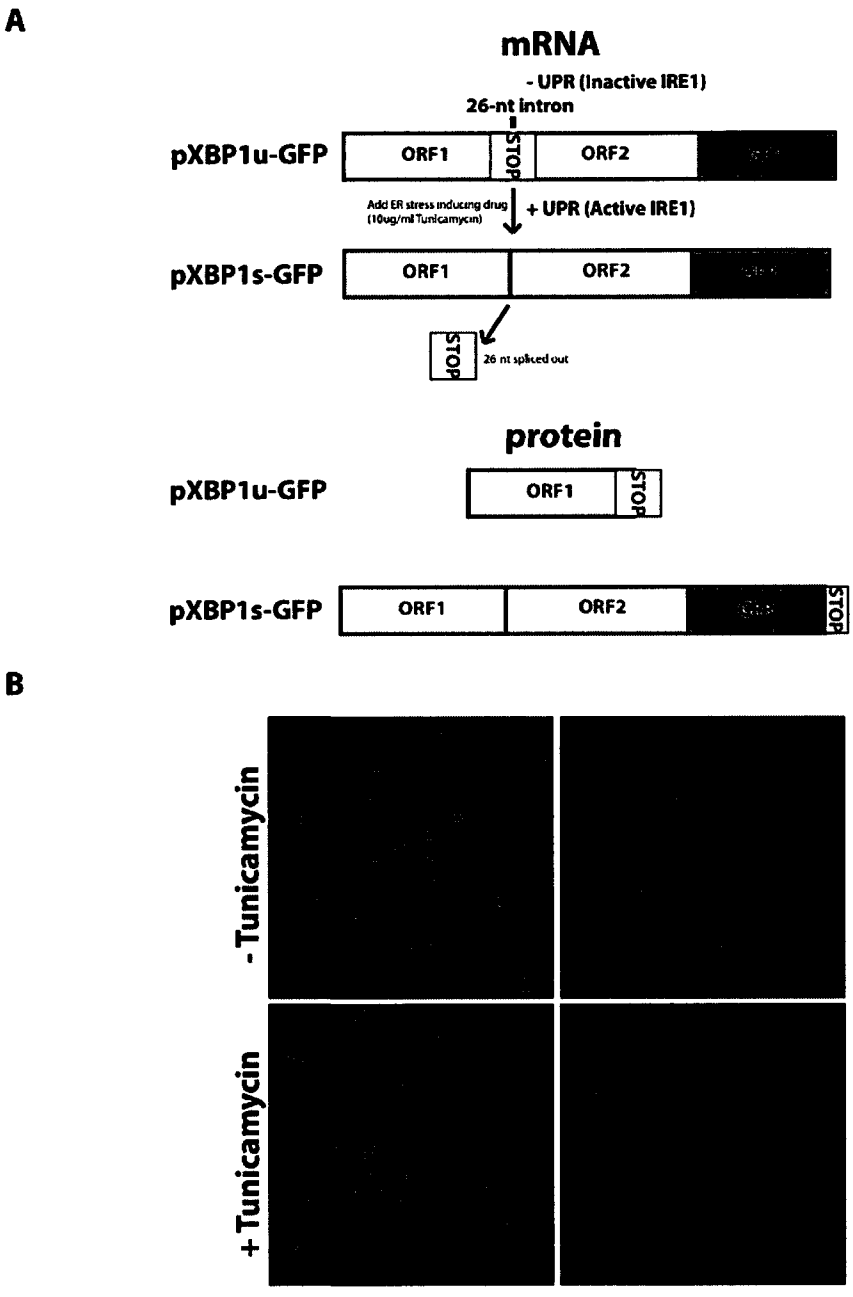

Figure 16. Diagram of pXBP1u-GFP plasmid employed to determine IRE1 activity. (*A*) Simplified cartoon of pXBP1-GFP unspliced and spliced mRNA sequences and their corresponding translated protein. (*B*) Fluorescent images of NSC-34 motor neurones cells treated without and with tunicamycin after 8 hours. Transfected cells were visualized by RFP and XBP1 by GFP.

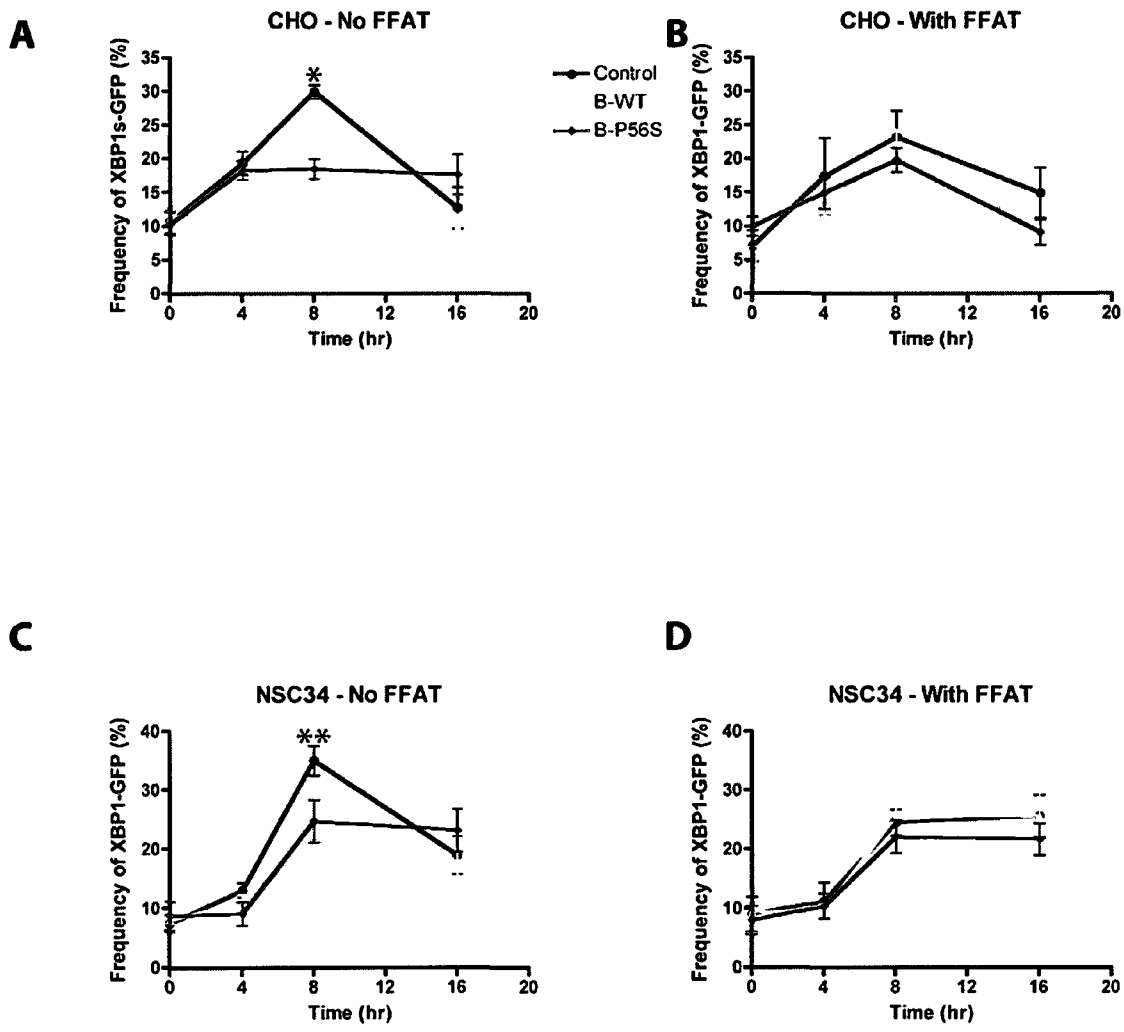

Figure 17. The effect of WT or P56S VAPB in the absence or presence of FFAT on IRE1 activity reported as XBP1s-GFP expression in CHO fibroblasts or NSC-34 motor neurones under chronic ER stress.

CHO fibroblasts or NSC-34 motor neurones were co-transfected with pXBP1u-GFP, pmRFP-N1, pcDNA3.1 (+)-Myc empty vector or pcDNA3.1 (+)-Myc/OSB-FFAT and either Flag-epitope tagged empty vector or wild-type or P56S mutant VAPB. ER stress was induced by tunicamycin and endogenous IRE1 activity was reported as the frequency of XBP1s-GFP cells at the indicated time points. An average of 100 cells were counted for each condition and each time point. The values represent the mean percentage ± S.E.M., n=5, of GFP expressing cells relative to cells expressing RFP as a transfection control. Statistical analysis comparing control to VAPB-WT and VAPB-P56S without FFAT at 8 hours in CHO and NSC-34 was performed using Student unpaired t-Test, with two-tailed distribution. *In CHO, control compared to VAPB-WT and VAPB-P56S, p=0.0001 and p=0.001, respectively **In NSC-34, control compared to VAPB-WT and VAPB-P56S, p=0.003 and p=0.046, respectively. Control (●),VAPB-WT ( ), and VAPB-P56S (◆).

Over-expression of VAPB-P56S inhibits XBP1s localization to the nucleus

The frequency of cells with XBP1s-GFP in over-expressed VABP-P56S cells was significantly less than the control suggesting that endogenous IRE1 splicing of XBP1u mRNA is inhibited. EM images of CHO fibroblasts over-expressing VAPB-P56S in the absence of FFAT showed expansion of the PNS of the NE (Fig. 6D) and it has been documented that VAPB-P56S inhibited XBP1-dependent activation of UPRE luciferase activity used to measure the activation of UPR target genes in the nucleus (Suzuki et al., 2009). Together, these findings suggest that expression of VAPB-P56S may inhibit transport of XBP1s protein to the nucleus and if this is validated, would cause rapid degradation of cytoplasmic XBP1 (Yoshida et al., 2006) resulting in a lower frequency of cells expressing XBP1s-GFP. To investigate if the expansion of the PNS affected the translocation of XBP1s-GFP into the nucleus, CHO fibroblasts were co-transfected with XBP1u-GFP and either pmRFP-N1 control vector or wild-type or P56S VAPB in the absence or presence of the FFAT motif of rabbit OSBP. The cells were fixed at 30 minutes after treatment with β-Mercaptoethanol, a water soluble reducing agent that readily crosses the plasma membrane and disrupts disulfide bonds (Yoshida et al., 2006) inducing unfolding of proteins in the ER, an oxidative environment (Malhotra and Kaufman, 2007a), and triggering ER stress. Treatment with β-Mercaptoethanol does not cause unfolding of protein in the cytoplasm, a reducing environment. Tunicamycin was not suitable for this experiment because it requires 8 hours for XBP1s-GFP to bhave maxiumum expression (Fig. 17) and nucleocytoplasmic transport events occur in a time-frame of about 30 minutes (Yoshida, 2007). To assess the transport of XBP1s-GFP into the nucleus, β-Mercaptoethanol was used since it is a more potent reagent for ER stress.

The caveat to using this reagent is that it inhibits production of adenosine kinase resulting in the cessation of ATP production, which may have non-specific effects on transportation events and cell survival (Back et al., 2005). The values were expressed as the GFP signal localized to the nucleus relative to the total GFP signal of the cell. DAPI, a fluorescent stain that binds to DNA was used to identify the nucleus. Immunofluorescence images of XBP1s-GFP cells displayed a heterogeneous mix of nuclear and cytoplasmic staining. Therefore to quantify XBP1s-GFP nuclear localization, cells were separated into three categories, less than 60%, 61-80%, and 81-100%, based on the relative GFP fluorescence in the nucleus. The less than 60% and 61-80% categories were not significantly different (Fig. 18B and 19B) regardless of the condition, therefore a cell with 81-100% of its relative GFP fluorescence in the nucleus (Fig. 21) was used as the cut-off to designate a cell as having XBP1s-GFP localized to the nucleus.

After 30 minutes of β-Mercaptoethanol treatment, the frequency of cells with XBP1s-GFP in the nucleus was lower in VAPB-P56S (15.1% ± 5.0%; Fig. 18B) compared to control (40.0% ± 6.1%, p=0.034; Fig. 18B) and VAPB-WT (46.8% ± 5.3%, p=0.013; Fig. 18B). XBP1s-GFP exclusion from the nucleus may explain the lower frequency of XBP1s-GFP expression in CHO over-expressing VAP-P56S. Co-transfection with the FFAT motif did not result in a difference (Fig. 19B) in the frequency of cells with XBP1s-GFP nuclear localization between the control, VAPB-WT or VAPB-P56S suggesting that FFAT is able to resolve the nuclear localization defect. The effect of the over-expression of VABP-P56S as it relates to the lower frequency of

cells expressing XBP1s-GFP can partially be explained by the inhibition of XBP1s-GFP localization to the nucleus, which may result in rapid degradation of the protein.

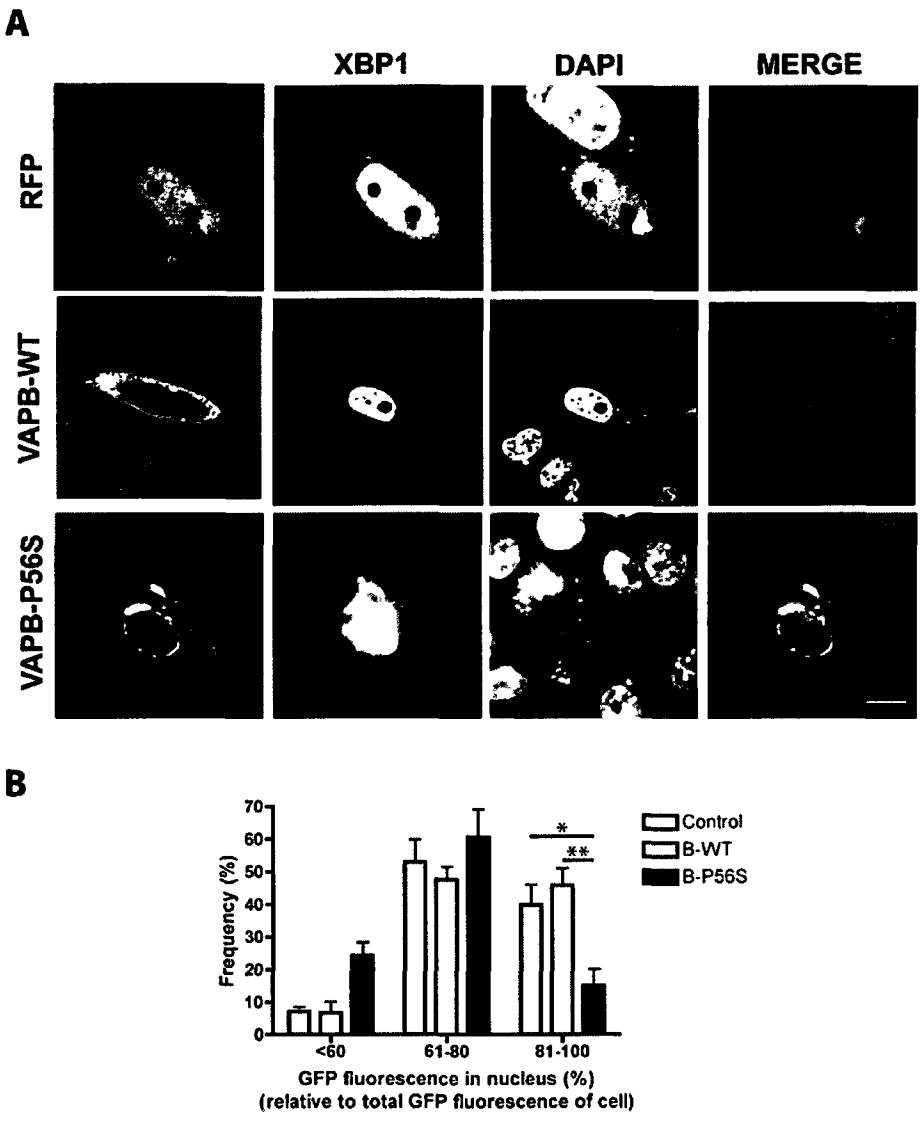

Figure 18. The effect of WT or P56S VAPB in the absence of FFAT on nuclear localization of XBP1s-GFP.

CHO fibroblasts were co-transfected with pXBP1u-GFP, pcDNA3.1 (+)-Myc empty vector and either pmRFP-N1 or wild-type or P56S mutant VAPB. ER stress was induced with β-Mercaptoethanol and CHO were fixed with 4% paraformaldehyde after 30 minutes. (*A*) Representative mages were captured by confocal microscopy and the proteins were visualized with either RFP (red) for control, anti-Flag (red) for VAP, GFP (green) for XBP1s or DAPI (blue) for the nucleus and merged (far right column) to illustrate co-localization. Scale bar: 10 μm. (*B*) Relative GFP fluorescence was taken as a ratio of nuclear GFP fluorescence to GFP fluorescence of the total cell. For each condition, an average of 50 RFP or VAPB cells were counted. The frequency was expressed as the mean percentage ± S.E.M., n=3. Statistical analysis using Student unpaired t-Test, with two-tailed distribution was used to compare VAPB-P56S to control or VAPB-WT without FFAT, *p=0.034 and **p=0.013, respectively.

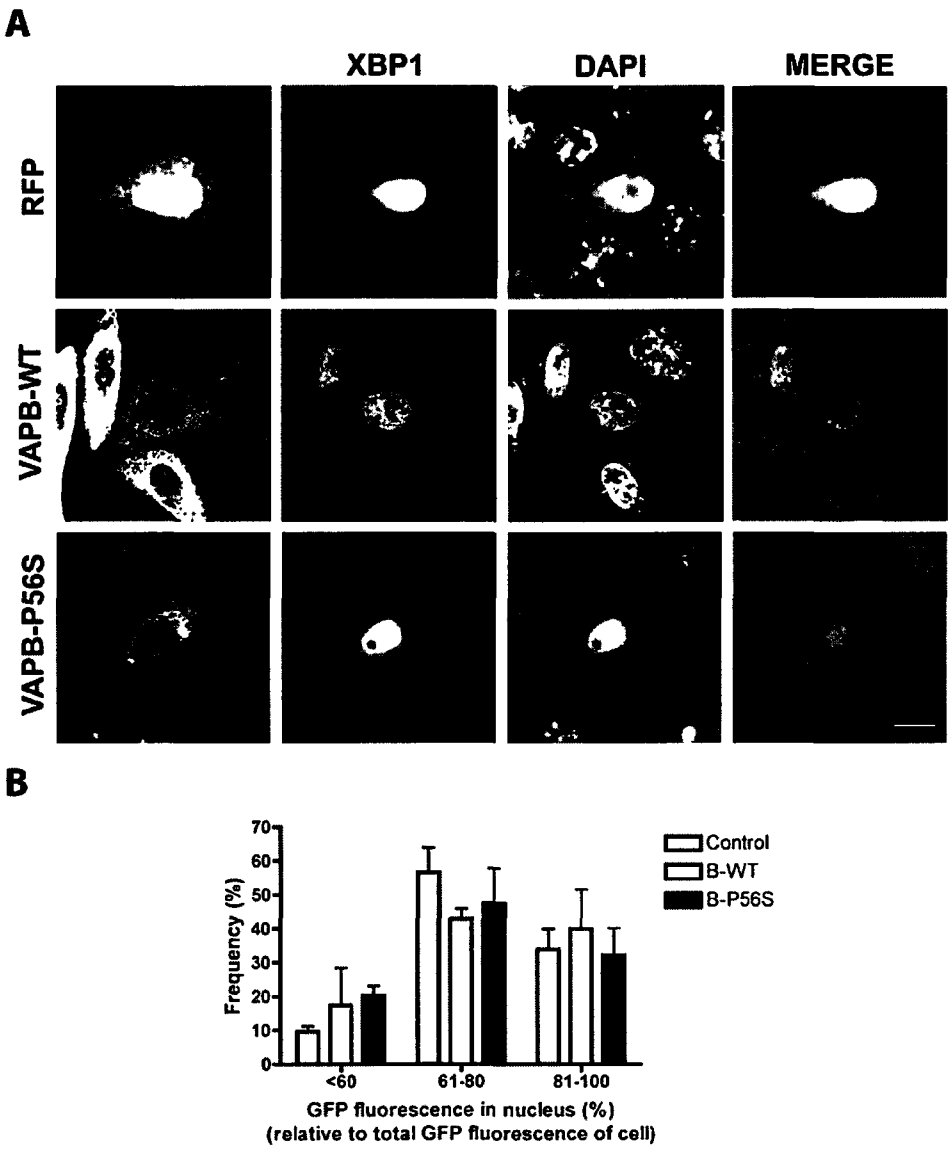

Figure 19. The effect of WT or P56S VAPB in the presence of FFAT on nuclear localization of XBP1s-GFP.

CHO fibroblasts were co-transfected with pXBP1u-GFP, pcDNA3.1 (+)-Myc/OSBP-FFAT and either pmRFP-N1 or wild-type or P56S mutant VAPB. ER stress was induced with β-Mercaptoethanol and CHO were fixed with 4% paraformaldehyde after 30 minutes. (*A*) Representative mages were captured by confocal microscopy and the proteins were visualized with either RFP (red) for control, anti-Flag (red) for VAP, GFP (green) for XBP1s or DAPI (blue) for the nucleus and merged (far right column) to illustrate co-localization. Scale bar: 10 μm. (*B*) Relative GFP fluorescence was taken as a ratio of nuclear GFP fluorescence to GFP fluorescence of the total cell. For each condition, an average of 50 RFP or VAPB cells were counted. The frequency was expressed as the mean percentage ± S.E.M., n=3.

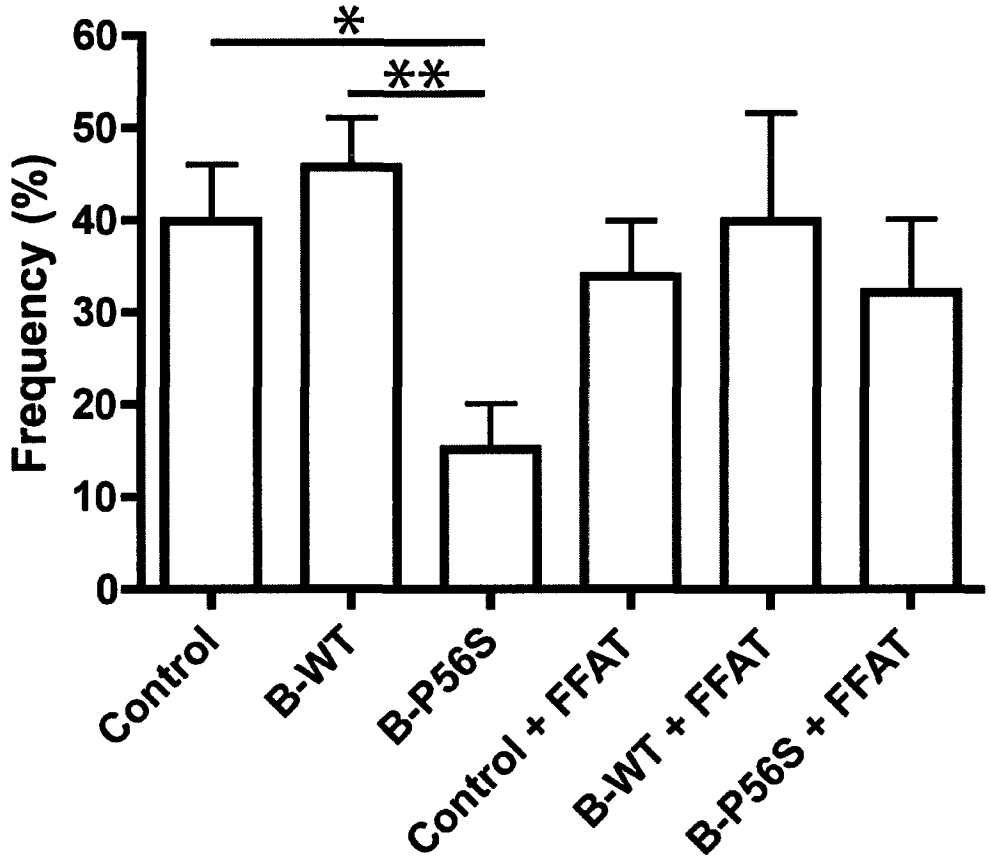

Figure 20. Distribution of WT or P56S VAPA or VAPB cells with XBP1s-GFP localized in the nucleus in the absence or presence of FFAT.
CHO fibroblasts were co-transfected with pXBP1u-GFP, pcDNA3.1 (+)-Myc empty vector or pcDNA3.1 (+)-Myc/OSBP-FFAT and either pmRFP-N1 or wild-type or P56S mutant VAPB. A cell with XBP1s-GFP with relative GFP fluorescence falling in the 81-100% category was defined as having XBP1s localized to the nucleus. For each condition, an average of 50 RFP or VAPB expressing cells were quantified. The frequency is given as the mean percentage ± S.E.M., n=3. Statistical analysis using Student unpaired t-Test, with two-tailed distribution was performed to compare VAPB-P56S to control and VAPB-WT without FFAT 30 minutes into the chase period, $*p=0.034$ and $**p=0.013$, respectively.

Over-expression of VAPB-P56S does not enhance the rate of XBP1s-GFP turnover

Over-expression of VAPB-P56S reduced endogenous IRE1 activity and this is partially due to failure of XBP1s protein translocation to the nucleus. A possible consequence of this effect is enhanced XBP1s-GFP protein degradation by proteasomes in the cytoplasm as supported by a study conducted by Mori's group (Yoshida et al., 2006). To test whether this might explain the lower expression of XBP1s-GFP, CHO fibroblasts over-expressing pFlag-CMV2 empty vector, VAPB-WT and VAPB-P56S were induced with tunicamycin for 8 hours to maximize the population of cells expressing of XBP1s-GFP (Fig. 17). The CHO were then treated with cycloheximide and cell lysates were collected immediately after treatment and at 2, 4, 6 and 8 hours. An immunoblot (Fig. 21A) was performed using the cell lysates and the protein content was determined by densitometry thereby allowing calculation of the rate of protein decay expressed as half-life value.

The half-life of each condition was calculated using the equation $t_{1/2} = t\ln(2)/\ln(N_0/N_8)$, where t=8 and the XBP1 density, N_8, after 8 hours for the control, VAPB-WT and VAPB-P56S were 0.37, 0.59, and 0.76, respectively. The results revealed a slower rate of XBP1s-GFP protein degradation (Fig. 21B) in cells over-expressing VAPB-WT (10.5 hours) or VAPB-P56S (20.2 hours) compared to the control (5.6 hours). This reduced turnover of XBP1s-GFP counters the rationale that a decrease in XBP1s-GFP response is due to greater protein degradation and the reason for this is unclear.

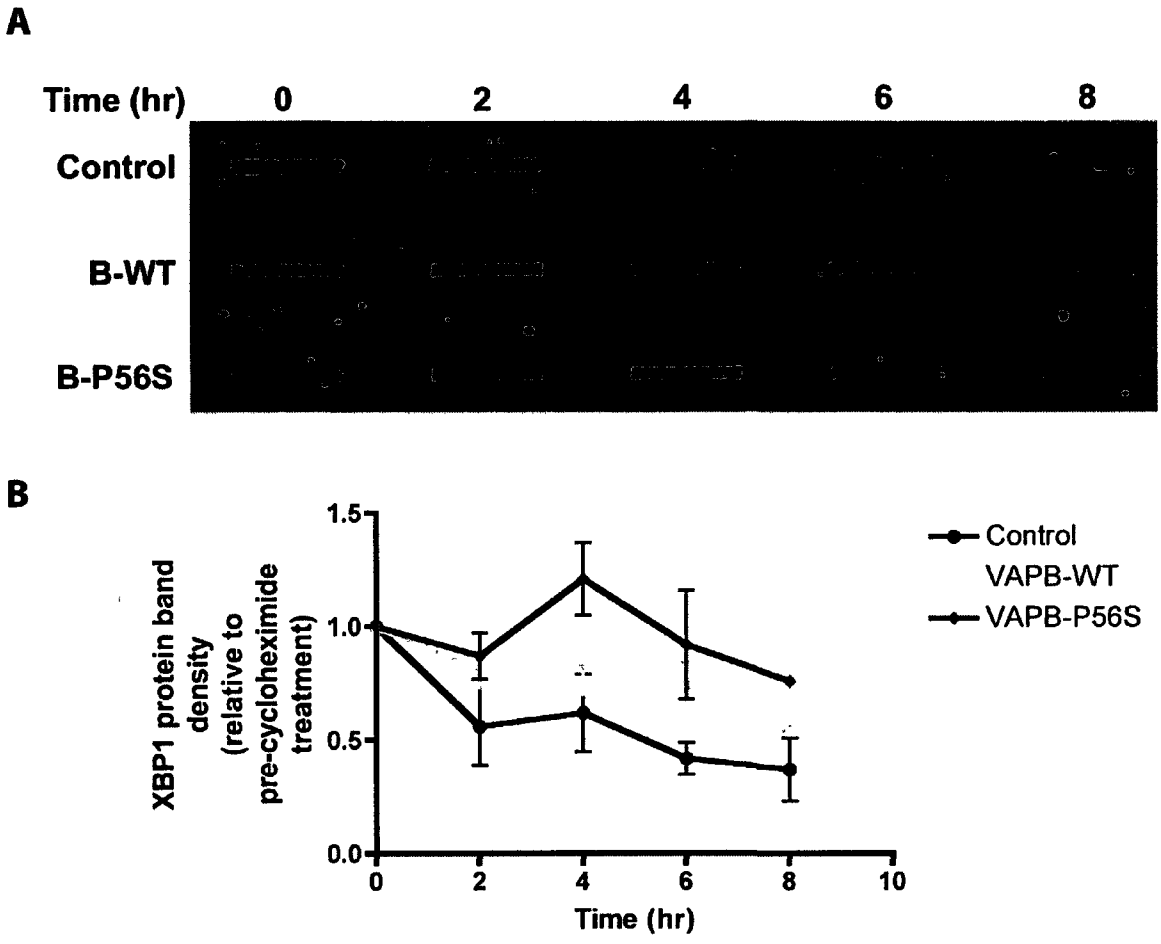

Figure 21. The effect of WT or P56S VAPB on XBP1s-GFP protein degradation. CHO fibroblasts were co-transfected with pXBP1u-GFP, pcDNA3.1 (+)-Myc empty and either Flag-tagged empty vector or wild-type or P56S mutant VAPB. ER stress was induced by tunicamycin for 8 hours to maximize XBP1s-GFP expression after which protein synthesis was stopped with cycloheximide. CHO were harvested at the indicated time points. (*A*) Thirty μg of total protein were loaded per condition and time point onto a Bio-Rad Slot Blot. XBP1s protein was visualized by rabbit anti-GFP and the amount of protein was measured by densitometry. (***B***) The amount of XBP1s-GFP remaining was calculated relative to the protein density at the initial time point, N_0. Values represent relative XBP1s-GFP band density, n=3. Control (●),VAPB-WT ( ), and VAPB-P56S (◆).

VAPB-P56S dampens ATF6 activity

ATF6 is reported to interact directly with VAPB (Gkogkas et al., 2008). Also, activation of ATF6 requires transport of ATF6 precursor from the ER to the Golgi complex for proteolytic processing and release of the TAD (Chen et al., 2002) and the active transcription domain of ATF6 must translocate from the cytoplasm to the nucleus in order to bind to and activate ER stress transcription elements (Wang et al., 2000). Given the inhibitory effects of over-expression of VAPB-P56S on anterograde transport of membrane-associate cargo protein and nucleocytoplasmic transport, the P56S mutation is predicted to inhibit ATF6 signaling. To investigate the effect of VAPB-P56S on ATF6 activity, a luciferase reporter construct, p5xATF6-GL3 (Wang et al., 2000) was used, whereby the firefly luciferase gene expression is controlled by five ATF6-dependent transcription elements. Thus, luciferase activity, expressed as a ratio of *Renilla* luciferase to correct for transfection efficiency, is a readout of ATF6 transcriptional activity. ER stress was induced by tunicamycin and the transfected cells were harvested before treatment and over 4, 8, 24, 32 and 48 hour and luciferase activity was assayed to indicate the level of ATF6 activation.

In CHO fibroblast, peak ATF6 activation occurred at 24 hours after tunicamycin treatment in all conditions (Fig. 22A). ATF6 activation in VAPB-P56S transfected CHO was significantly reduced (0.19 ± 0.03; Fig. 22A) compared to the control (0.43 ± 0.09, p=0.028; Fig. 22A) and VAPB-WT (0.34 ± 0.030; Fig. 22A) at 24 hours. Co-transfection of the FFAT motif did not have an effect on the control and VAPB-WT compared to the absence of FFAT but co-expression raised ATF6 luciferase activity in VAPB-P56S to levels similar to control and VAPB-WT. VAPB-P56S co-transfected with the FFAT

motif (0.38 ± 0.06, p=0.012; Fig. 22B) had a significantly higher ATF6 activation compared to VAPB-P56S cells not transfected with the FFAT motif (0.19 ± 0.03; Fig. 22A). These results indicate that expression of VAPB-P56S dampened ATF6 activation compared to control and VAPB-WT whereas co-expression of the FFAT motif was able to resolve the dampening effect.

In NSC-34 motor neurones, peak ATF6 activation for all three conditions occurred at 24 hours. Similar to the experiment in CHO, ATF6 activation in VAPB-P56S transfected CHO was significantly reduced (0.30 ± 0.04; Fig. 22C) compared to the control (0.50 ± 0.09, p=0.049; Fig. 22C) and VAPB-WT (0.66 ± 0.15, p=0.040; Fig. 22C) at 24 hours. Co-expression of the FFAT motif did not have an effect on control and VAPB-WT (Fig. 22D) compared to the conditions in the absence of FFAT (Fig. 22C). However, ATF6 activation for VAPB-P56S was comparable to control and VAPB-WT for the duration of the assay. VAPB-P56S co-transfected with FFAT (0.67± 0.09, p=0.001; Fig. 22D) had significantly higher ATF6 activation compared to the condition where the FFAT motif was absent (0.30 ± 0.04; Fig. 22C).

The results for the effect of over-expression of VABP-P56S as it relates to ATF6 activity parallel the trend observed for IRE1 activity suggesting that apoptosis by way of prolonged ATF6 activation may not be a contributing factor to motor neurone degeneration in ALS8.

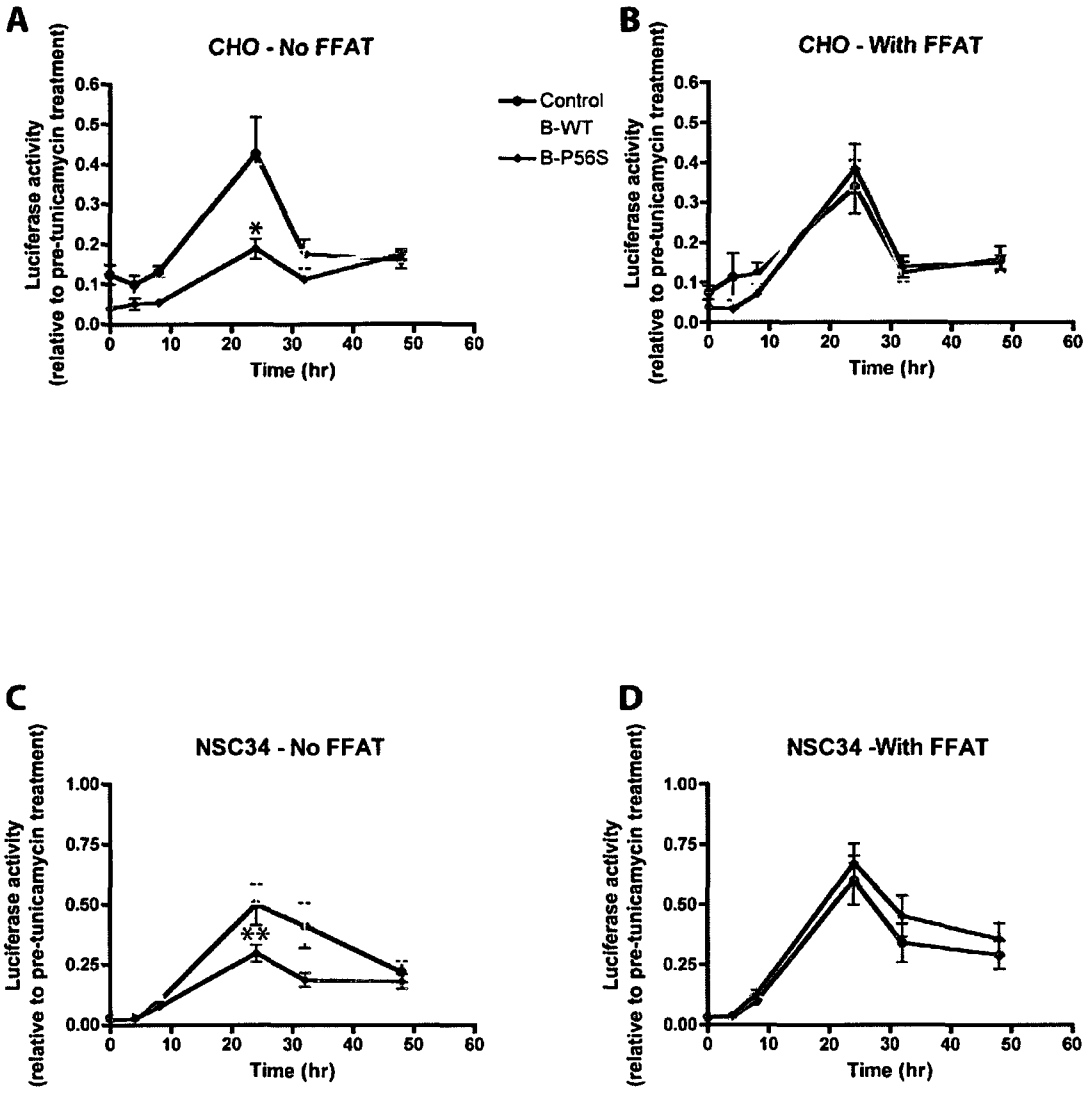

Figure 22. The effect of WT or P56S VAPB in the absence or presence of FFAT on ATF6 activity reported as ATF6-depedent luciferase activity in CHO fibroblasts or NSC-34 motor neurones under chronic ER stress.

CHO fibroblasts or NSC-34 motor neurones were co-transfected with p5xATF6-GL3, pcDNA3.1 (+)-Myc empty vector or pcDNA3.1 (+)-Myc/OSB-FFAT and either Flag-epitope tagged empty vector or wild-type or P56S mutant VAPB. ER stress was induced by tunicamycin and cells lysates were collected at the indicated time points. Relative Luciferase activity was taken as a ratio of ATF6 firefly luciferase activity to transfection control *Renilla* luciferase activity to indicate the level of ATF6 activation. Luciferase activity was expressed as the luminescence ratio of ATF6 to *Renilla* ± S.E.M, CHO n=8, NSC-34 n=6. Statistical analysis comparing VAPB-P56S to control and VAPB-WT at 24 hours in CHO and NSC-34 in was performed using Student unpaired t-Test, with two-tailed distribution. *In CHO, VAPB-P56S compared to control and VAPB-WT, p=0.028 and p=0.030, respectively **In NSC-34, VAPB-P56S compared to control and VAPB-P56S, p=0.049 and p=0.040, respectively. Control (●), VAPB-WT ( ), and VAPB-P56S (◆).

DISCUSSION

Over-expression of VAPA or VAPB have differential effects on ER morphology

The principal objective of this study was to characterize the cellular effects of VAPB-P56S and the mechanism by which these cellular effects may promote the loss of motor neurones in ALS8. The characterization of VAPA was conducted in parallel to assess whether the structural similarities between VAPA and VAPB (Nishimura et al., 1999) (Fig. 1) also included functional similarities. Over-expression of the wild-type variants of VAPA or VAPB in CHO fibroblasts displayed similar reticular pattern that partially co-localized with the ER chaperone, calreticulin (Fig. 3). However, over-expression of the P56S mutation in VAPA and VAPB revealed that the two VAP isoforms had distinct effects on the ER morphology. Over-expression of VAPB-P56S but not VAPA-P56S caused the loss of the characteristic reticular ER pattern (Fig. 3) and the formation of membrane aggregates that co-localized with calreticulin, suggesting that these structures are a product of the collapsed ER network. VAPA and VAPB localization to different subsets of the ER may explain the differential effect on ER morphology. In support of this, a recent study by Skehel's group revealed that HEK293 stained with antibodies against VAPA and VAPB showed that both proteins displayed reticular patterns of expression but had very little co-localization (Gkogkas et al., 2008). In addition, VAPB was initially identified as ERG30 (Soussan et al., 1999) and was predicted to localize to the ER-Golgi Intermediate Compartment (ERGIC). Co-staining with an ERGIC protein such as ERGIC-53 (Hauri et al., 2000) may clarify if the two

VAP isoforms localize to distinct compartments. Together, the differential effect on ER morphology suggested that VAPA and VAPB might also have dissimilar effects on cellular processes.

The impact of epitope tagging on VAP function has not been tested. The VAP constructs employed in this thesis were amino-terminal tagged with the Flag epitope. The Flag protein is approximately 1kDa in size suggesting that it may not affect VAP function whether the epitope is located at the N- or C-terminal of the VAP protein. The size of the epitope may have more impact on VAP function rather than the location of the epitope. For instance, a large C-terminal tagged epitope may affect VAP post-translational insertion into the ER membrane. The protein may fail to insert into the ER membrane and would then be degraded ablating the possibility to study VAP function.

Over-expression of VAPB-P56S causes expansion of ER tubules and the perinuclear space

Previous studies (Fasana et al., 2009; Teuling et al., 2007) documented that over-expression of the VAPB-P56S mutation caused reorganization of the ER. In this study, ultrastructure analysis by EM of CHO fibroblasts transfected with VAPB-P56S revealed structures that resembled enlarged vacuoles (Fig. 6C). These structures were designated as expanded ER tubules and not aggregates, as originally thought, to more accurately describe the phenotype. The formation of these structures may be a product of enhanced lipid synthesis at the ER stemming from the recruitment and constitutive interaction of endogenous FFAT-motif-containing lipid proteins to the ER by VAPB-P56S. This rationale is based on studies that have shown that the MSP domain of VAP interacts with the FFAT motif of lipid-binding proteins (Loewen and Levine, 2005), and that this

interaction maintains the lipid content and profile of the ER (Wyles et al., 2002). Also, constitutive interaction of VAPA with a mutated OSBP resulted in accumulation of ceramide, a lipid molecule, in the ER (Peretti et al., 2008). This interaction is predicted to be preserved in the VAPB-P56S mutation because the yeast orthologue of VAP, SCS2, containing a P51S mutation that is equivalent to P56S in human VAPB, is able to bind to the FFAT motif of Opi1p (Loewen and Levine, 2005). Moreover, the 56th residue of VAPB is not located within the hydrophobic FFAT-binding pocket of the MSP domain (Kaiser et al., 2005). Simultaneous expression of the FFAT motif of rabbit OSBP with VAPB-P56S corrected the ER morphology defect (Fig. 4 and 5) suggesting that exogenous FFAT motifs binds to the MSP domain of VAPB-P56S and outcompete endogenous FFAT motif-containing lipid proteins. These results reinforce the prediction that these expanded ER tubules are a product of enhanced lipid synthesis at the ER.

Over-expression of the FFAT motif and not the AAAT motif restored normal ER morphology shown by the EM images (Fig. 6). Despite transfection with the same amount of plasmid, previous experiments done in our lab have not been able to clarify the expression level of these two constructs by immunoblotting because they are small proteins of about 100 amino acids or 1kDa therefore resolving a protein band of this size is difficult. Moreover, the use of immunofluorescence to image expression levels of the motifs has not been successful because they are small, soluble proteins. Therefore, it is possible that the lack of effect of the AAAT motif can be explained by lower expression. However, we can rationalize that the over-expression of the FFAT motif has an effect because there is a change in ER morphology.

The result obtained in this study contradict the findings by Hoogenraad's group (Teuling et al., 2007), which showed that co-expression of the FFAT motif with VAPB-P56S did not resolve these expanded ER structures. This difference may be attributed to the different FFAT constructs used. Hoogenraad's group cloned the amino acid sequence of the FFAT domain from human Nir2 and fused it to the carboxyl-terminus of GFP sequence (Teuling et al., 2007) whereas the FFAT motif in this study was cloned from rabbit OSBP and fused to the much smaller Myc epitope at the amino-terminus of the FFAT motif. The GFP portion of the fusion protein might interfere with binding of the FFAT motif resulting in failure to correct the adverse effects of VAPB-P56S over-expression (Prosser et al., 2008). Furthermore, the EM images of the expanded ER tubules were inconsistent with previous studies. In these studies, over-expression of VAPB-P56S resulted in ER restructuring with tubular membrane structures that formed irregular branched networks derived from the ER (Teuling et al., 2007) or a form of organized smooth ER (OSER) described as parallel cisternae held together by a layer of cytosol (Fasana et al., 2009). Neither of these studies exhibited enlarged vacuolar-like ER structures as observed in this study. Cell line difference might account for this discrepancy as CHO fibroblasts were used in the current study as opposed to HeLa cells by the other two groups. This could be addressed in the future by EM analysis of transfected HeLa cells. The poor substrate adhesion properties of the NSC-34 motor neurones (Durham et al., 1993) despite poly-lysine coating the matrix would make them difficult to handle for EM. More importantly, the small cell body of these motor neurones would not be ideal where the interest is the effect of VAPB-P56S on ER morphology and not on motor function.

Altogether, over-expression of VAPB-P56S resulted in expansion of ER tubules and suggested that this phenotype might alter cellular processes that are associated with the ER. Co-expression of the FFAT motif prevented formation of these expanded ER tubules and is predicted to correct functional defects due to VAPB-P56S over-expression.

Interestingly, the P56S mutation of VAPB resulted in distortion of the nuclear envelope (Fig. 6D) reflected as an increase of the PNS between the inner and outer nuclear membrane (Fig. 7). This alteration in NE morphology has not been documented in previous studies, and suggested that VAPB-P56S may also alter functions associated with the NE.

VAPB-P56S inhibits anterograde transport of correctly folded, membrane-bound proteins

VAPA and VAPB are reported to have a function in intracellular trafficking of cargo proteins (Foster et al., 2000) but their exact function is unknown. A temperature-sensitive VSVG was used to monitor anterograde transport of cargo protein and illustrated that VAPA but not VAPB regulated anterograde transport of vesicle cargo protein by inhibiting ER exit of VSVG (Fig. 9 and 10). Therefore, the differential effect of the two VAP isoforms on the ER morphology also extends to protein function. The inhibition of ER exit may be due to the indirect interaction of the MSP domain of VAPA with microtubules (Prosser et al., 2008) resulting in the formation of VAPA-associated immobile anchor point on the ER. In this situation, over-expression of VAPA is expected to increase the number of these immobile anchor points and inhibit lateral movement of membrane-bound VSVG to ER exit sites (Prosser et al., 2008). This was supported by fluorescence recovery after photobleaching (FRAP) experiments where diffusion of

VSVG^{ts045}-GFP into the bleached areas was inhibited when VAPA-WT or VAPA-P56S but not VAPB-WT was over-expressed (Prosser et al., 2008). In the case of VAPA, co-expression of the FFAT motif restored anterograde transport of VSVG from the ER to the Golgi complex (Fig. 13 and 14). While changes in lipid composition could affect ER to Golgi complex transport, the FFAT motif could also affect the lateral diffusion of membrane proteins by altering ER-microtubule interaction. In this view, the FFAT motif would disrupt the indirect interaction between the MSP domain and microtubules resulting in the loss of immobile anchor points. In support of this argument, application of the FFAT peptide prevented co-precipitation of VAPA with polymerized microtubules (Prosser et al., 2008). Furthermore, this is consistent with FRAP experiments where possible disruption of membrane-microtubule interaction resulted in higher rate of recovery of VSVG^{ts045}-GFP fluorescence in bleached areas of VAPA-WT and VAPA-P56S expressing cells (Prosser et al., 2008). The results inferred that the VAP isoforms are functionally distinct and opens the possibility that VAPB is associated with retrograde transport of cargo protein. One of the earliest studies on VAPB by Elazar's group demonstrated that addition of antibodies against ERG30, the initial designation for VAPB, resulted in the accumulation of COPI-coated vesicles, which are involved in retrograde traffic from the Golgi complex to the ER (Soussan et al., 1999). In contrast to its wild-type variant, the VAPB-P56S mutation sequestered VSVG into these expanded ER tubules and inhibited ER exit of VSVG (Fig. 9 and 10) implying that VSVG was trapped in these structures and is immobile. Consequently, VSVG was not available for cargo selection during formation of transport vesicles (Gorelick and Shugrue, 2001) and was unable to move to the ER exit site. This was validated from FRAP experiments

showing that over-expression of VAPB-P56S prevented recovery of $VSVG^{ts045}$-GFP fluorescence in bleached areas suggesting that the VSVG is not mobile (Prosser et al., 2008). Co-expression of the FFAT motif with VAPB-P56S corrected the ER morphology and restored anterograde transport of VSVG (Fig. 13 and 14) implying that alteration to the ER compartment also alters ER-associated functions.

Over-expression of the different VAP constructs did not interfere with proper folding of VSVG as confirmed by conformation-specific I14 antibody (Figs. 11 and 12), therefore inhibition of ER exit is not due to misfolded VSVG. Furthermore, the comparison of protein transport of soluble CgB versus membrane-bound VSVG revealed that the inhibition of anterograde transport was specific to membrane-associated proteins (Fig. 15) and this outcome can be explained by the differences in their movement to the ER exit site. Unlike membrane-associated proteins that are restricted to movement in two-dimensions, soluble cargo proteins are not limited to the membrane (Jacobson et al., 1987) and can move freely within the ER lumen to the ER exit site.

Taken together, VAPA and VAPB are functionally different in regards to regulation of anterograde transport of cargo protein. Over-expression of VAPB-P56S altered ER morphology and altered ER function reflected as the inhibition of correctly folded, membrane-associated VSVG to exit the ER. This suggests that other membrane-bound proteins are also trapped in these expanded ER tubules. Consequently, this effect may increase the protein load in the ER, triggering ER stress and activating the UPR (Suzuki et al., 2009).

VAPB-P56S dampens IRE1 and ATF6 activation

The expression of VAPB has been documented to affect the level of activation of the IRE1 and ATF6 signaling pathways of the UPR. However, the ER of the cells in these studies were not stressed (Kanekura et al., 2006) or stressed for a maximum of 12 hours (Gkogkas et al., 2008) which may not be applicable in studying the effects of late-onset ALS8 associated VAPB-P56S.

The use of a GFP reporter that was translated upon splicing of XBP1u mRNA into the active XBP1s protein was used to monitor the level of IRE1 activity under chronic tunicamycin treatment. The results indicated that under conditions of chronic ER stress in CHO or NSC-34, over-expression of VAPB-WT or VAPB-P56S dampened the activity of IRE1 (Fig. 17) compared to control cells. Two possible explanations for the dampening of IRE1 activity indicated by a lower frequency of XBP1s-GFP was due to inhibition of endogenous IRE1 splicing of XBP1 mRNA or increased XBP1s protein degradation. I explored the latter possibility because EM images showed distortion of the NE exhibited by an increase in the PNS. This distortion could potentially prevent insertion into the NE of nuclear pore complexes (NPCs), large macromolecules that form aqueous channels that span the double-lipid bilayer of the NE and are tasked with regulating nucleocytoplasmic transport (Zwerger et al., 2010). Consequently, this defect may inhibit transport of XBP1s from the cytoplasm to the nucleus resulting in the accumulation of cytoplasmic XBP1s that are reported to be rapidly degraded by the proteasome machinery (Tirosh et al., 2006). Using the same XBP1-GFP reporter, a cell with 81-100% of its relative GFP fluorescence in the nucleus was designated as having XBP1s-GFP localized to the nucleus. In this context, my results indicated that under

conditions of acute ER stress, over-expression of VAPB-P56S but not VAPB-WT inhibited XBP1s-GFP transport from the cytoplasm to the nucleus (Fig. 18). It should also be noted that incomplete exclusion of XBP1s-GFP from the nucleus in cells over-expressing VAPB-P56S can be attributed to vertebrate cells that have approximately 2,000-4,000 NPCs in the NE (Capelson and Hetzer, 2009) thereby potentially allowing the cell to accommodate some loss of NPCs without completely disrupting nucleocytoplasmic transport. The limitation of this experiment was that it only tested the effects of nuclear import leaving the possibility that VAPB-P56S affects the permeability of the nucleus. This change in the permeability may be reflected as a loss of retention of proteins in the nucleus resulting in the proteins being transported back to the cytoplasm to be degraded. However, the XBP1s (residues 2-295)-GFP translated in this study contained the nuclear localization signal (NLS) (residues 62-70) and transcription activation domain (residues 55-93) (Yu et al., 2006). Therefore it is unlikely that once bound to the UPRE or ERSE, that XBP1s-GFP was transported out of the nucleus and degraded. The rate of protein degradation of XBP1s-GFP in cells over-expressing VAPB-WT or VAPB-P56S presented as protein half-life was lower (Fig. 21) compared to the control and this is inconsistent with the prediction that the lower frequency of XBP1s-GFP expression in cell over-expressing VAPB-P56S is due to rapid protein degradation of cytoplasmic XBP1s-GFP. Presently, the reason for this remains unclear. Co-expression of the FFAT motif cleared the defect at the NE (Fig. 6B and 7) and corrected XBP1s-GFP localization to the nucleus (Fig. 19) indicating that distortion of the NE has an effect on nucleocytoplasmic transport. Co-expression of the FFAT motif did not alter the frequency of XBP1s-GFP in VAPB-WT and VAPB-P56S over-

expressing cells compared to the condition where the FFAT motif was not expressed but instead dampened the control condition (Fig. 17). This outcome can be explained based on a previous study where FFAT-binding defective VAPB K87D/M89D nullified XBP1 splicing (Kanekura et al., 2006) suggesting that VAPB-induced activation of IRE1 signaling might be via its interaction with FFAT-motif containing proteins (Suzuki et al., 2009). Therefore, it is possible that the FFAT motif behaved as a competitive ligand for endogenous VAPB and prevented the interaction with endogenous FFAT-motif containing lipid proteins resulting in a decrease in XBP1s-GFP expression.

These results suggested that over-expression of VAPB-P56S dampened XBP1s-GFP expression and that this is due to inhibition of endogenous IRE1 splicing activity of XBP1u-GFP mRNA as it does not appear that XBP1s-GFP is being rapidly turned over (Fig. 21). Based on the FRAP experiments of VSVG, the lateral movement of membrane-associated IRE1 may be inhibited and prevent dimerization from occurring which is essential for IRE autophosphorylation and activation of endoribonuclease activity (Ron and Hubbard, 2008). This can be addressed by comparing the protein levels of phosphorylated IRE1 or the levels of unspliced versus spliced XBP1 mRNA by quantitative RT-PCR (Samali et al., 2010) between control and VAPB-P56S expressing cells induced by ER stress. Also, an alternative to measuring XBP1s expression by fluorescent microscopy is to employ a more sensitive reporter assay using a p4xXBPGL3 reporter that has a luciferase gene under the control of four tandem copies of the XBP1 consensus binding site (Samali et al., 2010).

The over-expression of VAPB-WT or VAPB-P56S before the treatment with tunicamycin did not activate IRE1 signaling (Fig. 17) and this is partially inconsistent

with previous studies by Matsuoka's group that showed that in the absence of any ER stress, VAPB-WT alone increased IRE1/XBP1 signaling while the P56S mutant did not result in activation (Kanekura et al., 2006; Suzuki et al., 2009). The difference in VAPB plasmid constructs may explain differential effect of VAPB-WT between their study and this one. Matsuoka's group used a vector with an elongation factor 1α (EF1α) promoter (Suzuki et al., 2009) and this study employed a vector with a cytomegalovirus (CMV) promoter. The EF1α promoter is reported to be a more efficient promoter for transgene expression than CMV (Teschendorf et al., 2002), which may have resulted in higher expression of VAPB-WT and the activation of IRE1. In addition, the effect of wild-type or P56S VAPB on IRE1 activity was determined by luminescence using a UPRE luciferase reporter plasmid that monitored both the IRE1 and ATF6 pathway (Suzuki et al., 2009). Thus, the effect of VAPB might not have been specific to IRE1 activity.

A luciferase reporter assay using an ATF6-dependent reporter demonstrated that over-expression of VAPB-P56S dampened ATF6-dependent luciferase activity (Fig. 22) in comparison to control and VAPB-WT in CHO and NSC-34, which is counter to results presented in an earlier study by Skehel's group (Gkogkas et al., 2008). Their study showed that over-expression of VAPB-WT or VAPB-P56S inhibited ATF6 activity, although the mutant provoked a more robust inhibition (Gkogkas et al., 2008). Similar cell culture and ATF6 luciferase reporter was used in both studies therefore the differential effect may be due to the time point at which the cells were collected. Skehel's group collected their cells at one time point, 12 hours after tunicamycin treatment (Gkogkas et al., 2008) in contrast to this study where the cells were collected at various intervals with a peak response at 24 hours (Fig. 22) and a final time point at 48

hours. It is possible that the effect seen by Skehel's group is due to their shorter tunicamycin treatment and a longer time course may have presented similar results this study. Co-expression of the FFAT motif with VAPB-P56S corrected the ATF6 activation by raising the relative luciferase activity to values similar to control and VAPB-WT suggested that resolving the formation of the expanded ER tubules restored the cellular mechanism needed to properly activate ATF6 signaling.

VAPB interacts directly with ATF6 (Gkogkas et al., 2008) and under this circumstance, over-expression of VAPB-P56S might dampen ATF6 activity by restricting the movement of endogenous membrane-associated ATF6 to ER exit sites similar to the effect seen with VSVG. A study by Mori's group reinforced this hypothesis as they have demonstrated that ATF6 and correctly folded proteins are transported to the Golgi apparatus using the same route and mechanism under conditions of ER stress (Nadanaka et al., 2004). Restricting the movement of membrane-associated ATF6 precursor would prevent proteolysis of the precursor and release of the activation domain at the Golgi complex. This hypothesis can be validated by FRAP or by employing a fluorescent or epitope-tagged ATF6 and observing ATF6 anterograde transport. The prediction would be that in control cells, ATF6 would translocate from the ER to the Golgi complex upon ER stress but VAPB-P56S over-expression would sequester ATF6 in these expanded ER tubules. Also, the dampening of ATF6 activity may be due to a defect in nucleocytoplasmic transport based on the results of XBP1s-GFP localization to the nucleus.

The techniques used to measure the IRE1 and ATF6 activation in this study were limited because they did not address whether specific UPR target genes were being

upregulated. This can be remedied by looking at protein levels by Western blotting or mRNA levels by RT-PCR of specific UPR target genes of IRE1 and ATF6 such as the ERAD genes ER degradation enhancer, mannosidase alpha-like 1 (EDEM1) and homocysteine-induced ER protein (HERP), respectively (Samali et al., 2010).

VAPB-P56S did not cause prolonged IRE1 or ATF6 activity

Walter's group showed that IRE1 activity, given as a measure of spliced XBP1 mRNA peaked at 4 hours and completely subsided by 12 hours when treated with tunicamycin (Lin et al., 2007). Similarly, ATF6 activity given as a measure of the protein level of the free cytosolic ATF6 fragment peaked at 8 hours and completely ceased at 24 hours (Lin et al., 2007). The peak activities of IRE1 and ATF6 for the control and VAPB in this study were recorded at later time points than Walter's group's findings and the difference may be due to dosage of tunicamycin. However, the results from this study suggested that over-expression of VAPB-P56S prevented activation of IRE1 and ATF6 signaling therefore prolonged IRE1 or ATF6 activity did not occur. The same study carried out by Walter's group showed that the PERK branch of the UPR did not diminish during chronic ER stress (Lin et al., 2007). They suggested that IRE1 triggered protective effects early on in ER stress, whereas ATF6 was intermediate and PERK response was long-lasting (Lin et al., 2009). Thus, IRE1, ATF6 and PERK have divergent effects where PERK might have more influence on determining the death of cells by promoting apoptosis (Lin et al., 2009). Presently, no studies have reported the effect of VAPB-P56S on the PERK pathway opening the possibility that prolonged UPR activation and apoptosis might occur via this proximal sensor. The preferred method to measuring PERK activation is by detection of downstream protein targets such as ATF4

or by looking at eIF2α phosphorylation levels because phosphorylation of PERK itself is difficult to detect due to low levels of expression and the lack of available commercial antibodies (Samali et al., 2010).

A defect of the nuclear envelope may trigger the loss of motor neurones

This study indicated that over-expression of VAPB-P56S caused the formation of expanded ER tubules (Fig.6c) resulting in the inhibition of anterograde transport (Fig. 9 and 10) of correctly folded (Fig. 12), membrane-associated VSVG from the ER to the Golgi complex (Fig. 15). Proteins unable to exit the ER are predicted to increase ER stress and trigger the UPR, however, the accumulation of proteins in the ER is cytotoxic and can possibly overwhelm a cellular process such as the UPR (Schroder and Kaufman, 2005). Under chronic ER stress, over-expression of VAPB-P56S was predicted to activate IRE1 and ATF6 signaling for a prolong period of time due to the stability of these expanded ER tubules (Kanekura et al., 2006) and trigger motor neurone death via the apoptotic pathway (Schroder and Kaufman, 2005). In contrast to this proposed model, over-expression of VAPB-P56S dampened the activation of IRE1 (Fig. 17) and ATF6 (Fig. 22), two of the three sensors of the UPR. In this study, CHO fibroblasts and NSC-34 motor neurones displayed similar deficits to activation of the UPR under chronic ER stress despite the fact that motor neurones are preferentially vulnerable to the P56S mutation of VAPB (Teuling et al., 2007). This suggests that an alternative mechanism may be responsible for the loss of motor neurones. One possibility is that defects at the nuclear envelope may underlie the mechanism responsible for selective damage of motor neurones.

EM images revealed that over-expression of VAPB-P56S caused morphological defects of the NE characterized by separation of the inner and outer nuclear membrane and expansion of the PNS (Fig. 6c and 7). Therefore, VAPB-P56S may be a form of nuclear envelopathy (Burke and Stewart, 2006), a general term assigned to diseases with defects of the nuclear envelope. It is possible that proteins localized to the nuclear lamina, on the inner nuclear membrane or spanning both nuclear membranes are affected by this defect. The expanded ER tubules associated with over-expression of VAPB-P56S may have caused a defect in the transport of renewing proteins of the NPCs (Busch et al., 2009; Kinoshita et al., 2009) or proteins associated with linker of the nucleocytoskeleton to the cytoskeleton (LINC) complexes (Razafsky and Hodzic, 2009), responsible for the physical connection between the two nuclear membranes. This can be addressed by employing fluorescent microscopy to test the localization of proteins of the LINC complex when VAPB-P56S is over-expressed. Candidate proteins for the outer and inner nuclear membrane could be Nesprin and Sun1 (Burke and Stewart, 2006), respectively. An alternative explanation is that expression of the VAPB-P56S mutation results in enhanced lipid synthesis of the outer nuclear membrane but not on the inner membrane. The consequence of this would be an increase in the surface area of the outer nuclear membrane that would not be matched by the inner nuclear membrane resulting in expansion of the PNS. The widening of PNS and the loss of surface area on the nucleus could affect insertion of NPCs leading to a decrease in NPCs on the nuclear envelope. This effect could explain the preferential vulnerability to VAPB-P56S in non-dividing cells such as motor neurones. In these cells, proteins that make up the pore of the NPCs, referred to as scaffold nucleoporins (Nups), are downregulated or do not renew whereas

only peripheral Nups are exchanged. Hetzer's group showed that scaffold Nups localized to the central channel were more prone to oxidative protein damage (D'Angelo et al., 2009) leading to increased nuclear permeability and leaking of cytoplasmic proteins into the nucleus. The decrease in NPCs found on the NE and the lack of a replacement mechanism for scaffold Nups in motor neurones predict that these cells would have less NPCs and those NPCs present would keep their scaffolding proteins for many years making them vulnerable to protein damage as the cell ages (D'Angelo et al., 2009). This may explain the tissue-specificity and late-onset nature of ALS8. One of the characteristics of SALS and FALS is the mislocalization of nuclear protein TAR-DNA-binding protein-43 (TDP-43) to the cytoplasm (Anagnostou et al., 2008) and a recent study demonstrated that transgenic mice expressing human VAPB-P56S in the brain and spinal cord regions of the nervous system showed mislocalization of TDP-43 to the cytoplasm as early as 18 months of age (Tudor et al., 2010). Interestingly, the mice had no clear disease motor phenotype or alteration in survival. Absence of disease in VAPB-P56S transgenic mice might reflect the less severe and late-onset disease phenotype seen in most ALS8 cases as these mice were not breed past 24 months of age (Tudor et al., 2010). Altogether, expression of VAPB-P56S altered NE morphology, which may affect its permeability and explain the preferential vulnerability of motor neurones to premature death in ALS8.

REFERENCES

Ackerman, S. L. and Cox, G. A. (2008). From ER to Eph receptors: new roles for VAP fragments. *Cell* **133**, 949-51.

Amarilio, R., Ramachandran, S., Sabanay, H. and Lev, S. (2005). Differential regulation of endoplasmic reticulum structure through VAP-Nir protein interaction. *J Biol Chem* **280**, 5934-44.

Anagnostou, G., Akbar, M. T., Paul, P., Angelinetta, C., Steiner, T. J. and de Belleroche, J. (2008). Vesicle associated membrane protein B (VAPB) is decreased in ALS spinal cord. *Neurobiol Aging.*

Back, S. H., Schroder, M., Lee, K., Zhang, K. and Kaufman, R. J. (2005). ER stress signaling by regulated splicing: IRE1/HAC1/XBP1. *Methods* **35**, 395-416.

Baker, A. M., Roberts, T. M. and Stewart, M. (2002). 2.6 A resolution crystal structure of helices of the motile major sperm protein (MSP) of Caenorhabditis elegans. *J Mol Biol* **319**, 491-9.

Beh, C. T. and Rine, J. (2004). A role for yeast oxysterol-binding protein homologs in endocytosis and in the maintenance of intracellular sterol-lipid distribution. *J Cell Sci* **117**, 2983-96.

Ben-Tekaya, H., Miura, K., Pepperkok, R. and Hauri, H. P. (2005). Live imaging of bidirectional traffic from the ERGIC. *J Cell Sci* **118**, 357-67.

Boillee, S., Vande Velde, C. and Cleveland, D. W. (2006). ALS: a disease of motor neurons and their nonneuronal neighbors. *Neuron* **52**, 39-59.

Bruijn, L. I., Miller, T. M. and Cleveland, D. W. (2004). Unraveling the mechanisms involved in motor neuron degeneration in ALS. *Annu Rev Neurosci* **27**, 723-49.

Burke, B. and Stewart, C. L. (2006). The laminopathies: the functional architecture of the nucleus and its contribution to disease. *Annu Rev Genomics Hum Genet* **7**, 369-405.

Busch, A., Kiel, T., Heupel, W. M., Wehnert, M. and Hubner, S. (2009). Nuclear protein import is reduced in cells expressing nuclear envelopathy-causing lamin A mutants. *Exp Cell Res* **315**, 2373-85.

Capelson, M. and Hetzer, M. W. (2009). The role of nuclear pores in gene regulation, development and disease. *EMBO Rep* **10**, 697-705.

Cashman, N. R., Durham, H. D., Blusztajn, J. K., Oda, K., Tabira, T., Shaw, I. T., Dahrouge, S. and Antel, J. P. (1992). Neuroblastoma x spinal cord (NSC) hybrid cell lines resemble developing motor neurons. *Dev Dyn* **194**, 209-21.

Chai, A., Withers, J., Koh, Y. H., Parry, K., Bao, H., Zhang, B., Budnik, V. and Pennetta, G. (2008). hVAPB, the causative gene of a heterogeneous group of motor neuron diseases in humans, is functionally interchangeable with its Drosophila homologue DVAP-33A at the neuromuscular junction. *Hum Mol Genet* **17**, 266-80.

Chang, H. J., Jesch, S. A., Gaspar, M. L. and Henry, S. A. (2004). Role of the unfolded protein response pathway in secretory stress and regulation of INO1 expression in Saccharomyces cerevisiae. *Genetics* **168**, 1899-913.

Chen, X., Shen, J. and Prywes, R. (2002). The luminal domain of ATF6 senses endoplasmic reticulum (ER) stress and causes translocation of ATF6 from the ER to the Golgi. *J Biol Chem* **277**, 13045-52.

Conforti, F. L., Sprovieri, T., Mazzei, R., Ungaro, C., Tessitore, A., Tedeschi, G., Patitucci, A., Magariello, A., Gabriele, A., Labella, V. et al. (2006). Sporadic ALS is not associated with VAPB gene mutations in Southern Italy. *J Negat Results Biomed* **5**, 7.

Cozzolino, M., Ferri, A. and Carri, M. T. (2008). Amyotrophic lateral sclerosis: from current developments in the laboratory to clinical implications. *Antioxid Redox Signal* **10**, 405-43.

D'Angelo, M. A., Raices, M., Panowski, S. H. and Hetzer, M. W. (2009). Age-dependent deterioration of nuclear pore complexes causes a loss of nuclear integrity in postmitotic cells. *Cell* **136**, 284-95.

Doms, R. W., Ruusala, A., Machamer, C., Helenius, J., Helenius, A. and Rose, J. K. (1988). Differential effects of mutations in three domains on folding, quaternary structure, and intracellular transport of vesicular stomatitis virus G protein. *J Cell Biol* **107**, 89-99.

Durham, H. D., Dahrouge, S. and Cashman, N. R. (1993). Evaluation of the spinal cord neuron X neuroblastoma hybrid cell line NSC-34 as a model for neurotoxicity testing. *Neurotoxicology* **14**, 387-95.

DuRose, J. B., Tam, A. B. and Niwa, M. (2006). Intrinsic capacities of molecular sensors of the unfolded protein response to sense alternate forms of endoplasmic reticulum stress. *Mol Biol Cell* **17**, 3095-107.

Ellgaard, L. and Helenius, A. (2001). ER quality control: towards an understanding at the molecular level. *Curr Opin Cell Biol* **13**, 431-7.

Fasana, E., Fossati, M., Ruggiano, A., Brambillasca, S., Hoogenraad, C. C., Navone, F., Francolini, M. and Borgese, N. (2009). A VAPB mutant linked to amyotrophic lateral sclerosis generates a novel form of organized smooth endoplasmic reticulum. *FASEB J.*

Forman, M. S., Lee, V. M. and Trojanowski, J. Q. (2003). 'Unfolding' pathways in neurodegenerative disease. *Trends Neurosci* **26**, 407-10.

Foster, L. J., Weir, M. L., Lim, D. Y., Liu, Z., Trimble, W. S. and Klip, A. (2000). A functional role for VAP-33 in insulin-stimulated GLUT4 traffic. *Traffic* **1**, 512-21.

Gkogkas, C., Middleton, S., Kremer, A. M., Wardrope, C., Hannah, M., Gillingwater, T. H. and Skehel, P. (2008). VAPB interacts with and modulates the activity of ATF6. *Hum Mol Genet* **17**, 1517-26.

Gorelick, F. S. and Shugrue, C. (2001). Exiting the endoplasmic reticulum. *Mol Cell Endocrinol* **177**, 13-8.

Hamamoto, I., Nishimura, Y., Okamoto, T., Aizaki, H., Liu, M., Mori, Y., Abe, T., Suzuki, T., Lai, M. M., Miyamura, T. et al. (2005). Human VAP-B is involved in hepatitis C virus replication through interaction with NS5A and NS5B. *J Virol* **79**, 13473-82.

Hauri, H. P., Kappeler, F., Andersson, H. and Appenzeller, C. (2000). ERGIC-53 and traffic in the secretory pathway. *J Cell Sci* **113 (Pt 4)**, 587-96.

Hetz, C., Thielen, P., Matus, S., Nassif, M., Court, F., Kiffin, R., Martinez, G., Cuervo, A. M., Brown, R. H. and Glimcher, L. H. (2009). XBP-1 deficiency in the nervous system protects against amyotrophic lateral sclerosis by increasing autophagy. *Genes Dev* **23**, 2294-306.

Hirano, M. (2008). VAPB: new genetic clues to the pathogenesis of ALS. *Neurology* **70**, 1161-2.

Jacobson, K., Ishihara, A. and Inman, R. (1987). Lateral diffusion of proteins in membranes. *Annu Rev Physiol* **49**, 163-75.

James, P. A. and Talbot, K. (2006). The molecular genetics of non-ALS motor neuron diseases. *Biochim Biophys Acta* **1762**, 986-1000.

Jiang, J. X., Choi, R. C., Siow, N. L., Lee, H. H., Wan, D. C. and Tsim, K. W. (2003). Muscle induces neuronal expression of acetylcholinesterase in neuron-muscle co-culture: transcriptional regulation mediated by cAMP-dependent signaling. *J Biol Chem* **278**, 45435-44.

Kabashi, E., Lin, L., Tradewell, M. L., Dion, P. A., Bercier, V., Bourgouin, P., Rochefort, D., Bel Hadj, S., Durham, H. D., Vande Velde, C. et al. (2010). Gain and loss of function of ALS-related mutations of TARDBP (TDP-43) cause motor deficits in vivo. *Hum Mol Genet* **19**, 671-83.

Kaiser, S. E., Brickner, J. H., Reilein, A. R., Fenn, T. D., Walter, P. and Brunger, A. T. (2005). Structural basis of FFAT motif-mediated ER targeting. *Structure* **13**, 1035-45.

Kanekura, K., Nishimoto, I., Aiso, S. and Matsuoka, M. (2006). Characterization of amyotrophic lateral sclerosis-linked P56S mutation of vesicle-associated membrane protein-associated protein B (VAPB/ALS8). *J Biol Chem* **281**, 30223-33.

Kanekura, K., Suzuki, H., Aiso, S. and Matsuoka, M. (2009). ER stress and unfolded protein response in amyotrophic lateral sclerosis. *Mol Neurobiol* **39**, 81-9.

Kaufman, R. J. (2002). Orchestrating the unfolded protein response in health and disease. *J Clin Invest* **110**, 1389-98.

Kinoshita, Y., Ito, H., Hirano, A., Fujita, K., Wate, R., Nakamura, M., Kaneko, S., Nakano, S. and Kusaka, H. (2009). Nuclear contour irregularity and abnormal transporter protein distribution in anterior horn cells in amyotrophic lateral sclerosis. *J Neuropathol Exp Neurol* **68**, 1184-92.

Kukihara, H., Moriishi, K., Taguwa, S., Tani, H., Abe, T., Mori, Y., Suzuki, T., Fukuhara, T., Taketomi, A., Maehara, Y. et al. (2009). Human VAP-C negatively regulates hepatitis C virus propagation. *J Virol* **83**, 7959-69.

Landers, J. E., Leclerc, A. L., Shi, L., Virkud, A., Cho, T., Maxwell, M. M., Henry, A. F., Polak, M., Glass, J. D., Kwiatkowski, T. J. et al. (2008). New VAPB deletion variant and exclusion of VAPB mutations in familial ALS. *Neurology* **70**, 1179-85.

Lee, M. C., Miller, E. A., Goldberg, J., Orci, L. and Schekman, R. (2004). Bi-directional protein transport between the ER and Golgi. *Annu Rev Cell Dev Biol* **20**, 87-123.

Lefrancois, L. and Lyles, D. S. (1983). Antigenic determinants of vesicular stomatitis virus: analysis with antigenic variants. *J Immunol* **130**, 394-8.

Lev, S., Ben Halevy, D., Peretti, D. and Dahan, N. (2008). The VAP protein family: from cellular functions to motor neuron disease. *Trends Cell Biol* **18**, 282-90.

Lin, J. H., Li, H., Yasumura, D., Cohen, H. R., Zhang, C., Panning, B., Shokat, K. M., Lavail, M. M. and Walter, P. (2007). IRE1 signaling affects cell fate during the unfolded protein response. *Science* **318**, 944-9.

Lin, J. H., Li, H., Zhang, Y., Ron, D. and Walter, P. (2009). Divergent effects of PERK and IRE1 signaling on cell viability. *PLoS One* **4**, e4170.

Lin, T. Y., Wang, S. M., Fu, W. M., Chen, Y. H. and Yin, H. S. (1999). Toxicity of tunicamycin to cultured brain neurons: ultrastructure of the degenerating neurons. *J Cell Biochem* **74**, 638-47.

Liu, C. Y. and Kaufman, R. J. (2003). The unfolded protein response. *J Cell Sci* **116**, 1861-2.

Loewen, C. J. and Levine, T. P. (2005). A highly conserved binding site in vesicle-associated membrane protein-associated protein (VAP) for the FFAT motif of lipid-binding proteins. *J Biol Chem* **280**, 14097-104.

Loewen, C. J., Roy, A. and Levine, T. P. (2003). A conserved ER targeting motif in three families of lipid binding proteins and in Opi1p binds VAP. *EMBO J* **22**, 2025-35.

Malhotra, J. D. and Kaufman, R. J. (2007a). Endoplasmic reticulum stress and oxidative stress: a vicious cycle or a double-edged sword? *Antioxid Redox Signal* **9**, 2277-93.

Malhotra, J. D. and Kaufman, R. J. (2007b). The endoplasmic reticulum and the unfolded protein response. *Semin Cell Dev Biol* **18**, 716-31.

Mitne-Neto, M., Ramos, C. R., Pimenta, D. C., Luz, J. S., Nishimura, A. L., Gonzales, F. A., Oliveira, C. C. and Zatz, M. (2007). A mutation in human VAP-B--MSP domain, present in ALS patients, affects the interaction with other cellular proteins. *Protein Expr Purif* **55**, 139-46.

Nadanaka, S., Yoshida, H., Kano, F., Murata, M. and Mori, K. (2004). Activation of mammalian unfolded protein response is compatible with the quality control system operating in the endoplasmic reticulum. *Mol Biol Cell* **15**, 2537-48.

Nehls, S., Snapp, E. L., Cole, N. B., Zaal, K. J., Kenworthy, A. K., Roberts, T. H., Ellenberg, J., Presley, J. F., Siggia, E. and Lippincott-Schwartz, J. (2000). Dynamics and retention of misfolded proteins in native ER membranes. *Nat Cell Biol* **2**, 288-95.

Nishimura, A. L., Al-Chalabi, A. and Zatz, M. (2005). A common founder for amyotrophic lateral sclerosis type 8 (ALS8) in the Brazilian population. *Hum Genet* **118**, 499-500.

Nishimura, A. L., Mitne-Neto, M., Silva, H. C., Richieri-Costa, A., Middleton, S., Cascio, D., Kok, F., Oliveira, J. R., Gillingwater, T., Webb, J. et al. (2004). A mutation in the vesicle-trafficking protein VAPB causes late-onset spinal muscular atrophy and amyotrophic lateral sclerosis. *Am J Hum Genet* **75**, 822-31.

Nishimura, Y., Hayashi, M., Inada, H. and Tanaka, T. (1999). Molecular cloning and characterization of mammalian homologues of vesicle-associated membrane protein-associated (VAMP-associated) proteins. *Biochem Biophys Res Commun* **254**, 21-6.

Olkkonen, V. M., Johansson, M., Suchanek, M., Yan, D., Hynynen, R., Ehnholm, C., Jauhiainen, M., Thiele, C. and Lehto, M. (2006). The OSBP-related proteins (ORPs): global sterol sensors for co-ordination of cellular lipid metabolism, membrane trafficking and signalling processes? *Biochem Soc Trans* **34**, 389-91.

Olkkonen, V. M. and Levine, T. P. (2004). Oxysterol binding proteins: in more than one place at one time? *Biochem Cell Biol* **82**, 87-98.

Peretti, D., Dahan, N., Shimoni, E., Hirschberg, K. and Lev, S. (2008). Coordinated lipid transfer between the endoplasmic reticulum and the Golgi complex requires the VAP proteins and is essential for Golgi-mediated transport. *Mol Biol Cell* **19**, 3871-84.

Perry, R. J. and Ridgway, N. D. (2006). Oxysterol-binding protein and vesicle-associated membrane protein-associated protein are required for sterol-dependent activation of the ceramide transport protein. *Mol Biol Cell* **17**, 2604-16.

Prosser, D. C., Tran, D., Gougeon, P. Y., Verly, C. and Ngsee, J. K. (2008). FFAT rescues VAPA-mediated inhibition of ER-to-Golgi transport and VAPB-mediated ER aggregation. *J Cell Sci* **121**, 3052-61.

Ratnaparkhi, A., Lawless, G. M., Schweizer, F. E., Golshani, P. and Jackson, G. R. (2008). A Drosophila model of ALS: human ALS-associated mutation in VAP33A suggests a dominant negative mechanism. *PLoS One* **3**, e2334.

Razafsky, D. and Hodzic, D. (2009). Bringing KASH under the SUN: the many faces of nucleo-cytoskeletal connections. *J Cell Biol* **186**, 461-72.

Ron, D. and Hubbard, S. R. (2008). How IRE1 reacts to ER stress. *Cell* **132**, 24-6.

Rutkowski, D. T. and Kaufman, R. J. (2004). A trip to the ER: coping with stress. *Trends Cell Biol* **14**, 20-8.

Samali, A., Fitzgerald, U., Deegan, S. and Gupta, S. (2010). Methods for monitoring endoplasmic reticulum stress and the unfolded protein response. *Int J Cell Biol* **2009**, 830307.

Schroder, M. and Kaufman, R. J. (2005). The mammalian unfolded protein response. *Annu Rev Biochem* **74**, 739-89.

Shang, J. (2005). Quantitative measurement of events in the mammalian unfolded protein response. *Methods* **35**, 390-4.

Shaw, P. J. (2005). Molecular and cellular pathways of neurodegeneration in motor neurone disease. *J Neurol Neurosurg Psychiatry* **76**, 1046-57.

Shen, J. and Prywes, R. (2005). ER stress signaling by regulated proteolysis of ATF6. *Methods* **35**, 382-9.

Shi, J., Lua, S., Tong, J. S. and Song, J. (2010). Elimination of the Native Structure and Solubility of the hVAPB MSP Domain by the Pro56Ser Mutation which Causes Amyotrophic Lateral Sclerosis. *Biochemistry*.

Skehel, P. A., Fabian-Fine, R. and Kandel, E. R. (2000). Mouse VAP33 is associated with the endoplasmic reticulum and microtubules. *Proc Natl Acad Sci U S A* **97**, 1101-6.

Sommer, T. and Jarosch, E. (2002). BiP binding keeps ATF6 at bay. *Dev Cell* **3**, 1-2.

Soussan, L., Burakov, D., Daniels, M. P., Toister-Achituv, M., Porat, A., Yarden, Y. and Elazar, Z. (1999). ERG30, a VAP-33-related protein, functions in protein transport mediated by COPI vesicles. *J Cell Biol* **146**, 301-11.

Suzuki, H., Kanekura, K., Levine, T. P., Kohno, K., Olkkonen, V. M., Aiso, S. and Matsuoka, M. (2009). ALS-linked P56S-VAPB, an aggregated loss-of-function mutant of VAPB, predisposes motor neurons to ER stress-related death by inducing aggregation of co-expressed wild-type VAPB. *J Neurochem* **108**, 973-985.

Szegezdi, E., Logue, S. E., Gorman, A. M. and Samali, A. (2006). Mediators of endoplasmic reticulum stress-induced apoptosis. *EMBO Rep* **7**, 880-5.

Teschendorf, C., Warrington, K. H., Jr., Siemann, D. W. and Muzyczka, N. (2002). Comparison of the EF-1 alpha and the CMV promoter for engineering stable tumor cell lines using recombinant adeno-associated virus. *Anticancer Res* **22**, 3325-30.

Teuling, E., Ahmed, S., Haasdijk, E., Demmers, J., Steinmetz, M. O., Akhmanova, A., Jaarsma, D. and Hoogenraad, C. C. (2007). Motor neuron disease-associated mutant vesicle-associated membrane protein-associated protein (VAP) B recruits wild-type VAPs into endoplasmic reticulum-derived tubular aggregates. *J Neurosci* **27**, 9801-15.

Tirosh, B., Iwakoshi, N. N., Glimcher, L. H. and Ploegh, H. L. (2006). Rapid turnover of unspliced Xbp-1 as a factor that modulates the unfolded protein response. *J Biol Chem* **281**, 5852-60.

Tudor, E. L., Galtrey, C. M., Perkinton, M. S., Lau, K. F., de Vos, K. J., Mitchell, J. C., Ackerley, S., Hortobagyi, T., Vamos, E., Leigh, P. N. et al. (2010). Amyotrophic lateral sclerosis mutant vesicle-associated membrane protein-associated protein-B transgenic mice develop TAR-DNA-binding protein-43 pathology. *Neuroscience*.

Urano, F., Bertolotti, A. and Ron, D. (2000). IRE1 and efferent signaling from the endoplasmic reticulum. *J Cell Sci* **113 Pt 21**, 3697-702.

Wacker, I., Kaether, C., Kromer, A., Migala, A., Almers, W. and Gerdes, H. H. (1997). Microtubule-dependent transport of secretory vesicles visualized in real time with a GFP-tagged secretory protein. *J Cell Sci* **110 (Pt 13)**, 1453-63.

Wang, Y., Shen, J., Arenzana, N., Tirasophon, W., Kaufman, R. J. and Prywes, R. (2000). Activation of ATF6 and an ATF6 DNA binding site by the endoplasmic reticulum stress response. *J Biol Chem* **275**, 27013-20.

Weir, M. L., Xie, H., Klip, A. and Trimble, W. S. (2001). VAP-A binds promiscuously to both v- and tSNAREs. *Biochem Biophys Res Commun* **286**, 616-21.

Wyles, J. P., McMaster, C. R. and Ridgway, N. D. (2002). Vesicle-associated membrane protein-associated protein-A (VAP-A) interacts with the oxysterol-binding protein to modify export from the endoplasmic reticulum. *J Biol Chem* **277**, 29908-18.

Xiong, Z. Q. and McNamara, J. O. (2002). Fas(t) balls and Lou Gehrig disease. A clue to selective vulnerability of motor neurons? *Neuron* **35**, 1011-3.

Yoshida, H. (2007). Unconventional splicing of XBP-1 mRNA in the unfolded protein response. *Antioxid Redox Signal* **9**, 2323-33.

Yoshida, H., Oku, M., Suzuki, M. and Mori, K. (2006). pXBP1(U) encoded in XBP1 pre-mRNA negatively regulates unfolded protein response activator pXBP1(S) in mammalian ER stress response. *J Cell Biol* **172**, 565-75.

Yu, C. Y., Hsu, Y. W., Liao, C. L. and Lin, Y. L. (2006). Flavivirus infection activates the XBP1 pathway of the unfolded protein response to cope with endoplasmic reticulum stress. *J Virol* **80**, 11868-80.

Zhang, K. and Kaufman, R. J. (2004). Signaling the unfolded protein response from the endoplasmic reticulum. *J Biol Chem* **279**, 25935-8.

Zhao, L. and Ackerman, S. L. (2006). Endoplasmic reticulum stress in health and disease. *Curr Opin Cell Biol* **18**, 444-52.

Zwerger, M., Kolb, T., Richter, K., Karakesisoglou, I. and Herrmann, H. (2010). Induction of a massive endoplasmic reticulum and perinuclear space expansion by expression of lamin B receptor mutants and the related sterol reductases TM7SF2 and DHCR7. *Mol Biol Cell* **21**, 354-68.